ISSN 1905-9094

GMSARN INTERNATIONAL JOURNAL

Vol. 3 No. 2
June 2009

Published by the

GREATER MEKONG SUBREGION ACADEMIC AND RESEARCH NETWORK
c/o Asian Institute of Technology
P.O. Box 4, Klong Luang, Pathumthani 12120, Thailand

GMSARN INTERNATIONAL JOURNAL

GMSARN MEMBERS

Asian Institute of Technology (AIT)	P.O. Box 4, Klong Luang, Pathumthani 12120, Thailand. www.ait.ac.th
Hanoi University of Technology (HUT)	No. 1, Daicoviet Street, Hanoi, Vietnam S.R. www.hut.edu.vn
Ho Chi Minh City University of Technology (HCMUT)	268 Ly Thuong Kiet Street, District 10, Ho Chi Minh City, Vietnam. www.hcmut.edu.vn
Institute of Technology of Cambodia (ITC)	BP 86 Blvd. Pochentong, Phnom Penh, Cambodia. www.itc.edu.kh
Khon Kaen University (KKU)	123 Mittraparb Road, Amphur Muang, Khon Kaen, Thailand. www.kku.ac.th
Kunming University of Science and Technology (KUST)	121 Street, Kunming P.O. 650093, Yunnan, China. www.kmust.edu.cn
National University of Laos (NUOL)	P.O. Box 3166, Vientiane Perfecture, Lao PDR. www.nuol.edu.la
Royal University of Phnom Penh (RUPP)	Russian Federation Blvd, PO Box 2640 Phnom Penh, Cambodia. www.rupp.edu.kh
Thammasat University (TU)	P.O. Box 22, Thamamasat Rangsit Post Office, Bangkok 12121, Thailand. www.tu.ac.th
Yangon Technological University (YTU)	Gyogone, Insein P.O. Yangon, Myanmar
Yunnan University	2 Cuihu Bei Road Kunming, 650091, Yunnan Province, China. www.ynu.edu.cn
Guangxi University	100, Daxue Road, Nanning, Guangxi, CHINA www.gxu.edu.cn

ASSOCIATE MEMBERS

Nakhon Phanom University	330 Apibanbuncha Road, Nai Muang Sub-District, Nakhon Phanom 48000, THAILAND www.npu.ac.th
Mekong River Commission	P.O. Box 6101, Unit 18 Ban Sithane Neua, Sikhottabong District, Vientiane 01000, LAO PDR www.mrcmekong.org
Ubon Rajathanee University	85 Sathollmark Rd. Warinchamrap UbonRatchathani 34190, THAILAND www.ubu.ac.th

GMSARN
INTERNATIONAL JOURNAL

GREATER MEKONG SUBREGION ACADEMIC AND RESEARCH NETWORK (http://www.gmsarn.org)

The Greater Mekong Subregion (GMS) consists of Cambodia, China (Yunnan & Guanxi Provinces), Laos, Myanmar, Thailand and Vietnam.

The Greater Mekong Subregion Academic and Research Network (GMSARN) was founded followed an agreement among the founding GMS country institutions signed on 26 January 2001, based on resolutions reached at the Greater Mekong Subregional Development Workshop held in Bangkok, Thailand, on 10 - 11 November 1999. GMSARN is composed of eleven of the region's top-ranking academic and research institutions. GMSARN carries out activities in the following areas: human resources development, joint research, and dissemination of information and intellectual assets generated in the GMS. GMSARN seeks to ensure that the holistic intellectual knowledge and assets generated, developed and maintained are shared by organizations within the region. Primary emphasis is placed on complementary linkages between technological and socio-economic development issues. Currently, GMSARN is sponsored by Royal Thai Government.

The GMSARN member institutions are the Asian Institute of Technology, Pathumthani, Thailand; The Institute of Technology of Cambodia, Phnom Penh, Cambodia; Kunming University of Science and Technology, Yunnan Province, China; National University of Laos, Vientiane, Laos PDR; Yangon Technological University, Yangon, Myanmar; Khon Kaen University, Khon Kaen Province, Thailand; Thammasat University, Bangkok, Thailand; Hanoi University of Technology, Hanoi, Vietnam; Ho Chi Minh City University of Technology, Ho Chi Minh City, Vietnam; The Royal University of Phnom Penh, Phnom Penh, Cambodia; Yunnan University, Yunnan Province and Guangxi University, Guangxi Province, China; and other associate members are Nakhon Phanom University, Nakon Phanom Province, Thailand; Mekong River Commission, Vientiane, Laos PDR and Ubon Rajathanee University, Ubon Ratchathani Province, Thailand.

GMSARN International Journal

Volume 3, Number 2, June 2009

CONTENTS

Feeder Reconfiguration for Loss Reduction in Distribution System with Distributed Generators by Tabu Search 47
N. Rugthaicharoencheep and S. Sirisumrannukul

Multi-objective Optimal Placement of Distributed Generation Using Bee Colony Optimization 55
S. Anantasate, C. Chokpanyasuwan, W. Pattaraprakorn, and P. Bhasaputra

Control of Line Side Converter for Doubly Fed Induction Generator with Active Power Filter and Load Balancing 65
S. Wangsathitwong, S. Sirisumrannukul, S. Chatratana, and W. Deleroi

System Study and Fault Level Reduction Techniques for a Small Scale Power Plant in Thailand 73
S. Tongsrichantra, T. Suwanasri, and C. Suwanasri

A Fuzzy Multi-Attribute Decision Making Approach for Multi-Objective Thermal Power Dispatch 81
S. Chalermchaiarbha and W. Ongsakul

Optimal Capacitor Placement in Unbalanced Loading Distribution System with Nonlinear Loads by Adaptive Particle Swarm Technique 91
S. Auchariyamet and S. Sirisumrannukul

Feeder Reconfiguration for Loss Reduction in Distribution System with Distributed Generators by Tabu Search

N. Rugthaicharoencheep and S. Sirisumrannukul

***Abstract*—** *Feeder reconfiguration is a procedure to alter topological structures of the network by changing the statuses of tie and disconnecting switches. It provides an effective way to control the tie and sectionalizing switches in the system to give an appropriate connection for several reasons such as loss reduction, load balancing, and fast restoration. The main objective of this paper is to minimize the system power loss in the presence of distributed generators that cause reverse power flows and voltage variations. The optimization problem is subject to system constraints consisting of load-point voltage limits, radial configuration format, no load-point interruption and current feeder capability limits. The feeder reconfiguration problem for active power loss minimization is solved by a Tabu search algorithm that effectively utilizes a memory to provide an efficient search for optimality. The developed methodology is tested with a 69-bus distribution system having 48 load points. The study results indicate that for a given set of distributed generators and their locations, the proposed method can identify optimal on/off patterns of the switches that yield the minimum loss while satisfying the constraints.*

***Keywords*— Feeder reconfiguration, Tabu search, Tie and sectionalizing switches, Loss reduction, Distributed generators.**

1. INTRODUCTION

Electricity is generated at central stations, powered up through transformers and transmitted over high voltage transmission lines, and passed down through low voltage distribution lines to final circuits for delivery to the customers. This centralized generation pattern, however, suffers a number of drawbacks, such as a high level of dependence on imported fuels that are very vulnerable, transmission losses, the necessity for continuous upgrading and replacement of the transmission and distribution facilities and therefore high operating cost, and environmental impact.

Over the last decade, distribution systems have seen a significant increase in small-scaled generators as they can compensate the disadvantages encountered in the centralized generation dispatch. These generators, also known as distributed generation (DG), are installed in the network to serve as a source of power at on or near the site where they are to be used. They can be driven by different types of resource and technology such as wind, solar, fuel cells, hydrogen, and biomass.

The introduction of DG units brings a number of technical issues to the system. Many technical effects of distributed generators on the distribution system have been reported in literature such as thermal rating of equipment, system fault levels, stability, reverse power flow capabilities of tap-changers, line drop compensation, voltage rise, power losses, power quality (such as flickers and harmonics) and protection [1]. Distributed generators may introduce positive or negative impacts to the system depending on the system's operating conditions and their characteristics and locations. The emphasis of this paper is paid toward economic benefits presented in terms of active power loss reduction. The active power loss in the distribution network, which varies with the square of the branch current, is appreciable and constitutes a large portion of the overall power system loss. It was reported in [2] that distribution systems cause a power loss about 5–13% of the total power generated. Therefore, reducing the loss will financially and technically benefit the utility.

DG units can normally, but not necessarily, help reducing current flow in the feeders and hence contribute to power loss reduction, mainly because they are usually placed near the load being supplied. Minimizing the power loss, of course, requires an optimization process that can determine the optimal size and location of DG units to be installed. However, in practice, such an optimal solution could not be implemented as distributed generation plants are generally not planned by the utility but are developed by entrepreneurs (e.g., small power producer). For this reason, the location and rating of generators are limited by a number of constraints such as land and resource availability, and environment. For example, the location of a combined heat and power plant is determined by the position of the heat load, and their operation is generally controlled in response to the energy demand of the host site or of a district heating scheme [3]. Therefore, these constraints complicate the issue of loss since the distribution network with DG units is no longer passive.

Many methods have been employed for reducing the active power loss, for example, increasing conductor size, shortening circuit lengths, adjusting transformer tap, and installing capacitors. Another efficient operation that can improve the performance of distribution systems is feeder reconfiguration. It is a process that changes the

N. Rugthaicharoencheep (corresponding author) and S. Sirisumrannukul are with Department of Electrical Engineering, Faculty of Engineering, King Mongkut's University of Technology North Bangkok, 1518, Pibulsongkram Rd., Bangsue, Bangkok, 10800, Thailand. Phone: +66-89-607-1641; Fax: +66-2-585-7350; E-mail: s4910190018@kmutnb.ac.th, spss@kmutnb.ac.th.

topology of a distribution system by altering the open/closed status of switches.

This paper emphasizes the advantage of feeder reconfiguration to the distribution system in the presence of DG units for loss reduction and bus voltage improvement. The major effect of DG units on the feeder reconfiguration problem lies on the fact that power flows in the distribution system, which is normally radially operated, are no longer unidirectional (i.e., power can be fed back to the grid). Such reversible power flow, therefore, complicates the feeder reconfiguration problem for loss minimization. The application of a Tabu search algorithm is developed to determine the optimal on/off patterns of the switches to minimize the system loss subject to system constraints. The effectiveness of the methodology is demonstrated by a practical sized distribution system consisting of 69 bus and 48 load points.

2. FEEDER RECONFIGURATION

Feeder reconfiguration in a distribution system is an operation in configuration management that determines the switching operations for many purposes such as decreasing network loss, balancing system load, and improving bus voltages or system reliability. The configuration may be varied via switching operations to transfer loads among the feeders. Two types of switches are used: normally closed switches (sectionalizing switches) and normally open switches (tie switches) [4].

There are a number of closed and normally opened switches in a distribution system. The number of possible switching actions makes feeder reconfiguration become a complex decision-making for system operators. Figure 1 shows a schematic diagram of a simplified primary circuit of a distribution system [4]. In the figure, CB1-CB6 are normally closed switches that connect the line sections, and CB7 is a normally open switch that connects two primary feeders. The two substations can be linked by CB8, while CB9, when closed, will create a loop. A flowchart for feeder reconfiguration algorithm is shown in Figure 2.

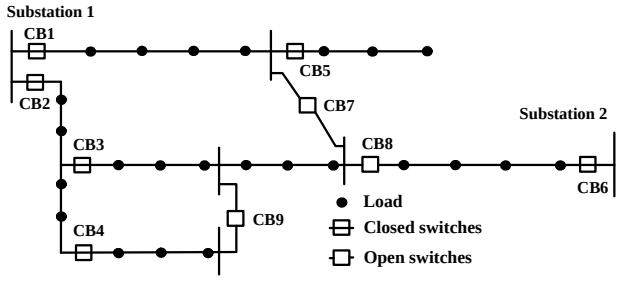

Fig.1. Schematic Diagram of a Distribution System.

3. PROBLEM FORMULATION

The objective function of the network configuration problem in this paper is to minimize the total power loss as:

$$\text{Minimize } Z = \sum_{n=1}^{N_L}\sum_{k=1}^{l}\left|I_{k,n}\right|^2 R_k \quad (1)$$

The objective function is subjected to the following constraints.

- Power flow equations:

$$P_{i,n} = \sum_{j=1}^{N_B}\left|Y_{ij}V_{i,n}V_{j,n}\right|\cos(\theta_{ij} + \delta_{j,n} - \delta_{i,n}) \quad (2)$$

$$Q_{i,n} = -\sum_{j=1}^{N_B}\left|Y_{ij}V_{i,n}V_{j,n}\right|\sin(\theta_{ij} + \delta_{j,n} - \delta_{i,n}) \quad (3)$$

- Bus voltage limits:

$$V^{\min} \le V_{i,n} \le V^{\max} \quad (4)$$

- Current transfer capability of feeders:

$$I_{k,n} \le I_k^{\max};\ k \in \{1,2,...,l\} \quad (5)$$

- Radial configuration format.
- No load-point interruption.

4. TABU SEARCH

Background

Tabu search (TS) is a meta-heuristic that guides a local heuristic search strategy to explore the solution space beyond local optimality. Tabu search was developed by Glover and has been used to solve a wide range of hard optimization problems, such as resource planning, telecommunications, financial analysis, scheduling, space planning, and energy distribution [5].

The basic idea behind the search is a move from a current solution to its neighborhood by effectively utilizing a memory to provide an efficient search for optimality. The memory is called “Tabu list”, which stores attributes of solutions. In the search process, the solutions are in the Tabu list cannot be a candidate of the next iteration. As a result, it helps inhibit choosing the same solution many times and avoid being trapped into cycling of the solutions [6]. The quality of a move in solution space is assessed by aspiration criteria that provide a mechanism (see Figure 3) for overriding the Tabu list. Aspiration criteria are analogous to a fitness function of the genetic algorithm and the Bolzman function in the simulated annealing.

Neighborhood

In the search process, a move to the best solution in the neighborhood, although its quality is worse than the current solution, is allowed. This strategy helps escape from local optimal and explore wider in the search space. A Tabu list includes recently selected solutions that are forbidden to prevent cycling. If the move is present in the Tabu list, it is accepted only if it has a better aspiration level than the minimal level so far. Figure 4 shows the main concept of a search direction in Tabu search [7].

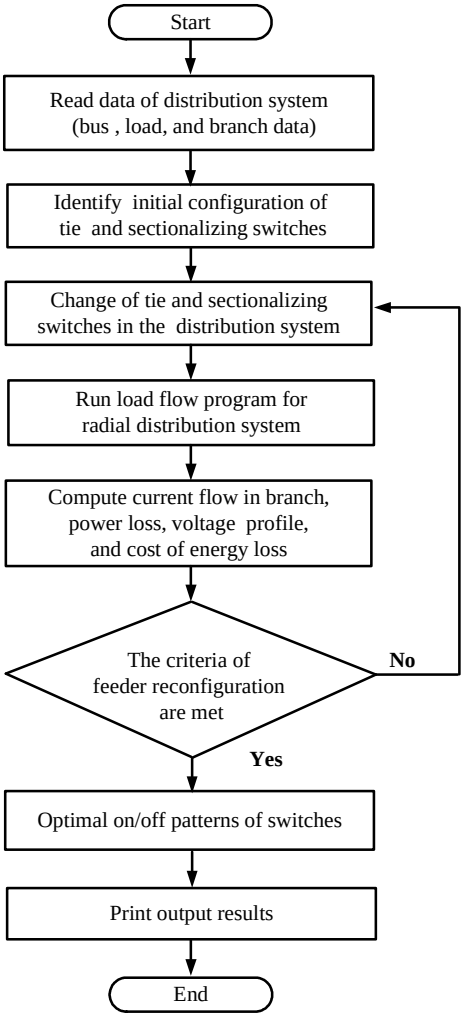

Fig.2. Flowchart of Feeder Reconfiguration.

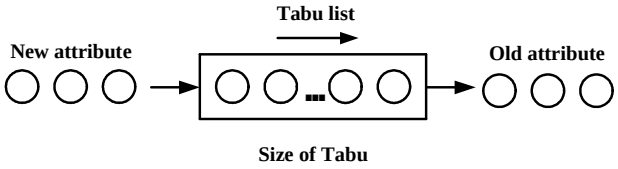

Fig.3. Mechanism of Tabu list.

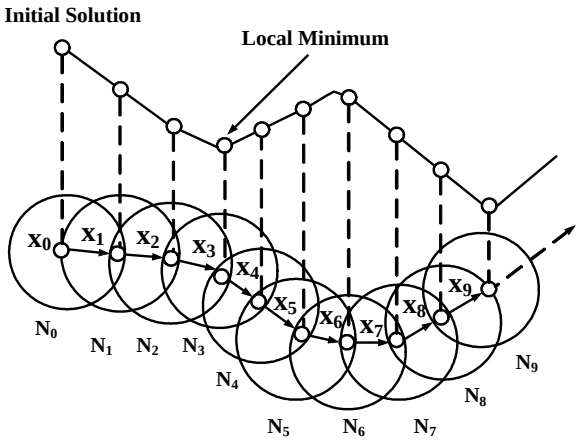

Fig.4. Search direction of Tabu Search.

5. SOLUTION ALGORITHM BY TABU SEARCH

The Tabu search algorithm is applied to solve the optimal or near optimal solution of the feeder configuration problem by taking the following steps:

Step 1: Read the bus, load and branch data of a distribution system including all the operational constraints.

Step 2: Randomly select a feasible solution from the search space: $S_0 \in \Omega$. The solution is represented by the switch number that should be opened during network reconfiguration.

Step 3: Set the size of a Tabu list, maximum iteration and iteration index $m = 1$.

Step 4: Let the initial solution obtained in step 2 be the current solution and the best solution: $S_{\text{best}} = S_0$, and $S_{\text{current}} = S_0$.

Step 5: Perform a power flow analysis to determine power loss, bus voltages, and branch currents.

Step 6: Calculate Z using (1) and check whether the current solution satisfies the constraints. A penalty factor is applied for constraint violation.

Step 7: Calculate the aspiration level of S_{best}: $f_{\text{best}} = f(S_{\text{best}})$. The aspiration level is the sum of Z and a penalty function

Step 8: Generate a set of solutions in the neighborhood of S_{current} by changing the switch numbers that should be opened. This set of solutions is designated as S_{neighbor}.

Step 9: Calculate the aspiration level for each member of S_{neighbor}, and choose the one that has the highest aspiration level, $S_{neighbor\_best}$.

Step 10: Check whether the attribute of the solution obtained in step 9 is in the Tabu list. If yes, go to step 11, or else $S_{current} = S_{neighbor\_best}$ and go to step 12.

Step 11: Accept $S_{neighbor\_best}$ if it has a better aspiration level than f_{best} and set $S_{current} = S_{neighbor\_best}$, or else select a next-best solution that is not in the Tabu list to become the current solution.

Step 12: Update the Tabu list and set $m = m + 1$.

Step 13: Repeat steps 8 to 12 until a specified maximum iteration has been reached.

Step 14: Report the optimal solution.

An application of the Tabu search algorithm is shown by a three-feeder distribution system in Figure 5 [8]. The system consists of 16 buses, 13 load points, 13 normally closed switches, and 3 normally open switches. The initial configuration states that switches located on branch No. 14, No. 15 and No. 16 are open. With this configuration, the initial power loss is 511.44 kW. Figure 6 shows moves from the current solution to two feasible solutions generated by the Tabu search: neighborhood solutions 1

and 2. The moves to solutions 1 and 2 give a power loss of 676.63 kW and 483.87 kW, respectively. The same process continues until 100 iterations. The optimal solution indicates that switch No. 16 remains open and the statuses of switches No. 7 and 8 are changed from 'closed' to 'open', giving a real power loss of 466.12 kW.

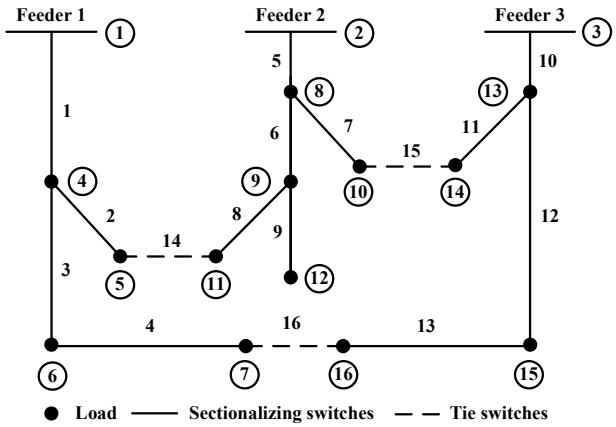

Fig.5. Single-line diagram of 16-bus distribution system.

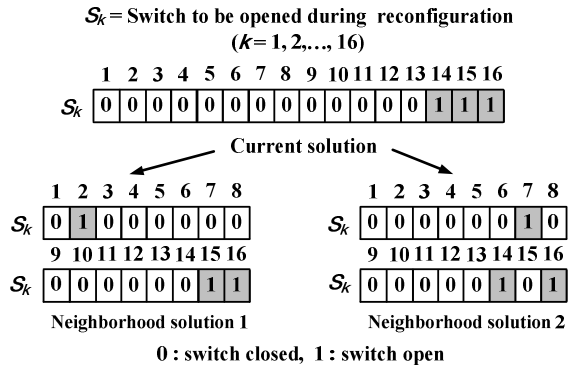

Fig.6. Neighborhood search for tie and sectionalizing Switches.

6. CASE STUDY

The test system for the case study is a 12.66 kV radial distribution system with 69 buses, 7 laterals and 5 tie-lines (looping branches), as shown in Figure 7. The current carrying capacity of branch No.1-9 is 400 A, No. 46-49 and No. 52-64 are 300 A and the other remaining branches including the tie lines are 200 A. Each branch in the system has a sectionalizing switch for reconfiguration purpose. The load data and branch data are provides in Table A1 and A2 [9]. The data associated with the loads in peak and off-peak periods are given in Table A3 [10]. Four cases are examined as follows:

Case 1: The system is without distributed generators and feeder reconfiguration

Case 2: The same as case 1 except that the feeders can be reconfigured by the available sectionalizing switches and the tie switches.

Case 3: The same as case 1 except that there are 4 small power producers who can provide only firm active power to the system by their DG units. The producers are located at buses 14, 35, 36, and 53 with capacities of 300, 200, 100, and 400 kW, respectively.

Case 4: The same as case 3 but with feeder reconfiguration.

The initial statuses of all the sectionalizing switches (switches No. 1-68) are closed while all the tie-switches (switch No. 69-73) open. The total loads for this test system are 3,801.89 kW and 2,694.10 kVAr. The feeder configuration algorithm, based on Tabu search as detailed in Section 5, is used to search the most appropriation topology of the system under a peak and off-peak load pattern. The minimum and maximum voltages are set at 0.95 and 1.05 p.u. The maximum iteration for the Tabu search algorithm is 100.

The test results for the four cases are summarized in Table 1. It is confirmed from case 3 that the distributed generators help reduce the system loss from 224.63 kW to 195.68 kW during the peak period and from 104.51 kW to 87.49 kW during the off-peak period, giving an annual saving of 478,406.50 Baht. However, if compared with Case 2, Case 3 sees a higher power loss. The minimum loss is seen in case 4, where there are changes in branch currents after the reconfiguration.

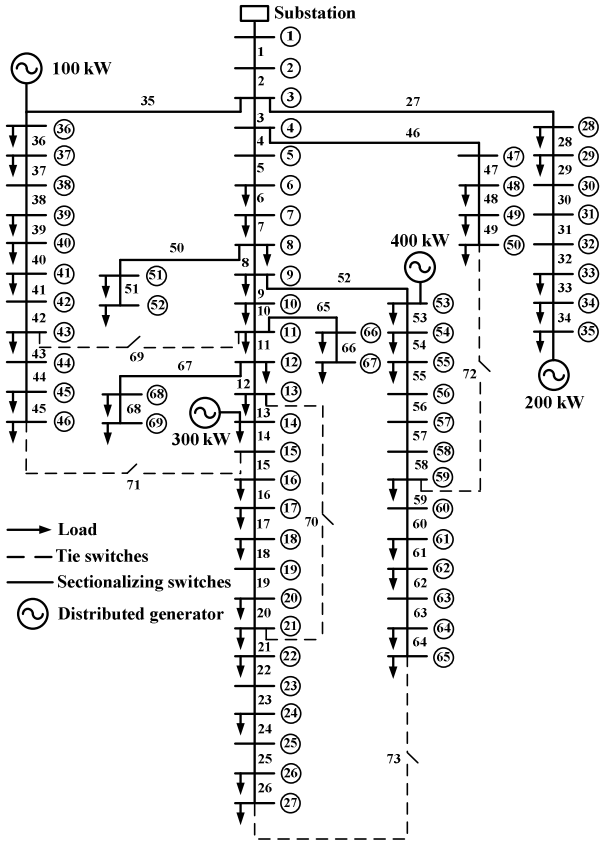

Fig.7. Single-line diagram of 69-bus distribution system.

Table 1. Results of Case Study

	Case 1	Case 2		Case 3	Case 4	
		TS	SA		TS	SA
Sectionalizing switches to be open	-	14, 56, 61	14, 57, 61	-	12, 52, 61	12, 18, 52, 61
Tie switches to be closed	-	71, 72, 73	71, 72, 73	-	71, 72, 73	70, 71, 72, 73
Power loss in peak period (kW)	224.63	98.56	99.58	195.68	82.58	82.92
Power loss in off-peak period (kW)	104.51	47.05	47.06	87.49	38.34	38.05
Total energy loss cost (Baht/year)	3,588,682.66	1,579,941.50	1,594,156.54	3,110,276.16	1,318,934.51	1,322,359.21

For example, the current flows in branch No. 3 to 11 are lower than those before reconfiguration. Because of the opening of switch No.12, these branches do not need to carry the currents to supply downstream load points at buses 13, 14, 16-18, 20-22, 24, and 25-26. However, the loads on these buses are not disconnected since tie-switch No.71 is closed so that the power is supplied through branch No.35-46 and 71, and therefore the current flows in these branches are increased.

In fact, feeder reconfiguration increases branch currents in some feeders while decreasing current flow in others but the latter effect outweighs the former. With this logical idea, feeder reconfiguration can, therefore, result in loss reduction. For this system, approximately 54-58% as much as loss reduction is achieved from the feeder reconfiguration for case 2 when compared with case 1 and for case 4 when compared with case 3. The solution convergence of this test system is shown in Figure 8, which reveals that the solution converges after iteration 51 for both peak and off-peak periods. The computation time for cases 2 and 4 is 924.61and 965.06 seconds.

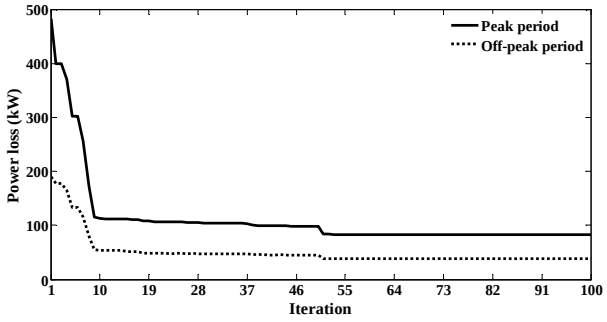

Fig.8. Convergence report of optimal solution.

The bus voltage profile for all the cases during peak period depicted in Figures 9 and 10 and off-peak period in Figures 11 and 12. It is observed that in cases 1 and 3, the voltages at buses 57-65 during peak period and at buses 61-65 in off-peak period are below 0.95 p.u. because a large load of 1,244 kW are drawn at bus 61. But for cases 2 and 4, all bus voltages satisfy the 0.95 p.u.-voltage constraint.

For the purpose of comparison, we have developed a simulated annealing (SA) algorithm applied to the feeder reconfiguration problem. The results from the two methods (i.e., Tabu search and simulated annealing) for case 2 and case 4 are provided in the Table 1. It can be observed that the power loss obtained from the two methods is comparable for on- and off-peak periods. However, the TS yields better savings in the energy loss cost mainly because the power loss in peak period, where the cost of energy is high, is lower. Note that for the TS in case 4, only 3 switching operations, instead of 4 as in the SA, are associated and is therefore preferred by the system operator.

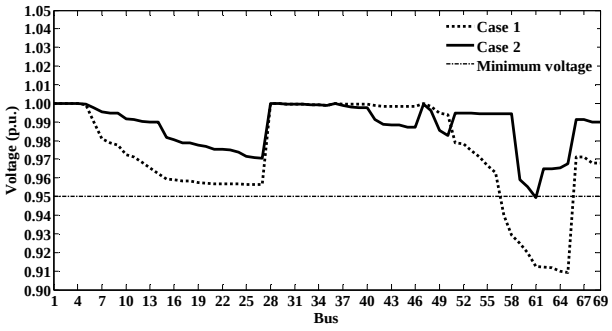

Fig.9. Bus voltage profile in peak period Case 1 and Case 2.

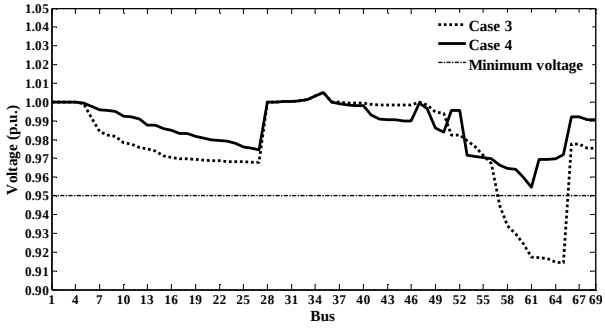

Fig.10. Bus voltage profile in peak period Case 3 and Case 4.

7. CONCLUSION

A Tabu search-based optimization technique has presented in this paper to find the most appropriate topology of the distribution system in the presence of distributed generators. The objective function of feeder reconfiguration is to minimize the total system loss. The objective function is subject to power flow equations, bus voltage limits, current transfer capability of feeders, radial configuration

format, and no load-point interruption. A 69-bus distribution system with four distributed generators is used to demonstrate the effectiveness of the proposed technique. Although the distributed generators contribute to loss reduction, some bus voltages violate the minimum voltage constraint. Such a problem can be remedied by feeder reconfiguration. Not only are these bus voltages improved above the limit, but also the system power loss can be further reduced. The decrease in loss produces significant savings on the annual energy loss cost, thus emphasizing the benefit of feeder reconfiguration.

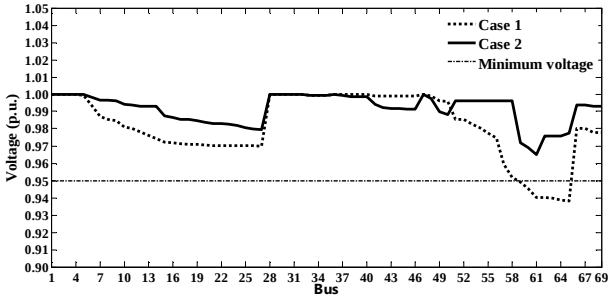

Fig.11. Bus voltage profile in off-peak period Case 1 and Case 2.

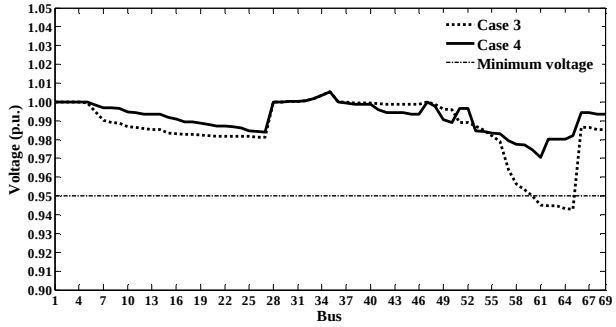

Fig.12. Bus voltage profile in off-peak period Case 3 and Case 4.

ACKNOWLEDGMENT

The first author would like to express his sincere thanks to the Rajamangala University of Technology Phra Nakhon (RMUTP), Thailand for financial support.

NOMENCLATURE

Z	total cost of energy loss
N_L	number of load levels
l	number of feeders
$I_{k,n}$	current flow in branch k at load level n
R_k	resistance of branch k
$P_{i,n}$	active power at bus i at load level n
N_B	number of buses
Y_{ij}	element (i, j) in bus admittance matrix
$V_{i,n}$	voltage of bus i at load level n
$V_{j,n}$	voltage of bus j at load level n
θ_{ij}	angle of Y_{ij}
$\delta_{i,n}$	voltage angle at bus i at load level n
$\delta_{j,n}$	voltage angle at bus j at load level n
$Q_{i,n}$	reactive power at bus i at load level n
$V^{\min}$	minimum voltage
$V^{\max}$	maximum voltage
$I_k^{\max}$	maximum current capability of branch k
S_0	initial solution
Ω	search space
S_{best}	best solution in search space
S_{current}	current solution in search space
f_{best}	objective function of S_{best}
S_{neighbor}	neighborhood solutions of S_{current}
$S_{neighbor\_best}$	best solution of S_{neighbor}

REFERENCES

[1] Yasin, Z. M., and Rahman, T. K. A. 2006. Service Restoration in Distribution Network with Distributed Generation. In *Proceeding of Research and Development, 4th Student Conference.* Shah Alam, Selangor, Malaysia, 27-28 June.

[2] Sivanagaraju, S., Srikanth, Y., and Jagadish Babu, E. 2006. An efficient genetic algorithm for loss minimum distribution system reconfiguration. *Electric Power Components and Systems*, 34: 249–258, 2006.

[3] Jenkins, N., et. al. 2000. *Embedded Generation*, London: The Institute of Electrical Engineer.

[4] Baran, M. E., and Wu, F. F. 1989. Network reconfiguration in distribution systems for loss reduction and load balancing. *IEEE Transactions on Power Delivery*, 4(2): 1401-1407.

[5] Dengiz, B., and Alabas, C. 2000. Simulation optimization using tabu search. In *Proceedings of Winter Simulation Conference.* Orlando, USA, 10-13 December.

[6] Glover, F. *Tabu search-part I*, ORSA J. Computing, vol.1, no.3, 1989.

[7] Hiroyuki, M., and Yoshihiro, O. 2000. Parallel tabu search for capacitor placement in radial distribution system. In *Proceedings of Power Engineering Society Winter Meeting*, January.

[8] Su, C. T., and Lee, C. S. 2003. Network reconfiguration of distribution systems using improved mixed-integer hybrid differential evolution. *IEEE Transactions Power Delivery*, 18(3): 1022-1027.

[9] Savier, J. S., and Das, D. 2007. Impact of network reconfiguration on loss allocation of radial distribution systems. *IEEE Transactions on Power Delivery*, 22(4): 2473-2480.

[10] The Provincial Electricity Authority (2008). Very Small Power Producer (VSPP) Rate [On line available]

from the Word Wide Web: http://www.pea.co.th/vspp/vspp.htm/.

APPENDIX

Table A1. Load Data of 69-bus Distribution System

Bus No.	P_L (kW)	Q_L (kVAr)	Bus No.	P_L (kW)	Q_L (kVAr)
6	2.60	2.20	37	26.00	18.55
7	40.40	30.00	39	24.00	17.00
8	75.00	54.00	40	24.00	17.00
9	30.00	22.00	41	1.20	1.00
10	28.00	19.00	43	6.00	4.30
11	145.00	104.00	45	39.22	26.30
12	145.00	104.00	46	39.22	26.30
13	8.00	5.00	48	79.00	56.40
14	8.00	5.50	49	384.70	274.50
16	45.50	30.00	50	384.70	274.50
17	60.00	35.00	51	40.50	28.30
18	60.00	35.00	52	3.60	2.70
20	1.00	0.60	53	4.35	3.50
21	114.00	81.00	54	26.40	19.00
22	5.00	3.50	55	24.00	17.20
24	28.00	20.00	59	100.00	72.00
26	14.00	10.00	61	1,244.00	888.00
27	14.00	10.00	62	32.00	23.00
28	26.00	18.60	64	227.00	162.00
29	26.00	18.60	65	59.00	42.00
33	14.00	10.00	66	18.00	13.00
34	19.50	14.00	67	18.00	13.00
35	6.00	4.00	68	28.00	20.00
36	26.00	18.55	69	28.00	20.00

Base 100 MVA, 12.66 kV

Table A2. Branch Data of 69-bus Distribution System

Branch Number	Sending end bus	Receiving end bus	R (Ω)	X (Ω)
1	1	2	0.0005	0.0012
2	2	3	0.0005	0.0012
3	3	4	0.0015	0.0036
4	4	5	0.0251	0.0294
5	5	6	0.3660	0.1864
6	6	7	0.3811	0.1941
7	7	8	0.0922	0.0470
8	8	9	0.0493	0.0251
9	9	10	0.8190	0.2707
10	10	11	0.1872	0.0619
11	11	12	0.7114	0.2351
12	12	13	1.0300	0.3400
13	13	14	1.0440	0.3450
14	14	15	1.0580	0.3496
15	15	16	0.1966	0.0650
16	16	17	0.3744	0.1238
17	17	18	0.0047	0.0016
18	18	19	0.3276	0.1083
19	19	20	0.2106	0.0690
20	20	21	0.3416	0.1129
21	21	22	0.0140	0.0046

Table A2. (Continued)

Branch Number	Sending end bus	Receiving end bus	R (Ω)	X (Ω)
22	22	23	0.1591	0.0526
23	23	24	0.3463	0.1145
24	24	25	0.7488	0.2475
25	25	26	0.3089	0.1021
26	26	27	0.1732	0.0572
27	3	28	0.0044	0.0108
28	28	29	0.0640	0.1565
29	29	30	0.3978	0.1315
30	30	31	0.0702	0.0232
31	31	32	0.3510	0.1160
32	32	33	0.8390	0.2816
33	33	34	1.7080	0.5646
34	34	35	1.4740	0.4873
35	3	36	0.0044	0.0108
36	36	37	0.0640	0.1565
37	37	38	0.1053	0.1230
38	38	39	0.0304	0.0355
39	39	40	0.0018	0.0021
40	40	41	0.7283	0.8509
41	41	42	0.3100	0.3623
42	42	43	0.0410	0.0478
43	43	44	0.0092	0.0116
44	44	45	0.1089	0.1373
45	45	46	0.0009	0.0012
46	4	47	0.0034	0.0084
47	47	48	0.0851	0.2083
48	48	49	0.2898	0.7091
49	49	50	0.0822	0.2011
50	8	51	0.0928	0.0473
51	51	52	0.3319	0.1114
52	9	53	0.1740	0.0886
53	53	54	0.2030	0.1034
54	54	55	0.2842	0.1447
55	55	56	0.2813	0.1433
56	56	57	1.5900	0.5337
57	57	58	0.7837	0.2630
58	58	59	0.3042	0.1006
59	59	60	0.3861	0.1172
60	60	61	0.5075	0.2585
61	61	62	0.0974	0.0496
62	62	63	0.1450	0.0738
63	63	64	0.7105	0.3619
64	64	65	1.0410	0.5302
65	11	66	0.2012	0.0611
66	66	67	0.0047	0.0014
67	12	68	0.7394	0.2444
68	68	69	0.0047	0.0016
Tie line				
69	11	43	0.5000	0.5000
70	13	21	0.5000	0.5000
71	15	46	1.0000	0.5000
72	50	59	2.0000	1.0000
73	27	65	1.0000	0.5000

Table A3. Load Levels and Cost Data

Load level	Load (p.u.)	Duration (hr)	Cost of energy (Baht/kW)
Off-peak	0.7	4, 015	1.1154
Peak	1.0	4, 745	2.9278

Multi-objective Optimal Placement of Distributed Generation Using Bee Colony Optimization

S. Anantasate, C. Chokpanyasuwan, W. Pattaraprakorn, and P. Bhasaputra

Abstract*— *In this paper, the proposed bee colony optimization (BCO) is used to determine optimal placement and number of the distributed generation (DG) to simultaneously minimize the real power loss and violation function of contingency analysis subject to power balance constrains, and power generation limits. The simulation results on the IEEE 30 bus system show that BCO can obtain the optimal solution with less computing time than simulated annealing (SA), genetic algorithm (GA) and tabu search algorithm (TSA). The average computing time of BCO is 82.62%, 74.40% and 83.83% less than GA, SA and TSA, respectively.

***Keywords*— Distributed Generation, Multi-objective Optimal Placement, Bee Colony Optimization.**

1. INTRODUCTION

Electric power grids have brought substantial benefits to the Southeast Asia Region as well as Greater Mekong Subregion (GMS) and hold the potential to provide further benefits if strengthened and extended. The benefits include more reliable power supply, lower electricity costs to consumers, and reduced environmental impacts. Power grid enhancements can make electric supply more reliable by improving the ability of economies to cope with the outage of specific generating units or types of generating units, as well as by limiting the scope of power outages. Enhanced power grids can lower electricity costs by reducing needs for electric generating capacity and allowing cheaper fuel to be substituted for more expensive fuel. Grids lower needs for generating capacity by allowing peak demand in one area to be served in part by spare capacity in a neighbouring area where demand is not at its peak. Grids lower fuel costs by allowing generation from nuclear, hydro and coal-fired power plants to displace generation from gas-fired plants.

A plan for power grid interconnections in Southeast Asia has been elaborated under the auspices of the Association of South East Asian Nations (ASEAN). The plan initially included fourteen cross-border projects, supported by national power utilities. These are shown as 14 projects in the Figure 1 below. The power grid master plan is extremely ambitious relative to transmission capacity in place, even though several elements of the plan build upon existing interconnections. The planned 700 MW link between Singapore and Peninsular Malaysia, to be completed by 2010, will add to an existing 500 MW link. The planned interconnections between Thailand and Laos, to add 2,015 MW of transmission capacity in 2008 and another 1,578 MW in 2010, will build upon earlier links of 75 MW in 1972, 45 MW and 214 MW in 1998 and 126 MW in 1999 [1].

Particular support has been evident for components of the ASEAN Power Grid to be located in the Greater Mekong Subregion that includes Cambodia, Laos, Myanmar, Thailand and Vietnam as well as Yunnan Province in southern China. A Greater Mekong Subregion transmission study was performed by the Mekong River Commission in 1996. Finally, an Inter-Governmental Agreement (IGA) on Regional Power Trade in the Greater Mekong Subregion was signed by ministers of the subregion's six economies in November 2002. The IGA set up a Regional Power Trade Coordination Committee to establish rules governing regional power trade. It is anticipated that power trade pursuant to the agreement will allow members to coordinate and cooperate in the planning and operation of their systems to minimize costs while maintaining satisfactory reliability; fully recover their costs and share equitably in the resulting benefits; and promote reliable and economical electric service to the customers of each country.

Conversely, a few proposed new power links in the Greater Mekong Subregion, see Figure 2, go beyond what as been proposed in the broader ASEAN context. The 500 kV lines in northeastern Thailand would be reinforced by 2015 to accommodate greater power flows southward. A 230 kV line would be built by 2019 from Lower Sre Pok to Sambor and Phnom Penh in Cambodia, as well as from Sambor to Tan Dinh in Vietnam. A 500 kV HVDC transmission line would link the Jinghong and Nuozhadu hydro projects in the Yunnan province of China to Thailand by 2013, while a 230 kV line would link the Malutang hydro plant in Yunnan with Vietnam by 2019 [2].

In this paper, integrated electricity system planning is reviewed in section 2. The metaheuristic optimization methods are reviewed in section 3. Section 4 shows the problem formulation of minimizing the real power loss along with violation of system contingency. The solution algorithm based on the BCO approach is shown in section 5. In section 6, simulation result showing multi-

S. Anantasate (corresponding author), C. Chokpanyasuwan, and P. Bhasaputra are with the Electrical Engineering Department (EED), Thammasat University (TU), Klong Luang, Pathumthani 12121, Thailand. E-mail: sumetha@pttep.com; asia_design2005@yahoo.com and bporr@engr.tu.ac.th.

W. Pattaraprakorn is with Chemical Engineering Department, TU, Thailand. E-mail: pworarat@engr.tu.ac.th.

objective optimal placement of DG is demonstrated. The validity of the solution algorithm is verified by comparing the searching results with those by the BCO. Lastly, conclusion is given in section 7.

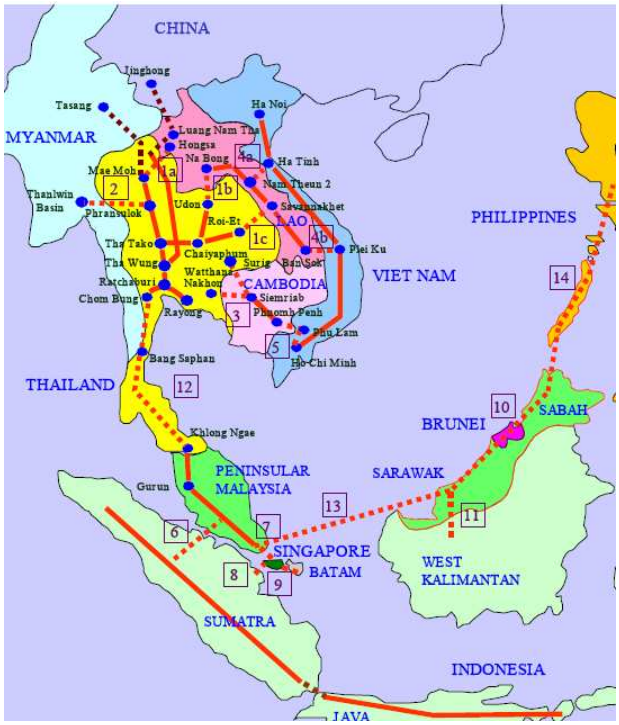

Source: ASEAN Centre for Energy. Key: Existing lines solid, proposed lines dashed.

Fig. 1. Southeast Asian Power Grid Endorsed by ASEAN Leaders.

2. INTEGRATED ELECTRICITY SYSTEM PLANNING

International power grid interconnections provide links between the electricity transmission systems of two or more adjoining countries and thus allow those countries to share power generation resources. As different countries are differently endowed with natural resources, energy trade among countries for centuries has helped to reduce energy prices and increase energy supply in importing countries, while providing a means of income for exporting countries.

International grid interconnections can be as modest as the one-way transfer of a small amount of electricity from one country to another, or as ambitious as the full integration of the power systems and markets of all of the countries in a region. Whatever the scale, international power grid interconnections can help to contribute toward the process of sustainable development. Grid interconnections can help to increase the supply and/or reliability of electricity [3].

The need to embed the consideration of power interconnection and generation projects into the broader consideration of electricity system planning, and even overall energy sector planning but deserves special additional mention. All costs and benefits of a long-term project like the power interconnection and generation must be measured relative to other means of providing the same energy services. As technology progresses, the number of other means of providing those energy services is growing rapidly, including not only construction of new large power plants, but also on-site renewable or fossil-fueled distributed generation for businesses and homes, energy efficiency improvements, fuel switching, and even alternative social organizations.

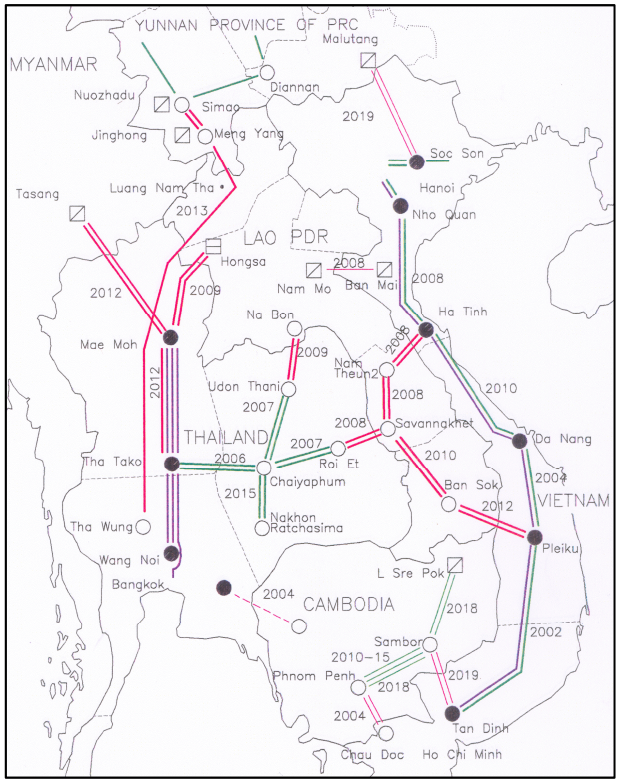

Source: Doorman et al. Note: Existing substations are shown as filled circles, planned substations as empty circles. Hydro plants are shown as squares with a diagonal slash, fossil-fuelled plants as squares with a horizontal slash.

Fig. 2. Extended Power Cooperation Scenario for Greater Mekong Subregion.

Distributed generation (DG) is a small generator spotted throughout a power system network, providing the electricity locally to load customers. DG is an alternative for industrial and commercial customers. DG makes use of the latest modern technology which is efficient, reliable, and simple enough so that it can compete with traditional large generators in some areas. Placement of DG is an interesting research area due to economical reason. Appropriate size and optimal location are the keys to achieve it.

Recently, the need for more flexible electric systems, changing in the regulatory and economic scenarios is providing impetus to the development of DG. Various kinds of DG are becoming available and it is expected that will grow in future years [4-7].

The local DG has some merits from the viewpoint of location limitations as well as transient and voltage stability in power system. The exact solution of the DG allocation can be obtained by a complete enumeration of all feasible combinations of placement and capacity rating of DG, which could be very large number and

various sizes, while the load flow is run for each feasible combination to evaluate the quality of solution. However, the high dimension of the feasible solution is the real difficulty in solving the problem. This paper presents methodology for optimal placement and number of DG in distribution systems by solving an optimization problem of system contingencies and real power loss.

3. REVIEW METAHEURISTIC OPTIMIZATION METHODS

Recently, the metaheuristic optimization methods are being successfully applied to combinatorial optimization problems in power systems. Methods and procedures of the DG placement are varied according to objective and the problem solution viewpoints. In [8], a GA based DG allocation method is presented where the power losses in an existing network is minimized. In [9], Rau and Wan employ gradient and second order methods to determine the optimal DG location for the minimization loss, line loading and reactive power requirement in the network. Kim et al in [10] suggest a combination of fuzzy non-linear goal programming and genetic algorithm techniques to locate DG and minimize overall power losses. In [11], Nara et al apply tabu search method to the same problem. Griffin et al in [12] demonstrate an iterative method that provides an approximation for the optimal placement of DG for loss minimization. In [13], Kim et al apply Hereford ranch algorithm to optimal placement of fixed capacity DG in order to minimize the losses of network. Celli et al in [14] propose a multi-objective formulation for the sizing and sitting of DG units into distribution feeders for simultaneous minimization of cost of network upgrading, losses, energy not supplied and customer energy. Willis in [15] offers a "2/3 rule" to place DG on a radial feeder with uniformly distributed load, where it is suggested to install DG of approximately 2/3 capacity of the incoming generation at approximately 2/3 of the length of line. El-Khattam et al in [16] use a heuristic approach to determine the optimal DG size and location in distribution feeders from an investment point of view. Wang and Nehrir in [17] present analytical approaches for determining optimal location of DG units with unity power factor in power system to minimize the power losses. In [18], Harrison and Wallace employ an optimal power flow technique to maximize DG capacity with respect to voltage and thermal constraints. Popovic et al in [19] use a sensitivity analysis to maximize DG capacity in the network without violation of security constraints. Keane and O'Malley in [20] present a method based on linear programming to determine the optimal allocation of DG with respect to technical constraints. In [21] Carpenellis et al propose a methodology based on multi-objective programming and decision theory which to find the best development plan for the system by using the DG as a development option. In [22], Borges and Falcao propose a methodology for optimal DG allocation and sizing in order to minimize the network losses and to guaranteeing acceptable reliability level and voltage profile.

In the literatures, several optimization techniques have been applied to DG placement, such as genetic algorithm (GA) [8], [10], [14], [21], [22], [27], tabu search algorithm (TSA) [11], [24-26], simulated annealing (SA) [28], heuristic algorithms [12], [16] and analytical based methods [9], [15], [17]. This paper presents a model to determine optimal location of DG in a distribution system in order to minimize the electrical losses and violation of system contingency, i.e. line overload and bus overvoltage, which they is solved using bee colony optimization (BCO) [23], [29-30] as the optimization tool by comparing with GA, SA and TSA. In this algorithm, DG is considered as constant power sources. The methods proposed are applied to the IEEE 30-bus test system to demonstrate their effectiveness.

4. PROBLEM FORMULATION

The problems of the system in the future are shortage of reactive power support, undervoltage at various buses, increased system losses and the tendency of voltage collapse initiation. Addition of proper DG in the system can overcome these problems. The contingency is analyzed to assess the ability of the network to provide electric power of sufficient quality to connected customers. DG optimization to alleviate the problem of the system is determined.

The main objective here is to minimize the real power loss along with violation of system contingency while subjected to power balance constraints and power generation limit. This is a case of nonlinear combinatorial problem with multiple objectives. This multi-objective optimization problem is converted to a single objective problem with the help of suitable weights, and the mathematical formulation of the problem is expressed as equation (1).

$$\text{Minimize } \omega_1 P_L(S) + \omega_2 Vf_{contin}(S) \tag{1}$$

subject to:

$$P_i = |V_i| \sum_{j=1}^{N} |Y_{ij}||V_j| \cos(\theta_i - \theta_j - \delta_{ij}) \tag{2}$$

$$Q_i = |V_i| \sum_{j=1}^{N} |Y_{ij}||V_j| \sin(\theta_i - \theta_j - \delta_{ij}) \tag{3}$$

$$P_{Gi,\min} \le P_{Gi} \le P_{Gi,\max}, \forall_i \in NG \tag{4}$$

$$Q_{Gi,\min} \le Q_{Gi} \le Q_{Gi,\max}, \forall_i \in NG \tag{5}$$

where

$$Vf_{contin}(S) = Vvf_{contin}(S) + Olf_{contin}(S) \tag{6}$$

Weights considered in Equation (1) reflect the relative priority of each term present in the objective function. In the present work, the weight is used to convert multi-objective optimization problem to a single objective problem. Since the main objective is to achieve a small quantity of power loss and violation of system contingency (voltage violation and line overloading), penalty is imposed to the both terms. Varying these weights can lead to alternative solutions. The

experimental results of the optimal values of weight for the IEEE 30 bus system are shown in section 6.

5. BEE COLONY OPTIMIZATION

A great number of traditional engineering models and algorithms used to solve complex problems are based on control and centralization. Various natural mechanisms (social insect colonies) show that very simple individual organisms can create systems able to perform highly complex tasks by dynamically interacting with each other. Bee swarm behavior in nature is, first and foremost, characterized by autonomy and distributed functioning and self-organizing [23]. In the last couple of years, the researchers started studying the behavior of social insects in an attempt to use the swarm intelligence concept in order to develop various artificial systems.

Bee in the Nature

Self-organization of bees is based on a few relatively simple rules of individual insect's behavior. In spite of the existence of a large number of different social insect species, and variation in their behavioral patterns, it is possible to describe individual insects' as capable of performing a variety of complex tasks [31]. The best example is the collection and processing of nectar, the practice of which is highly organized. Each bee decides to reach the nectar source by following a nestmate who has already discovered a patch of flowers. Each hive has a so-called dance floor area in which the bees that have discovered nectar sources dance, in that way trying to convince their nestmates to follow them. If a bee decides to leave the hive to get nectar, she follows one of the bee dancers to one of the nectar areas. Upon arrival, the foraging bee takes a load of nectar and returns to the hive relinquishing the nectar to a food storer bee. After she relinquishes the food, the bee can (a) abandon the food source and become again uncommitted follower, (b) continue to forage at the food source without recruiting the nestmates, or (c) dance and thus recruit the nestmates before the return to the food source. The bee opts for one of the above alternatives with a certain probability. Within the dance area, the bee dancers "advertise" different food areas. The mechanisms by which the bee decides to follow a specific dancer are not well understood, but it is considered that "the recruitment among bees is always a function of the quality of the food source" [31]. It is also noted that not all bees start foraging simultaneously. The experiments confirmed, "new bees begin foraging at a rate proportional to the difference between the eventual total and the number presently foraging".

The basic principles of collective bee intelligence in solving combinatorial optimization problems were for a first time used in [29] and [30]. The authors introduced the Bee System and tested it in the case of Traveling Salesman Problem. The Bee Colony Optimization Meta-heuristic that has been proposed in this paper represents further implementing it to solve combinatorial optimization problems of optimal placement of distributed generation.

Bee Colony Optimization Meta-heuristic

The BCO is a relatively new member of swarm intelligence. Within the BCO, agents called - artificial bees collaborate in order to solve difficult combinatorial optimization problem. All artificial bees are located in the hive at the beginning of the search process. During the search process, artificial bees communicate directly. Each artificial bee makes a series of local moves, and in this way incrementally constructs the solution of the problem. Bees are adding components to the current partial solution until they create one or more feasible solutions. The search process is composed of iterations.

The first iteration is finished when bees create for the first time one or more feasible solutions. The best discovered solution during the first iteration is saved, and then the second iteration begins. Within the second iteration, bees again incrementally construct solutions of the problem, etc. There are one or more partial solutions at the end of each iteration. The analyst-decision maker prescribes the total number of iterations.

When flying through the space our artificial bees perform forward pass or backward pass. During forward pass, bees create various partial solutions. It is executed via a combination of individual exploration and collective experience from the past. After that, backward pass is performed of returning to the hive. In the hive, all bees participate in a decision-making process. Every bee can obtain the information about solutions' quality generated by all other bees. In this way, bees exchange information about quality of the partial solutions created. Bees compare all generated partial solutions. Based on the quality of the partial solutions generated, every bee decides whether to abandon the created partial solution and become again uncommitted follower, continue to expand the same partial solution without recruiting the nestmates, or dance and thus recruit the nestmates before returning to the created partial solution. Depending on the quality of the partial solutions generated, every bee possesses certain level of loyalty to the path leading to the previously discovered partial solutions. During the second forward pass, bees expand previously created partial solutions, and after that perform again the backward pass and return to the hive. In the hive bees again participate in a decision-making process, perform third forward pass, etc. The iteration ends when one or more feasible solutions are created.

The advantage of BCO in solving optimization problems is that bee colony is as dynamical system gathering information from an environment and adjusting its behavior in accordance to it. They established a robotic idea on the foraging behavior of bees. Usually, all these robots are physically and functionally identical, so that any robot can be randomly replaced by the others. The swarm possesses a significant tolerance; the failure in a single agent does not stop the performance of the whole system. They also developed a minimal model of forage selection that leads to the emergence of collective intelligence which consists of three essential components: food sources, employed foragers and unemployed foragers. The model defines two leading modes of the behavior: recruitment to a

nectar source and abandonment of a source.

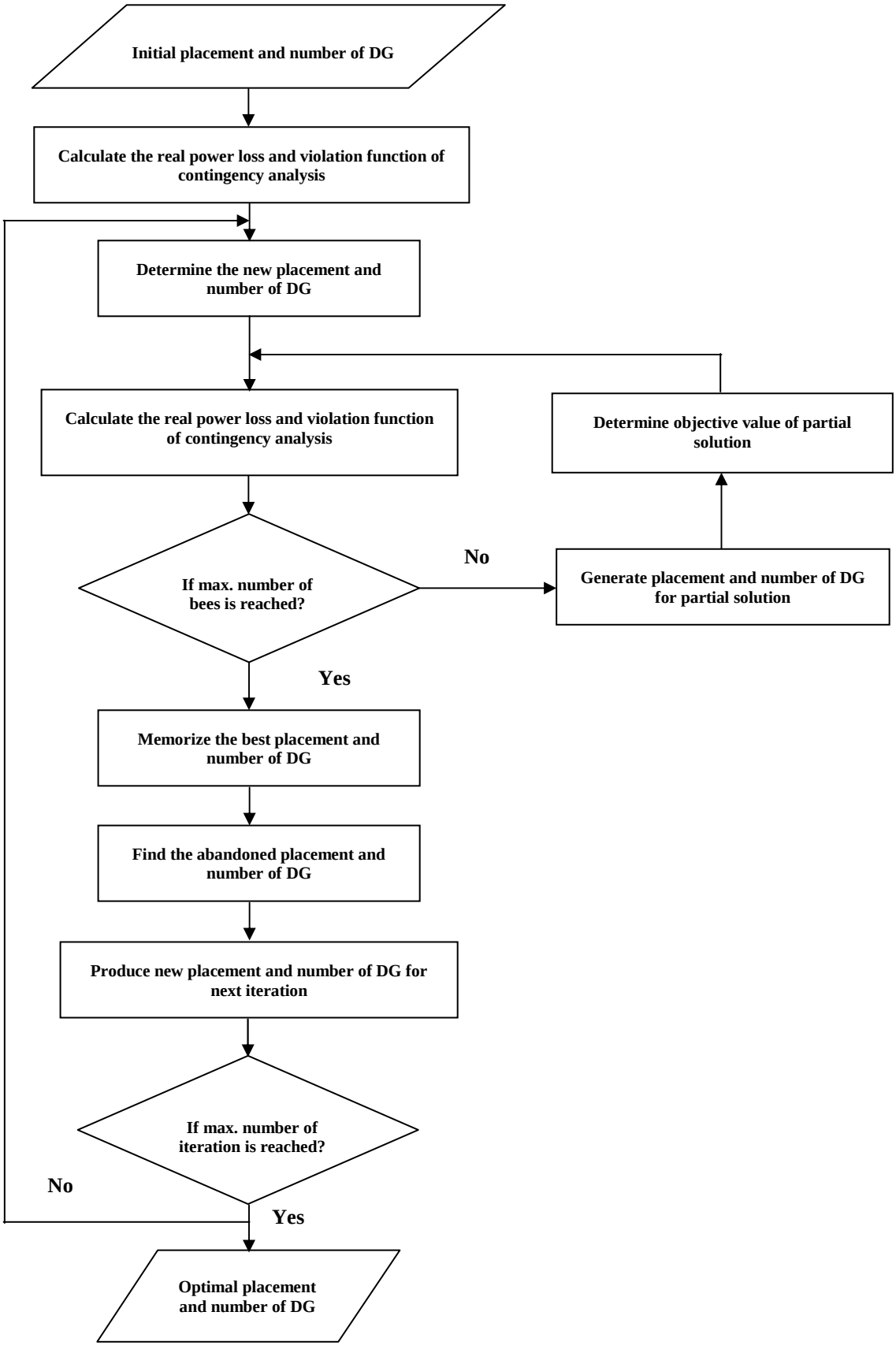

Fig. 3. Flow chart of the BCO algorithm.

Comparison with the other algorithms such as GA and SA suggests that BCO works more efficiently due to the parallelism of the multiple independent bees. For TSA, BCO algorithms work more efficiently due to TSA records the closest results to the best known solutions and have the most number of best solutions. Further, it also manages to achieve best results in the shortest execution time. These spectacular results are attributed to the efficient critical block neighborhoods. Moreover, a tabu list that keeps track of the most recent tabu moves prevents the search algorithm to be locked in local minimums.

Algorithm

Like Dynamic Programming, the BCO also solves combinatorial optimization problems in stages. Each of the defined stages involves one optimizing variable. The flowchart of the artificial BCO algorithm is given in Figure 3.

6. SIMULATION RESULTS

The test system is the 30-bus system, which has total load 232.3 MW and 77.3 MVar. The total active power loss and reactive power loss without DG is 4.77 MW and 0.60 MVar, respectively. The maximum number of DG is 2.

The parameters of BCO are set as follow; number of bees = 20, maximum of iteration = 50, number of partial solution = 5, and maximum generation (run) = 1000.

The simulation results on the IEEE 30-bus system show that BCO can obtain the optimal solution with the least computing time comparing with GA, SA and TS. The average computing time of BCO is 82.62%, 74.40% and 83.83% less than GA, SA and TS respectively. Table 1 compares the results of BCO and other heuristic methods.

Table 1. Comparison results of BCO with other heuristic search methods based on 1,000

Heuristic Approaches	Average Total CPU Time (sec)
GA	7.0293
SA	4.7729
TSA	7.5553
BCO	1.2219

ω_1 and ω_2 as well as normalization of $P_L(S)$ and $Vf_{contin}(S)$ to the same based for calculation of multi-objective optimization has been concluded and presented in Table 2. The results show that the optimal value of ω_1 and ω_2 for the IEEE 30 bus system is 0.3 and 0.7, respectively.

The results of each single objective optimal placement of minimizing system loss and violation function of contingency analysis are summarized in Table 3 and 4, respectively. When single objective of minimizing system loss is considered, the optimal placement of DG is of bus 19 and 20, which the system loss is reduced 27% comparing with system without DG. Meanwhile, when considering single objective of minimizing violation function of contingency analysis, the optimal placement of DG is of bus 19 & 21, which violation function of contingency analysis is reduced 43.75% comparing with system without DG.

Table 2. Weight factor and normalization for finding multi-objective optimization

ω_1	ω_2	min Loss	min Cont.	P_L (S)	Vf_{contin} (S)	Opt. Eq.(1)	Bus
0.3	0.7	3.74	4.14	0.78	0.56	0.63	19,21
0.4	0.6	3.74	4.14	0.78	0.56	0.65	19,21
0.5	0.5	3.74	4.14	0.78	0.56	0.67	19,21
0.6	0.4	3.48	4.68	0.73	0.64	0.69	19,20
0.7	0.3	3.48	4.68	0.73	0.64	0.70	19,20

The effect of location and number of DG to each single objective optimal placement of minimizing real power loss and violation function of contingency analysis are presented in Figure 4 and 5, respectively.

Table 3. The simulation results of the single objective optimal placement of minimizing real power loss

System with 2 DG	Min. Power Loss		Max. Power Loss	
DG Size (MW)	Loss (MW)	DG Location (Bus)	Loss (MW)	DG Location (Bus)
2 x 10	3.48	19 & 20	4.81	2 & 27
Comparing with system without DG (4.77 MW)	System loss reduced 27%		System loss increased 1.26%	

Table 4. The simulation results of the single objective optimal placement of minimizing violation function of contingency analysis

System with 2 DG	Min. Contingency		Max. Contingency	
DG Size (MW)	System Cont. (p.u.)	DG Location (Bus)	System Cont. (pu)	DG Location (Bus)
2 x 10	4.14	19 & 21	8.16	23 & 27
Comparing with system without DG (7.36 MW)	System contingency reduced 43.75%		System contingency increased 10.87%	

In Table 5, the optimal placement of DG to achieve multi-objective of minimizing real power loss together with violation function of contingency analysis is of Bus 19 and 21, which it can significantly reduce the system loss from 4.77 MW to 3.74 MW or 22% reduction, while violation function of contingency analysis can be reduced from 7.36 p.u. to 4.14 p.u. or 43% reduction, when comparing to the system without DG. The effect of DG allocation to the multi-objectives optimal placement is demonstrated in Figure 6.

Table 5. The simulation results of the multi-objective optimal placement of DG

Number of DG **DG Size (MW)**	2 DG 2 x 10
1. Without DG in the system: - System loss (MW) - System contingency (p.u.)	 4.77 7.36
2. With DG in the system: - Optimal placement (Bus No.) - System loss (MW) - System contingency (p.u.)	 19 & 21 3.74 4.14

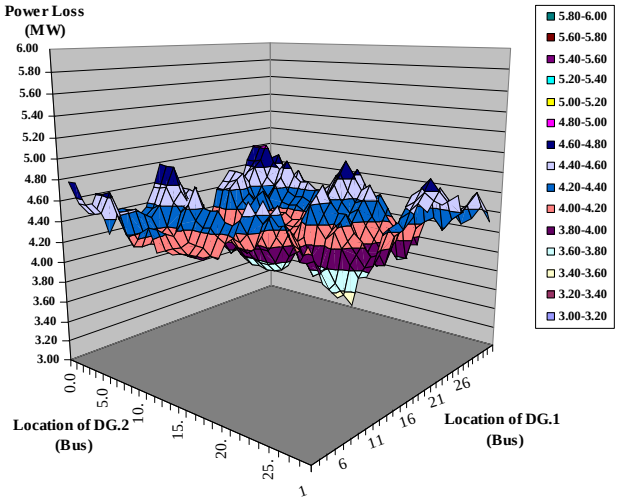

Fig. 4. Effect of allocation of DG to the single objective optimal placement of minimizing real power loss.

7. CONCLUSION

In this paper, the efficiency and success of BCO approach implemented to determine the multi-objective optimal placement of DG to simultaneously minimize the real power loss and violation function of contingency analysis has been demonstrated. The effectiveness of the BCO to solve the DG allocation problem has been illustrated through the IEEE 30-bus system, which it is executed with the BCO comparing to other heuristic search methods of GA, SA and TSA. Comparison with the other algorithms such as GA suggests that BCO algorithms work more efficiently due to the parallelism of the multi-bees. The result proves that the BCO is the best against GA, SA and TSA in terms of computing time and number of iteration, which average computing time of BCO is 82.62%, 74.40% and 83.83% less than GA, SA and TSA, respectively.

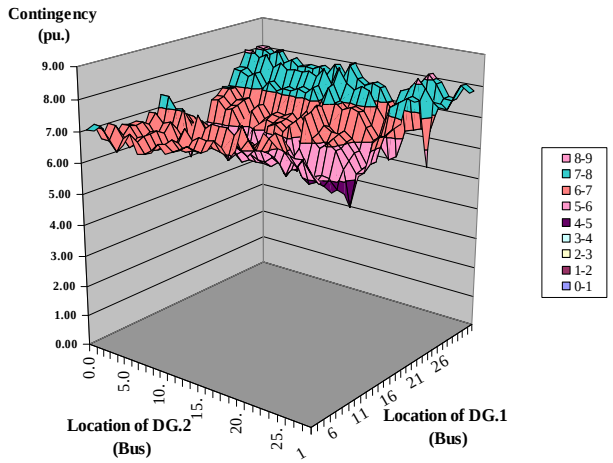

Fig. 5. Effect of allocation of DG to the single objective optimal placement of minimizing violation function of contingency analysis.

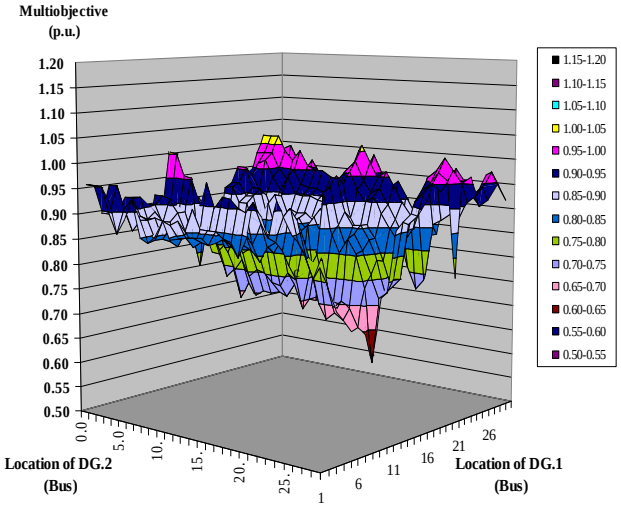

Fig. 6. Effect of allocation of DG to the multi-objective optimal placement.

NOMENCLATURE

P_i	active power at bus i,
Q_i	reactive power at bus i,
P_{Gi}	active power generation at generator number i,
Q_{Gi}	reactive power generation at generator number i,
$\|V_i\|$	voltage magnitude at bus i,
$\|V_j\|$	voltage magnitude at bus j,
$\|Y_{ij}\|$	magnitude of the the i-jth element of the bus admittance matrix,
δ_{ij}	angle of the i-jth element of the bus admittance matrix,
θ_i	phase angle of the voltage V_i,

θ_j phase angle of the voltage V_j,

NG set of generation bus indices,

N set of bus indices,

$P_L(S)$ real power loss of solution **S**,

S solution of number and location of the DG,

ω_1 weight factor of the real power loss,

ω_2 weight factor of the violation function of contingency analysis,

$Vf_{contin}(S)$ violation function of contingency analysis of solution **S**,

$Vvf_{contin}(S)$ voltage violation function of contingency analysis of solution **S**,

$Olf_{contin}(S)$ overloaded line function of contingency analysis of solution **S**.

REFERENCE

[1] Electric Power Grid Interconnections in the APEC Region. Presented by Asia Pacific Energy Research Centre, Institute of Energy Economics, Japan, 2004.

[2] Regional Cooperation Strategy on Interconnected Power Networks in Indochina. Presented by JBIC Institute, Japan Bank for International Cooperation, Japan, 2002.

[3] Multi-Dimensional Issues in International Electric Power Grid Interconnections. Presented by Department of Economic and Social Affairs, Devision for Sustainable Development, United Nations, New York, 2005.

[4] Impact of Increasing Contribution of Dispersed Generation on the Power System – Final Report. CIGRE WG 37-23, Sep 1998.

[5] Dispersed generation - Preliminary report. presented at the CIRED Conf., Nice, France, Jun 2-5, 1999.

[6] Barker, P. and Mello, R.W. 2000. Determining the impact of distributed generation on power systems. In *Proc. IEEE Power Eng.Soc.Summer Meeting*, vol. 3 Seattle, WA, 16-20 July, pp. 1645-1656.

[7] Willis, H.L. and Scott, W.G. 2000. *Distributed Power Generation*. New York, Marcel Dekker.

[8] Mardaneh, M. Gharehpetian, G.B. 2004. Sitting and Sizing of DG Units Using GA and OPF Based Technique. *IEEE Region 10 Int. Conference on Computers, Communications Control and Power Engineering*, *IEEE TENCON 2004*, Chiang Mai, Thailand.

[9] Rau, N.S. and Wan, Y.H. Nov. 1994. Optimum location of resources in distributed planning. *IEEE Transactions on Power Systems*, vol. 9, pp. 2014–2020.

[10] Kim, K.H. Lee, Y.J. Rhee, S.B. Lee, S.K., and You, S.K. 2002. Dispersed generator placement using fuzzy-GA in distribution systems. In *Proc. 2002 IEEE Power Engineering Society. Summer Meeting*, vol. 3, Chicago, IL, pp. 1148–1153.

[11] Nara, K. Hayashi, Y. Ikeda, K. and Ashizawa, T. 2001. Application of tabu search to optimal placement of distributed generators. *IEEE Power Engineering Society Winter Meeting*, pp. 918–923.

[12] Griffin, T. Tomsovic, K. Secrest, D. and Law, A. 2000. Placement of dispersed generation systems for reduced losses. In *Proc. 33rd Annu. Hawaii Int. Conf. Systems Sciences*, Maui, HI.

[13] Kim, J.O. Nam, S.W. Park, S.K. and Singh, C. Oct. 1998. Dispersed generation planning using improved Hereford ranch algorithm. *Electric Power System Research*, vol. 47, no. 1, pp. 47–55.

[14] Celli, G. Ghaiani, E. Mocci, S. and Pilo, F. May 2005. A multiobjective evolutionary algorithm for the sizing and sitting of distributed generation. *IEEE Transactions on Power Systems*, vol. 20, no. 2, pp. 750–757.

[15] Willis, H.L. July 2000. Analytical methods and rules of thumb for modeling DG distribution interaction. In *Proc. 2000 IEEE Power Engineering Society Summer Meeting*, vol. 3, Seattle, WA, pp. 1643–1644.

[16] El-Khattam,W. Bhattacharya, K. Hegazy, Y. and Salama, M.M.A. Aug. 2004. Optimal investment planning for distributed generation in a competitive electricity market. *IEEE Transactions on Power Systems*, vol. 19, no. 3, pp. 1674–1684.

[17] Wang, C. and Nehrir, M.H. Analytical approaches for optimal placement of distributed generation sources in power systems. *IEEE Transactions on Power Systems*, vol. 19, no. 4, pp. 2068–2076.

[18] Harrison, G. and Wallace, A. Jan. 2005. Optimal power flow evaluation of distribution network capacity for the connection of distributed generation. *Proc. Generation, Transmission and Distribution*, vol. 152, no. 1, pp. 115–122.

[19] Popovic, D.H. Greatbanks, J.A. Begovic, M. and Pregelj, A. June-July 2005. Placement of distributed generators and reclosers for distribution network security and reliability. *International Journal of Power and Energy Systems*, vol. 27, no. 5-6, pp. 398–408.

[20] Keane, A. and O'Malley, M. 2005. Optimal Allocation of Embedded Generation on Distribution Networks. *IEEE Transactions on Power Systems*, vol. 20, no. 3, pp. 1640–1646.

[21] Carpinelli, G. Celli, G. Mocci, S. Pilo, F. and Russo, A. 2005. Optimisation of embedded generation sizing and sitting by using a double trade-off method. *IEE Proceeding of Generation Transmission Distribution*, vol. 152, no. 4, pp. 503–513.

[22] Borges, C.L.T. and Falcao, D.M. July 2006. Optimal distributed generation allocation for reliability, losses, and voltage improvement. *International Journal of Power and Energy Systems*, vol. 28, no. 6, pp. 413–420.

[23] Nakrani, S. and Tovey, C. 2004. On honey bees and dynamic allocation in an internet server colony. *Adaptive Behavior*, 12(3-4): p.223-240.

[24] Glover, F. 1993. A user's guide to tabu search. *Annual Operational Research*, vol. 41, pp. 3-28.

[25] Glover, F. 1990. Artificial intelligence, heuristic frameworks and tabu search. *Management Decision Economic*, vol. 11, pp. 365-375.

[26] Nara, K. Hayashi, Y. Ikeda, K. and Ashizawa, T. 2001. Application of tabu search to optimal placement of distributed generators. *Power Engineering Society Winter Meeting*, IEEE vol. 2, pp.918-923.

[27] Marin, F.J. and Garcia-Lagos, F. 2003. Genetic algorithm for opimal placement of phasor measurement units in electrical networks. *IEEE Trans. Power Systems*, vol. 39, no. 19.

[28] Jovan, M. and Dragoslav, M. 2008. Optimal planning of radial distribution networks by simulated annealing technique. *IEEE Trans. Power Systems*, vol. 23, no.2.

[29] Lucic, P. and Teodorovic, D. 2001. Bee System: Modeling Combinatorial Optimization Transportation Engineering Problems by Swarm Intelligence. In preprints of the *TRISTAN IV Triennial Symposium on Transportation Analysis*, Sao Miguel, Azores Islands, Portugal , pp. 441-445.

[30] Lucic, P. and Teodorovic, D. 2003. Computing with Bees: Attacking Complex Transportation Engineering Problems. *International Journal on Artificial Intelligence Tools*, vol. 12, pp. 375-394.

[31] Camazine, S. Sneyd, J. 1991. A Model of Collective Nectar Source by Honey Bees: Self-organization Through Simple Rules. *Journal of Theoretical Biology*, vol.149, pp.547-571.

Control of Line Side Converter for Doubly Fed Induction Generator with Active Power Filter and Load Balancing

S. Wangsathitwong, S. Sirisumrannukul, S. Chatratana, and W. Deleroi

Abstract*— *A control system of line side converter for a doubly fed induction generator with active power filter and load balancing capability is presented. The control scheme is based on the model of the system on synchronously rotating reference frame (d-q axis). The d-q axis current components are used to control active power and reactive power, respectively. In this reference frame, the d-q current components of the nonlinear load are composed of dc and ac quantities. The dc component of d-axis current represents the fundamental of active current while ac components represents harmonic currents and unbalanced load currents. The q-axis current correspond to reactive power, harmonic currents and unbalanced load currents. The elimination of ac component of the d-axis current and q-axis current by appropriate compensation ensures that the converter is operating at unity power factor with active power filter function and load balancing capability. Simulation results of a line side converter with unbalanced nonlinear load confirm good performance of the proposed control method.

***Keywords*— Doubly fed induction generator, Line side converter, Active power filter, Load balancing.**

1. INTRODUCTION

Wind energy is one of the fastest growing renewable energy systems. Many large wind farms employ doubly fed induction generator (DFIG) with variable speed wind turbines [1]. More than 60% of the yearly installations of new wind farms employ DFIG. The main advantage of DFIG wind turbine system is cost-effective for an inverter because its rating is typically 25% of rating of total system and the operating speed range of the DFIG is ±33% around the synchronous speed. Approximately 2 to 3% efficiency improvement can be obtained due to the small size of power converters.

A typical configuration of a DFIG system with nonlinear load is shown in figure 1. The stator side of a DFIG is directly connected to the line while the rotor side is fed through two back-to-back power converters with dc link. In order to cover a wide speed range from subsynchronous to supersynchronous speeds, these power converters must be bi-directional power converters.

The dc link capacitor is capable of absorbing the instantaneous power difference between line side and machine side converter. Therefore, these two converters can be separately controlled. The configuration of a PWM voltage source line side converter is shown in figure 2. The function of the line side converter is to regulate the dc bus voltage at a reference value and to ensure that the converter operates at unity power factor. The control technique of the converter is based on the model of the system on the synchronously rotating reference frame (d-q axis) [2], [3]. Steady state balanced sinusoidal three phase voltages and currents, which are transformed onto the d-q axis, become dc values and can be easily controlled by PI controller. The active power and reactive power are decoupled from each other and the power flow between the line and the dc link can be independently controlled.

Today, the increasing use of power electronics equipment causes unbalanced non-sinusoidal currents in the ac supply system. These harmonic currents are the causes of various undesirable phenomena in the power quality such as losses, malfunction of sensitive devices, electromagnetic interference, faulty timing signals, increasing heat and shorten motor life. Normally, active power filters (APF) are used to compensate harmonic currents and reactive current component to improve the power quality. Furthermore, the APF can balance the load currents.

The control methods for rotor side converter of DFIG system with APF operation have been investigated [4] – [6]. The stator currents of the DFIG are controlled by rotor side converter to compensate the harmonic currents. These control schemes produce non-sinusoidal currents in the stator of the machine which can cause negative effect on the DFIG.

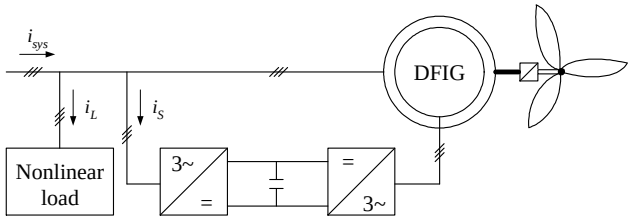

Fig.1. Schematic diagram of DFIG for wind turbine system with nonlinear load.

S. Wangsathitwong (corresponding author) and S. Sirisumrannukul are with King Mongkut's University of Technology North Bangkok (KMUTNB), Bangkok, Thailand. Phone: +66-2-9132500 ext.6304, Fax: +66-2-5874356. E-mail: ssww@kmutnb.ac.th and spss@kmutnb.ac.th.

S. Chatratana is with Technology Management Center, National Science and Technology Development Agency (NSTDA), 111 Thailand Science Park, Paholyothin Rd., Patumthani, Thailand. E-mail: somchaich@nstda.or.th.

W. Deleroi was with Delft University of Technology, Delft, Netherlands. E-mail: werner.deleroi@skynet.be.

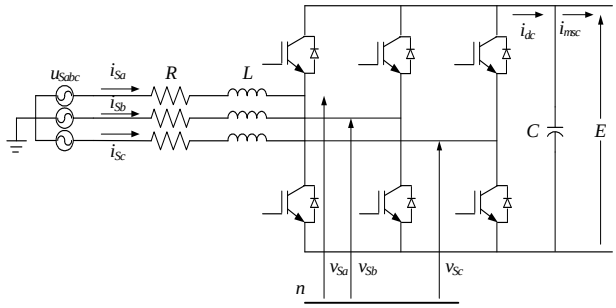

Fig.2. Equivalent circuit of the ac system with line side converter

The control scheme of the line side converter is more flexible. The function of line side converter can be enhanced to operate as a shunt APF to compensate harmonic currents. The line side converter with APF operation will then be capable of simultaneously compensating current harmonics, reactive power and unbalanced load current. The advantage of the proposed method is that the harmonic currents are directly compensated by the converter which would give faster response and better accuracy than the method of compensation through the rotor side converter.

There are several control methods of shunt APF for the application of line side converter with APF [7], [8]. For the synchronously rotating reference frame model, the compensated currents can be directly derived from the real load currents without the need of line voltage information. Furthermore, the reference current signals are not affected by unbalanced voltage or voltage distortion. These advantages increase the robustness of the system and simplify the design of controllers. The harmonic current and reactive power can be separately control by individual control loop [9].

This paper presents a control method of the line side converter for DFIG in conjunction with active power filter and load balancing. The rotor side converter of the DFIG is controlled in the same way as in normal operation while the line side converter is assigned to regulate dc link voltage, to compensate non-sinusoidal currents, to control reactive power and to balance three phase currents. With these functions, the load currents are measured and transformed on to the d-q axis of the synchronously rotating reference frame. The non-sinusoidal, reactive and unbalanced current components are extracted from the d-q components and used as references for currents compensation. Based on this scheme, the line side converter can compensate both the non-sinusoidal currents and unbalanced currents directly.
This paper is organized as follows: The mathematical model of line side voltage source converter and the proposed control method are investigated in Section 2, together with the block diagram of the control system. The simulation results to verify the control performances are shown in Section 3. The conclusion is given in Section 4.

2. MATHEMATICAL MODEL AND CONTROL METHOD

2.1 Nonlinear Model Analysis and Proposed Method

The line side converter is a three phase AC/DC converter which is connected to the three phase power supply on one side with a capacitor on the dc side. The voltage equations of the system are:

$$\begin{bmatrix} u_{Sa} \\ u_{Sb} \\ u_{Sc} \end{bmatrix} = R \begin{bmatrix} i_{Sa} \\ i_{Sb} \\ i_{Sc} \end{bmatrix} + L \frac{d}{dt} \begin{bmatrix} i_{Sa} \\ i_{Sb} \\ i_{Sc} \end{bmatrix} + \begin{bmatrix} v_{Sa} \\ v_{Sb} \\ v_{Sc} \end{bmatrix} \tag{1}$$

The power equation of dc link voltage can be written, as:

$$Ei_{msc} + EC\frac{dE}{dt} = Ei_{dc} = P_{dc} \tag{2}$$

Transforming (1) onto the synchronously rotating reference frame and align d-axis of reference frame with the complex vector of the phase voltage of the supply, results in:

$$u_{Sd} = Ri_{Sd} + L\frac{di_{Sd}}{dt} - \omega Li_{Sq} + v_{Sd} \tag{3}$$

$$u_{Sq} = 0 = Ri_{Sq} + L\frac{di_{Sq}}{dt} + \omega Li_{Sd} + v_{Sq} \tag{4}$$

The three phase instantaneous supply powers are,

$$\begin{aligned} s &= \frac{2}{3} u_{Sdq} i^{*}_{Sdq} \\ &= p + jq \end{aligned} \tag{5}$$

$$p = \frac{2}{3} u_{Sd} i_{Sd} \tag{6}$$

$$q = -\frac{2}{3} u_{Sd} i_{Sq} \tag{7}$$

If the power loss in the converter can be neglected, the instantaneous dc power in (2) and ac power in (6) are the same. Therefore, the dc bus voltage can be controlled via i_{Sd}. The i_{Sd} demand is derived from the dc bus voltage error through a standard PI controller, while i_{Sq}, demand determines the reactive power or power factor on the line side of the converter. The errors of both i_{Sd} and i_{Sq} act as inputs of PI controllers to generate the line side converter terminal voltage reference signal v_{Sd} and v_{Sq}.

For APF application, the nonlinear load currents are transformed onto the d-q axis frame. These two quantities are composed of the dc components and ripples or ac components as described in (8) and (9).

$$i_{Ld} = \bar{i}_{Ld} + \tilde{i}_{Ld} \tag{8}$$

$$i_{Lq} = \bar{i}_{Lq} + \tilde{i}_{Lq} \tag{9}$$

Based on (6) and (7), the dc component of (8) is related to the conventional fundamental active load current whereas the ac component is related to the harmonic currents and the negative sequence of the unbalanced load currents. The compensated d-axis current is calculated by extracting the ac component from the d-axis current. The q-axis load current in (9) represents reactive load current, harmonic current and unbalanced load. In order to avoid negative effects the q-axis load current should be zero. Therefore, the reference currents required by APF to compensate non-sinusoidal load currents, reactive power and unbalanced load current are

$$i_{Ld}^{*} = -\tilde{i}_{Ld} \tag{10}$$

$$i_{Lq}^{*} = -i_{Lq} \tag{11}$$

The compensated d-q axis currents, in (10) and (11), are fed and added to the conventional current controller of the line side converter. The block diagram of the proposed method is shown in figure. 3. The low pass filter is used to extract balanced active power load current, which is in the form of dc current, from d-axis current. Then the harmonic current and unbalanced load current can be determined by subtracting the dc current from the d-axis current.

2.2 Design of Control Loop

The design of both the current loop and dc voltage loop controller can be carried out according to the pole placement method [10]. The process transfer function can be described as the first order model.

$$G_p(s) = \frac{K_p}{1+sT}$$

The transfer function of PI controller is

$$G_c(s) = K\left(1+\frac{1}{sT_i}\right)$$

With simplified block diagram of control in figure 4, the closed loop characteristic equation becomes

$$s^2 + s\frac{1+K_pK}{T} + \frac{K_pK}{TT_i} = 0 \tag{12}$$

The analysis of the characteristic equation shows that the control loop is stable for all positive values of K and T_i [11].

The standard form of second order characteristic equation is

$$s^2 + 2\zeta\omega_n s + \omega_n^2 = 0 \tag{13}$$

Comparing (12) and (13), the controller parameter can then be designed as in (14) and (15).

$$K = \frac{2\zeta\omega_n T - 1}{K_p} \tag{14}$$

$$T_i = \frac{2\zeta\omega_n T - 1}{\omega_n^2 T} \tag{15}$$

The two closed loop poles in (12) can be chosen arbitrarily by assigning the controller constant terms, K and T_i, as in (14) and (15).

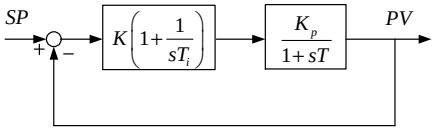

Fig.4. Block diagram of process controller.

It should be noted that the assumption of plant (converter) as a first order system is used in the simplified model. Thus it is obvious that the design of gain and time constant of controller depends on how close is the approximation. However, the results from (14) and (15) are good enough as initial values. Taking into account of dead time of the switches and time delay of the system should improve the design results considerably.

Design of Current Loop

In current control loop, the d-q axis terminal reference voltages in (3) and (4) can be made independent of each other by feeding forward the control components to compensate the two cross coupling terms. As a result, the d-q axis current control loops have been fully decoupled. Then according to (14) and (15), the d-q axis current PI controller parameter can be selected.

$$K_i = 2\zeta\omega_n L - R \text{ and } T_{ii} = \frac{2\zeta\omega_n L - R}{L\omega_n^2} \tag{16}$$

Design of DC Voltage Loop

Similarly, the dc voltage controller parameters can then be designed with the terms in (14) and (15) as in (17).

$$K_v = 2\zeta\omega_n C - 1/R_{dc} \text{ and } T_{iv} = \frac{2\zeta\omega_n C - 1/R_{dc}}{C\omega_n^2} \tag{17}$$

2.3 Linearized Model and Stability Analysis

The nonlinear equations in (2)-(7) can be linearized [12] and the linear control analysis such as stability and design technique can be directly applied. The linear relation between converter terminal voltage, v_S, and dc bus voltage, E, is expressed as

$$v_S = mE \tag{18}$$

Equations (2)-(4) can be rewritten in state-space equations as

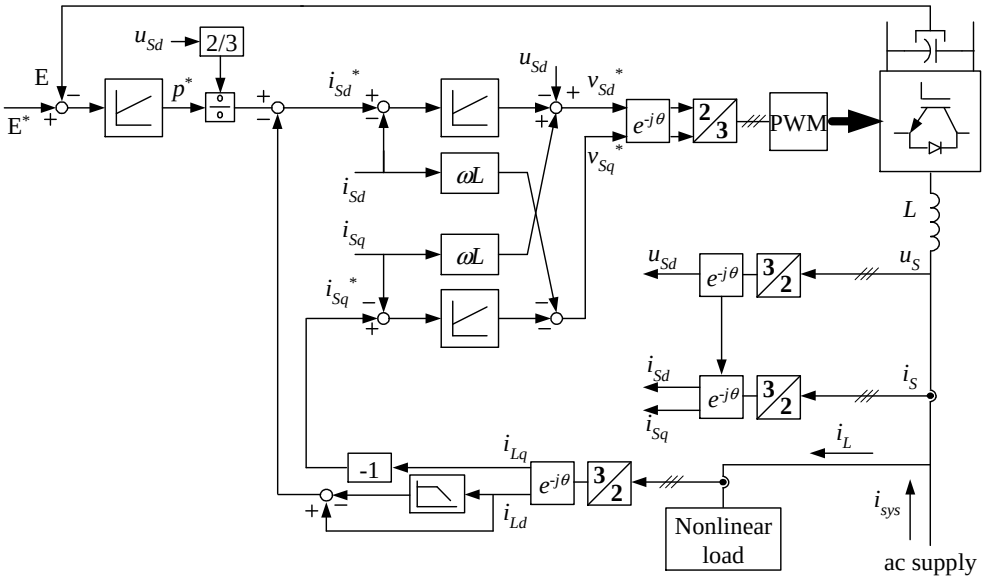

Fig.3. Block diagram of the control system of line side converter with APF and load balancing.

$$L\frac{di_{Sd}}{dt} = -Ri_{Sd} + \omega Li_{Sq} + (u_{Sd} - v_{Sd}) \tag{19}$$

$$L\frac{di_{Sq}}{dt} = -Ri_{Sq} - \omega Li_{Sd} - v_{Sq} \tag{20}$$

$$C\frac{dE}{dt} = i_{dc} - \frac{E}{R_{dc}} \tag{21}$$

If it is assumed that the dc power is equal to converter terminal active power, the expression for the dc power is

$$P_{dc} = Ei_{dc} = \frac{2}{3}v_S(i_{Sd}\cos\delta - i_{Sq}\sin\delta) \tag{22}$$

$$\frac{v_S}{m}i_{dc} = \frac{2}{3}v_S(i_{Sd}\cos\delta - i_{Sq}\sin\delta)$$

$$i_{dc} = \frac{2}{3}m(i_{Sd}\cos\delta - i_{Sq}\sin\delta) \tag{23}$$

Rearranging (19) – (23) in the standard form results in

$$\frac{d}{dt}\begin{bmatrix} i_{Sd} \\ i_{Sq} \\ E \end{bmatrix} = \begin{bmatrix} -\frac{1}{T_S} & \omega & -\frac{m}{L}\cos\delta \\ -\omega & -\frac{1}{T_S} & \frac{m}{L}\sin\delta \\ \frac{2}{3}\frac{m}{C}\cos\delta & -\frac{2}{3}\frac{m}{C}\sin\delta & -\frac{1}{T_{dc}} \end{bmatrix}\begin{bmatrix} i_{Sd} \\ i_{Sq} \\ E \end{bmatrix} + \begin{bmatrix} \frac{1}{L} & 0 \\ 0 & \frac{1}{L} \\ 0 & 0 \end{bmatrix}\begin{bmatrix} u_S \\ 0 \end{bmatrix} \tag{24}$$

$$\frac{d}{dt}\begin{bmatrix} \Delta i_{Sd} \\ \Delta i_{Sq} \\ \Delta E \end{bmatrix} = \begin{bmatrix} -\frac{1}{T_s} & \omega & -\frac{m_0}{L}\cos\delta_0 \\ -\omega & -\frac{1}{T_s} & \frac{m_0}{L}\sin\delta_0 \\ \frac{1}{2}\frac{m_0}{C}\cos\delta_0 & -\frac{1}{2}\frac{m_0}{C}\sin\delta_0 & -\frac{1}{T_{dc}} \end{bmatrix}\begin{bmatrix} \Delta i_{Sd} \\ \Delta i_{Sq} \\ \Delta E \end{bmatrix} + \begin{bmatrix} \frac{m_0}{L}E_0\sin\delta_0 & -\frac{E_0}{L}\cos\delta_0 \\ \frac{m_0}{L}E_0\cos\delta_0 & \frac{E_0}{L}\sin\delta_0 \\ -\frac{1}{2}\frac{m_0}{C}(i_{Sd0}\sin\delta_0 + i_{Sq0}\cos\delta_0) & \frac{1}{2C}(i_{Sd0}\cos\delta_0 - i_{Sq0}\sin\delta_0) \end{bmatrix}\begin{bmatrix} \Delta\delta \\ \Delta m \end{bmatrix} \tag{25}$$

where $T_s = \frac{L}{R}$ and $T_{dc} = R_{dc}C$.

The linearization for small perturbation is represented by the first order terms of Taylor's expansion given in (24). The linear difference equations are given in (25). Therefore, the characteristic equation is

$$\lambda^3 + \left(\frac{2}{T_S} + \frac{1}{T_{dc}}\right)\lambda^2 + \left(\frac{2}{T_S T_{dc}} + \frac{1}{T_S^2} + K + \omega^2\right)\lambda + \left(\frac{1}{T_S^2 T_{dc}} + \frac{K}{T_S} + \frac{\omega^2}{T_{dc}}\right) = 0 \tag{26}$$

when $K = \frac{1}{2}\frac{m_0^2}{LC}$

It can be seen that there is no δ term in the characteristic equation. Thus switching angle does not affect the position of characteristic roots. Reassigning the coefficients of the polynomial in terms of a_0, a_1 an a_2, (26) gives:

$$\lambda^3 + a_2\lambda^2 + a_1\lambda + a_0 = 0$$

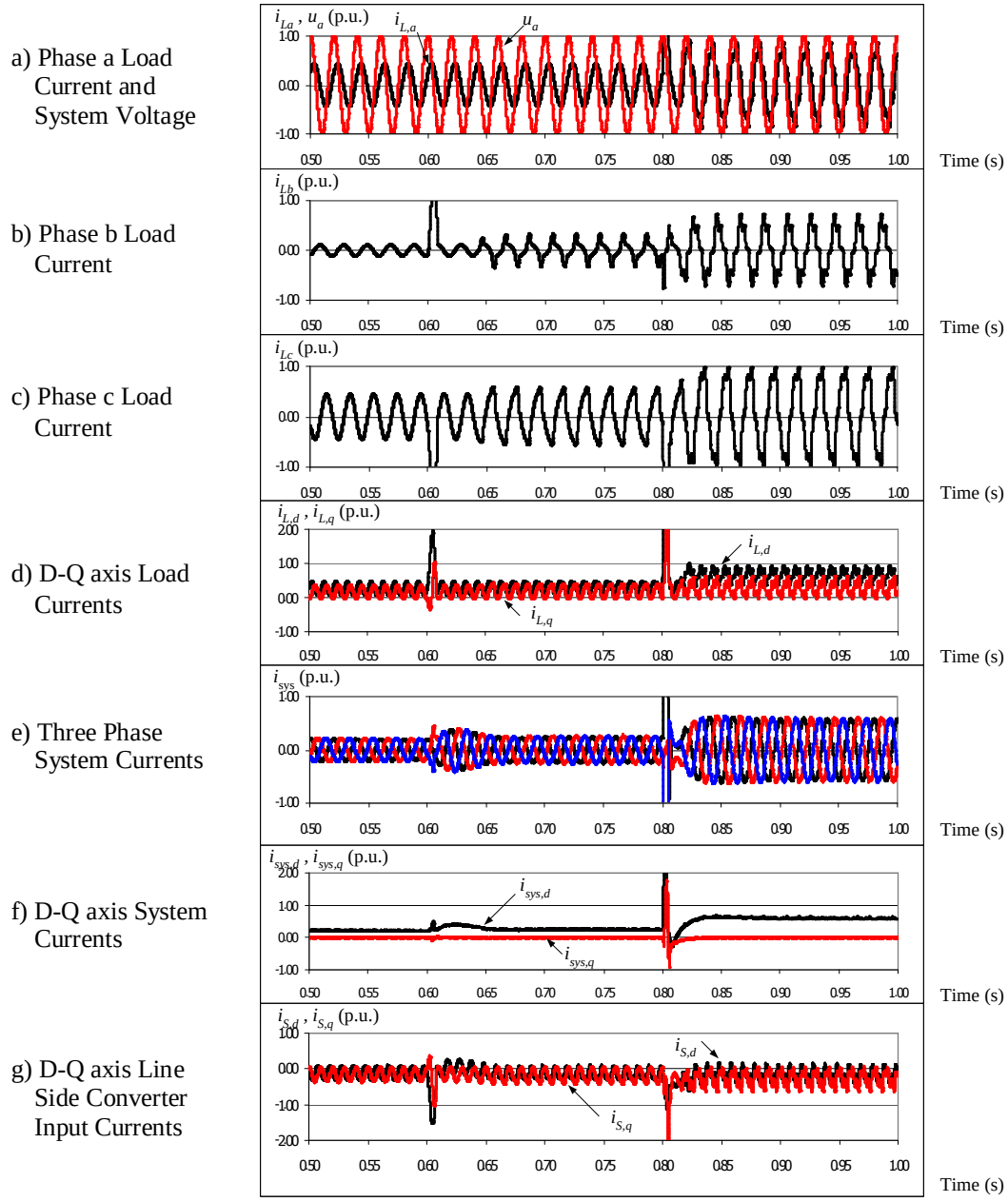

Fig.5. Simulation results of the proposed method.

The Routh-Hurwitz criterion can be used to determine stability analysis of this system.

$$\begin{array}{c|cc} \lambda^3 & 1 & a_1 \\ \lambda^2 & a_2 & a_0 \\ \lambda^1 & a_1 - a_0 / a_2 & \\ \lambda^0 & a_0 & \end{array}$$

For the system to be stable, the component of Routh array in the λ^1 row must be greater than 0, which results in

$$\frac{4}{T_S} + \frac{2}{T_{dc}} + \frac{2T_{dc}}{T_S^2} + KT_{dc} + KT_S + 2\omega^2 T_{dc} \geq 0 \qquad (27)$$

Obviously, for all positive values of system parameters the system is stable.

3. SIMULATION RESULTS

The proposed method was simulated with the circuit in Fig. 1, to verify the control performances of the system. The test conditions were started by applying linear unbalanced load with lagging power factor at t = 0.0 sec. At t = 0.6 sec a single phase nonlinear load was connected between phase b and phase c. The nonlinear effect was increased by additional three phase nonlinear load at t = 0.8 sec. The responses of the load currents (i_{Labc}), the ac system currents (i_{sys}) and the compensation currents (i_S) are shown in figure 5. Note that the waveforms of steady state load currents (i_L) in figure 5a, 5b and 5c from t = 0.5 to 0.6 sec are unbalanced sinusoidal with lagging power factor. During this period,

figure 5d shows that there are ac components in both d-q axis currents. For compensation currents (i_S) in figure 5g, the d-axis current of the system becomes dc value with zero q-axis current. The q-axis current in fact remains zero all the times which indicates unity power factor operation of the converter. The three phase currents of the system (i_{sys}) are balanced as shown in figure 5e.

When the nonlinear load is connected between phase b and c at t = 0.6 sec. and the control system responded in less than 0.1 sec (figure 5e). Figures 5a – 5c show the increase in nonlinear three phase loads at t = 0.8 sec. The control system increases the compensated currents accordingly as shown in Figure 5g. After short transients the system recovers back to balanced operation with sinusoidal currents at unity power factor which are shown in figure 5e and 5f. The performance of the line side converter with APF are clearly indicated in figures 5e and 5f with three phase system currents and d-q axis currents for both steady state and dynamic behaviors. It can be seen that the system currents remain sinusoidal, balanced and lower than load currents. As a result, d-q axis system currents are constant due to the compensated current from the line side converter in figure 5g. The negative d-axis current in Figure 5g at t = 0.8 sec indicates that the line side converter is in generating mode for a short time.

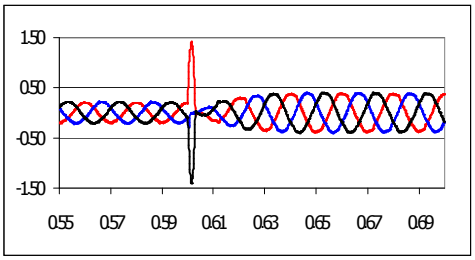

Fig.6. Three phase system current without reactance error.

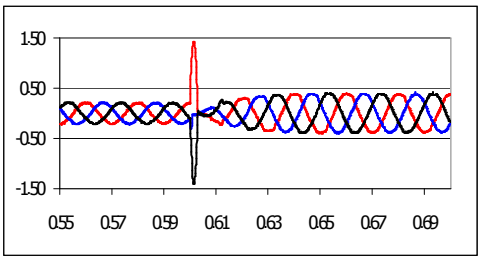

Fig.7. Three phase system current with reactance err

The robustness of proposed control system of the line side converter has been tested by keeping all the parameters of the controllers fixed, but reducing the reactance of the filter whose value is used in the feed forward component of current control loop by 10% of its original value. The original system and the system with reactance error were tested with the same operating conditions and with the linear unbalanced loads were connected to the system. At t = 0.6 sec the balanced nonlinear load are switched on. The results are shown in Figure 6 for the response of the original system and in Figure 7 for the system with reactance error, respectively. It can be seen that both responses are nearly the same even with large error of the reactance value.

4. CONCLUSION

The control of line side converter with active power filter and load balancing capability for DFIG has been demonstrated. The control scheme is based on the model of the system on synchronously rotating reference frame (d-q axis). It was proposed that the elimination of ac component of the d-axis current and q-axis current by appropriate compensation ensures that the converter is operating at unity power factor with active power filter function and load balancing capability. The potential benefit of the proposed method is the combination the active power filter function and load balancing function in a single converter. From the simulation results, the system was proved to be able to operate with balanced sinusoidal current waveforms and at unity power factor even when it was connected to the unbalanced nonlinear loads. The loading capability of the system is increased due to supply system currents are lower than load currents. The overall system efficiency is improved owing to the absence of harmonic currents and reactive current.

NOMENCLATURE

C	DC bus capacitance
E	DC bus voltage
i_{dc}	DC bus current
$\bar{i}_{Ldq}$	DC component of d-q axis load currents
$\tilde{i}_{Ldq}$	AC component of d-q axis load currents
i_{msc}	Machine side converter dc current
i_{Sabc}	Three phase line side converter input currents
i_{Sdq}	D-Q axis line side converter input currents
i_{sys}	Three phase system currents
$i_{sys,dq}$	D-Q axis system currents
K, K_p	Controller and process gain
L	Line side filter inductance
m	Proportional factor
p, q	Instantaneous line side converter input active power and reactive power, respectively
P_{dc}	DC bus power
R	Line side filter resistance
R_{dc}	DC equivalent resistance
s	Instantaneous line side converter input apparent power
T	Process time constant
T_{dc}	DC bus time constant
T_i	Controller integral time
T_s	Line side filter time constant
u_{Sabc}	Three phase system voltages
u_{Sdq}	D-Q axis system voltages
v_S,	Fundamental component of line side converter instantaneous voltage

v_{Sabc} Three phase line side converter terminal voltages

v_{Sdq} D-Q axis line side converter terminal voltages

θ Reference angle in synchronously rotating reference frame

ω System voltage frequency

δ Line side converter terminal voltage phase angle

REFERENCES

[1] Ackerman, T. 2005. *Wind Power in Power System. Chichester*. John Wiley & Sons.

[2] Pena, R. Clare, J.C. and Asher, G.M. 1996. Doubly fed induction generator using back-to-back converter and its application to variable-speed wind-energy generation. *IEE Proc.-Electr. Power Appl.*, vol. 143, no. 3, pp. 231-241.

[3] Leonhard, W. 1996. *Control of Electrical Drive*. Berlin German: Springer.

[4] Toufik, B. Machmoum, M. and Poitiers, F. 2005. Doubly fed induction generator with active filtering function for wind energy conversion system. In *Proceedings of Power Electronics and Application Conference*. 11-14 September.

[5] Jain, A. K. Ranganathan and V. T. 2008. Wound rotor induction generator with sensorless control and integrated active filter for feeding nonlinear loads in a stand-alone grid. *IEEE Trans. Ind. Electron.*, vol. 55, no. 1, pp. 218-228.

[6] Abolhassani, M. T. Enjeti, P and Toliyat, H. 2008. Integrated doubly fed electric alternator/active filter (IDEA), a viable power quality solution, for wind energy conversion systems. *IEEE Trans. Energy Convers*., vol. 23, no. 2, pp. 642-650.

[7] Akagi, H. Watanabe, E. H. Aredes, M. 2007. *Instanneous Power Theory and Aplications to Power Conditioning*. IEEE Press.

[8] Chen, D. Xie, S. 2004. Review of the control strategies applied to active power filters. In *Proceedings of Electric Utility Deregulation, Restructuring and Power Technologies Conference*. April.

[9] Tremblay, E. Chandra, A and Lagace, P. J. 2006. Grid-side converter of DFIG wind Turbines to enhance power quality of distribution network. In *Proceedings of Power Engineering Society General Meeting*. 18-22 June.

[10] Astrom, K. J. Hagglund, T. 1995. PID Controller: Theory, Design, and Tuning. Instrument Society of America.

[11] Rashid, M. H. 2001. *Power Electronics Handbook*. Academic Press.

[12] Voraphonpiput, N. and Chatratana, S. 2004. STATCOM Analysis and Controller Deesign for Power System Voltage Regulation. In *Proceedings of Transmission and Distribution Conference*. Dalian, China, 1-6.

System Study and Fault Level Reduction Techniques for a Small Scale Power Plant in Thailand

Sithiwoot Tongsrichantra, Thanapong Suwanasri, and Cattareeya Suwanasri

Abstract*— *Nowadays, the increasing fault level in Thailand power system is of prime concern due to the increasing number of small power producers (SPPs) and independent power producers (IPPs). One of the SPP in Thailand is chosen to find the optimal solution for fault current reduction. Therefore, the data of existing system is comprehensively collected and all equipment was drawn in single line diagram with their associated parameters. Then the short circuit simulation at various locations was performed according to IEC60909 to verify the equipment rating. Practically, the fault current reduction techniques were performed by using current limiting reactor (CLR) and fault current limiter (FCL). These devices were evaluated in term of their function, fault current limiting capability, power losses and suitable installation locations. The evaluation procedure consists of short circuit study at various locations in the plant to determine their fault current limiting capability. Moreover, load flow analysis was performed to evaluate the associated losses in case of the CLR. Loss evaluation is a necessary part for the CLR consideration. Consequently, the suitable installation location was determined based on effective fault current reduction, possibility of installation and their generated losses. Finally, from the technical and cost comparison, the optimum solution can be determined.

***Keywords*— Fault level, short circuit, current limiting reactor (CLR), fault current limiter (FCL), Load flow.**

1. INTRODUCTION

Fault is defined as a physical condition that causes a device, a component, or an element to fail in performing its required manner, for example a short circuit or broken wires [1]. Electric power system designers often face fault-current problems when expanding existing buses because the power demand continues to grow due to economic growth and increasing in electricity consumption. In some areas, additional generation from co-generators, small power producers (SPPs) and independent power producers (IPPs) raises the fault duty throughout a system. In addition, industrial use of computers and other power-quality-sensitive equipment has forced the utilities to provide higher quality and more reliable power. As a result, generation capacity as well as power interconnection keeps increasing for more efficient system. Increasing power generation does, however, increase the maximum available fault current at any point in the system. Older but still operational equipment gradually becomes underrated through system growth.

Unfortunately, there is no available record of annual number of faults occurring at SPP in Thailand. However the fault can be classified according to its associated causes as follow:

1) External system fault (electricity utilities)
2) Equipment failure, ageing or malfunction
3) Human errors

When fault occurred, the interrupting device must be able to interrupt such fault current. The significant fault types to be considered are;

1) Three - phase fault
2) Phase - phase fault
3) Phase to earth fault.

In this paper we consider mainly three phase fault, which is the worst and very rare case. However, its severity and consequential damages are very high and it is used to select the rating of interrupting devices.

Primary equipment, such as switchgear, transformers, cabling, and bus bar can be very expensive to be upgraded, replaced and reconfigured to higher fault level. There is a challenge to work out on this problem while keeping the additional costs in economics. In Thailand, according to the revised power development plan (PDP 2007), the total generation capacity in 2009 will reach 32,456 MW while the generation capacity contributed by very small scale power plants (VSPP) is approximately 14%. Such a contribution becomes higher due to the nation energy policy promoting in renewable energy usage. As a result, the fault level throughout the system also increases accordingly.

In this paper, the sample case is one of the Thai SPPs facing the mentioned fault level due to the interconnected network growth. By system modeling and using short circuit calculation based on IEC 60909 standards; it was found that the most of existing equipment interrupting capacity are over duties. Therefore, the fault current reduction techniques were

S. Tongsirchantra and T. Suwanasri are with Electrical Power Engineering Program (EPE), the Sirindhorn International Thai – German Graduate School of Engineering (TGGS), King Mongkut's University of Technology North Bangkok (KMUTNB), 1518 Pibulsongkram Rd., Bangsue, Bangkok, 10800, Thailand. E-mail: sithiwoot@ieee.org, sithiwoot@pe.co.th and thanapongs@kmutnb.ac.th.

C. Suwanasri (corresponding author) is with Department of Electrical and Computer Engineering, Faculty of Engineering, Naresuan University, Phitsanulok 65000, Thailand. Phone: +66-55-261-000 ext. 4342; Fax: +66-55-261-062; E-mail: cattareeyaa@nu.ac.th

studied and discussed in order to avoid unsafe operation and consequential damages caused by short circuit current. In all possible study cases, the repeated short circuit calculation is also carried out to check their effective outcome. In addition, the loss evaluation by load flow calculation based on Newton – Raphson method is also performed in case of using Fault Current Limiter.

2. BASIC THEORY

In general, there are four techniques to lower the short circuits such as;

1) Pre-planned for power circuit breaker (CB) and equipment uprating
2) Replacement by high impedance power transformer
3) Installation of series current limiting reactor (CLR)
4) Installation of fault current limiter (FCL)

The last two techniques will be proposed and discussed in this paper. The CLR is a typically and widely used technique due to its simple construction, reliability and proven technology. Nevertheless, the application of FCL is increasingly implemented in industrial plants in Thailand especially in case the system power (kW) losses are of prime main concern.

2.1 Current Limiting Reactor (CLR)

The CLR introduces higher impedance to the system by series–connected reactance in order to protect the equipment during fault condition. It reduces short circuit level to meet the system needs as well as stresses on busses, insulators, circuit breakers and other high voltage devices. It is, sometimes, connected between the neutral of the system and earth for limiting the phase to earth current under system fault conditions. It is also used as load sharing reactor for balancing the current in parallel circuits [2], [3].

Current Limiting Reactor Types

1. Air core reactor with the advantage of no saturation under fault condition, low losses, and long life
2. Dry type reactor
3. Indoor/outdoor reactor
4. Single phase /three phase reactor

A Sample Calculation

$$X_R = \frac{V_S}{\sqrt{3}}\left[\frac{1}{I_{SCA}} - \frac{1}{I_{SCB}}\right] \quad (1)$$

where

X_R = reactor reactance [Ω]

V_S = system voltage [V]

I_{SCA} = S/C current after series – connected reactor [kA]

I_{SCB} = S/C current before series – connected reactor [kA]

Advantages

1. Reduce fault current
2. Match impedance of parallel feeders
3. Increase equipment and capacitor life
4. Perfect mechanical strength to withstand high short circuit force
5. Limited temperature rise enables longer lifetime
6. Special surface protection against UV and pollution class 5 area
7. Simple design for determining an appropriate impedance
8. Maintenance-free design

Disadvantages

1. Energy costs increase as losses become a more significant component of total operating cost
2. Operating losses consist of
   a) the resistance and eddy-current loss in the winding due to load current,
   b) losses caused by circulating current in parallel windings,
   c) stray losses caused by magnetic flux in other metallic parts of the reactor
3. Minimum magnetic clearance for the reactor is required as shown in Fig. 1.
4. Voltage drop due to its connection, thus voltage regulation is required (maybe shunt capacitor bank).
5. Magnetic flux effects to human life and metallic structure in vicinities

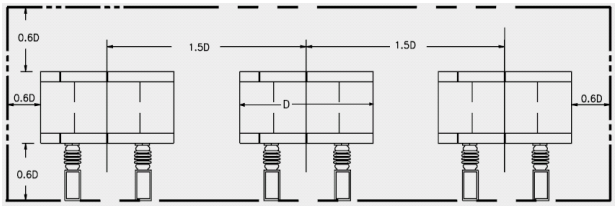

Fig.1. Minimum of magnetic clearance to other reactors and metallic parts [4].

2.2 Fault Current Limiter (FCL)

Technical Principle/Function

Fault current limiter is very quickly capable of detecting and limiting a short circuit current by use of a small explosive charge to open a conductor. This diverts the current to a parallel fuse which quenches the short circuit current.

Types

Fault current limiter of ABB is one of the FCL products in the FCL industrial market. ABB current limiting device (Is – limiter) consists of 2 components as shown in Fig. 2.

A. Current path uninfluenced
B. Current commutated to fuse

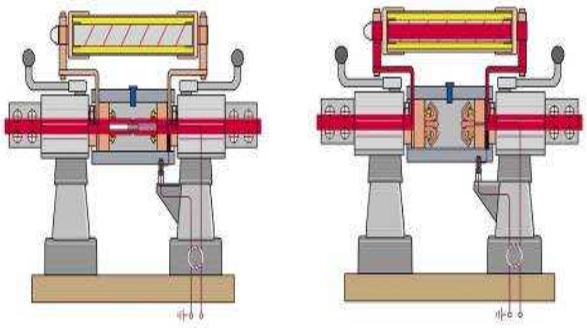

(A) (B)

Fig.2. Current limiting devices by ABB [5], [6].

Operation

In Fig. 3, when a short circuit is detected and exceeding the pre-determined magnitude and the rate of current rise, an explosive charge in the main current carrying conductor is detonated. This ruptures the main current carrying path thus diverting the current to the fuse which quenches it. The entire operation takes place within a few milliseconds [8]. After operation, the devices are isolated and insert containing the fuses and the ruptured conductors are removed and replaced with spares. One device is installed in each phase of a three phase system, and a circuit breaker is always required in series with it, in order to perform normal circuit opening and closing duties. Moreover, there is another supplier who supplies FCL as well. G&W produces the so-called triggered current limiter (TCL) [9]. It offers a high continuous current alternative to the technique by providing effective fault current limitation without the significant losses, and without equipment upgrade or replacement.

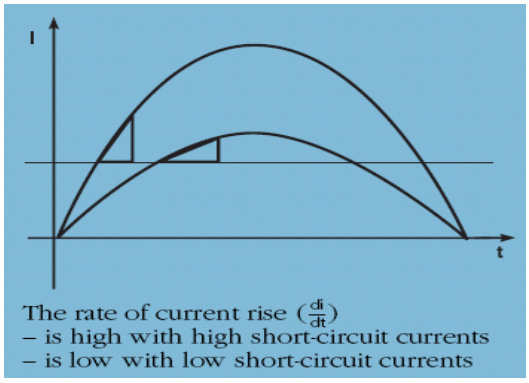

Fig.3. Rate of current rise [7].

The fuse characteristics of both suppliers are shown in Fig. 4. Note that the multiple breaks in the main current path provide faster commutation of fault current to the current limiting fuse element, while providing improved dielectric withstand of the broken gaps.

Co-ordination

From a coordination standpoint, the triggered current limiter is catastrophic protection devices. Since these are electronically sensed and triggered units, their operating criteria is pre-set and not dependent on time versus current, temperature, element size (or melting I^2t) or preconditions [10], [11], [12]. In addition, the FCLs as per G&W design are not dependent on rate-of-rise of fault current, but instead, are responsive to magnitude only.

Calculation of Tripping Value [13]

The tripping value is the expected rms value of the first half wave of a short-circuit current flowing through the Is – limiter, in which case the Is – limiter must trip during the first current rise. Since the use of this device is still relatively rare, the calculation of the tripping value is not generally known. Practical experience to date shows the tripping value should be greater or equal to twice the operating current in order to prevent it from tripping on unintentional fault.

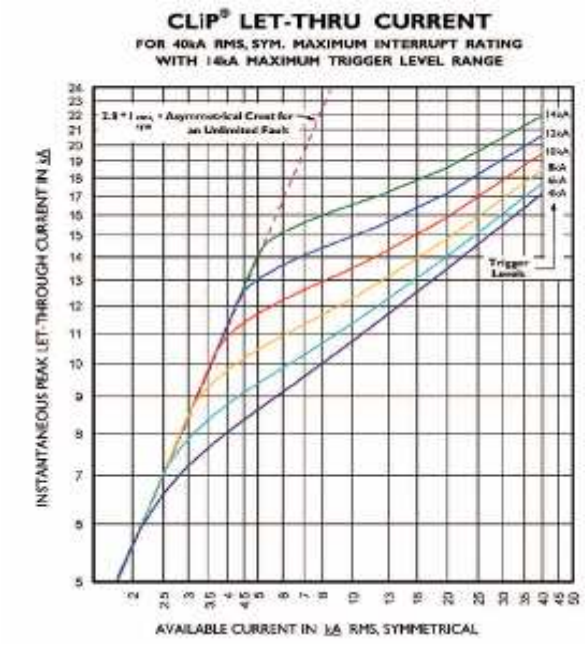

(A) The Let-Through current plot of 40kA rated CLiPs unit (G&W)

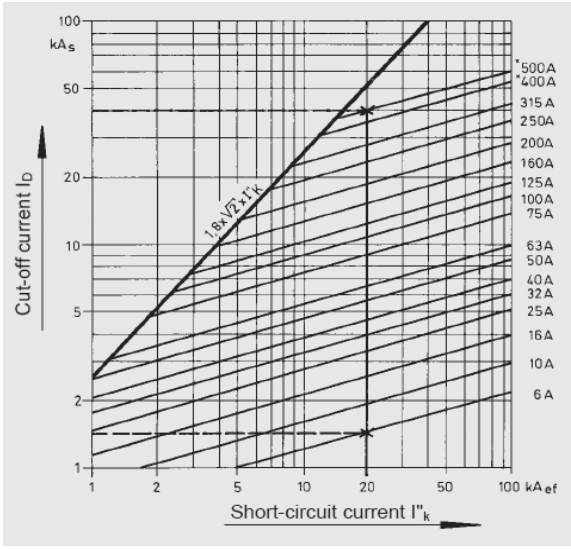

(B) cut-off characteristic of HRC fuse of ABB.

Fig.4. Example of fuse characteristic, peak let - through current VS symmetrical fault current.

The *Is* – limiter trips when the rate of current rise (di/dt) reaches or exceeds a specified level, while the current flowing through it has instantaneous values between the upper and lower measuring range limit or i_1 and i_2 respectively. The lower measuring range limit i_2 should be selected at approximately 1,000 to 3,000A above the peak value of the operating current. The measuring range (i_1-i_2) is in general 1,000 to 4,000A. As a result, the advantages and disadvantages are concluded bellows.

Advantages

1. Faster operation than relay
2. Technical and economic advantages when used in transformer or generator feeders, in switchgear sectionalizing and connected in parallel with reactors.
3. In comparison with reactors, the Is-limiter avoids voltage drops and does not contribute to the peak short-circuit current.
4. Voltage in the part of the system is not affected by the operation of an Is-limiter
5. The series network impedance remains unchanged.
6. Improvement of the current distribution at the feeder transformers.
7. The load dependent losses of the feeder transformers are reduced.
8. Increased reliability of the power supply. On failure of one feeder transformer, the load is taken over by the other feeder transformers without current interruption.
9. The cost for a required new switchboard with higher short-circuit capacity will be saved.

Disadvantages

1. Analysis of the proper and reliable thermal technique is still required.
2. Spare part and 'back up' system are needed.
3. Skill of worker
4. Failure consequence: any possibility that a failure of the current limiting device to operate could overstress switchgear.
5. Any legal constraints that could prevent the use of this type of current limiting device
6. Co-ordination with other protective devices is not possible.
7. Their intrinsic safety
8. Testing of operation
9. Triggering integrity

3. WORK PROCEDURE

In the study, the system in question consists of a fully condensing steam turbine generator with its capacity of 55MW at 11.4kV rated voltage, its local loads and the interconnected line synchronizing with the Provincial Electricity Authority (PEA) of Thailand. In this system, summary of simulation results concerning all critical possible short circuit cases are carried out and summarized as the technical references for further study or action by project and engineering teams in the future. The normal operating loads and supply of the SPP are shown in Fig. 5.

At first, all possible short circuit cases and fault current reduction studies are modelled and simulated by commercial simulating software namely ETAP based on IEC 60909 standards.

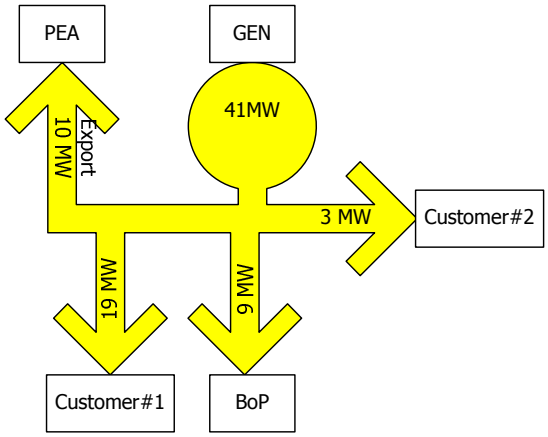

Fig.5. Load flow diagram of a chosen SPP

This study will help the SPP in the selection process of appropriate fault current reduction devices. All fault study cases are determined so as to help the SPP crystal clear in detail of bus fault current at all possible locations. Moreover, study reports also provide the voltage information on the healthy buses in the system. This can similarly help the SPP to perform the proper setting of under voltage relay in order to avoid nuisance tripping.

Short circuit simulations are divided into two main scenarios which are "with" and "without" fault current reduction devices such as the FCL and CLR. Precisely, both cases are simulated with full possible connected loads and actual operating loads by ETAP. According to operating record, actual operating loads are based on the total plant generation of 41MW with 10 MW exporting power to utility (PEA). In additions to short circuit study, load flow analyses using Newton-Raphson method are also performed in order to evaluate the reactor losses in the relevant cases.

4. RESULTS

Current Limiting Reactor (CLR) Cases

In CLR simulation cases, additional reactor(s) shall effectively reduce short circuit current contributed from short circuit sources such as generator, large rotating machine and utility grid. Obviously, reactor should be connected in front of generator, utility grid or between switchgear bus-1A and bus-1B as shown in Fig. 6.

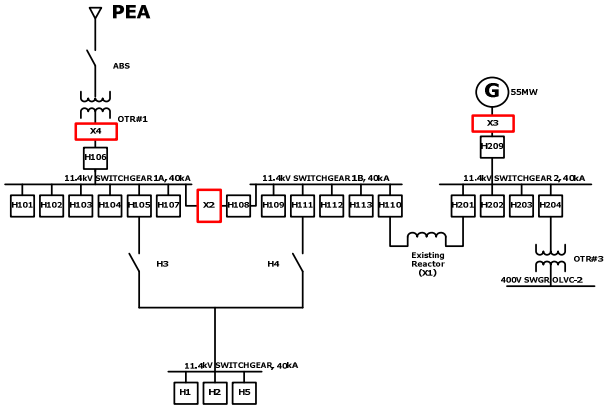

Fig.6. Installation diagram of additional reactors.

where:

X1 = Existing reactor (between Bus-1B and Bus-2)

X2 = New reactor#2 (between Bus-1A and Bus-1B)

X3 = New reactor#3 (between Generator and Bus-2)

X4 = New reactor#4 (between OTR#1 and Bus-1A)

Ideal (full) Operating Loads with Reactor

In case of ideal operating loads (the case where all installed loads are in service) the short circuit simulation results are summarized in Fig. 7.

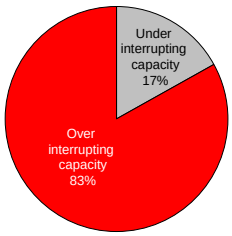

A) Ideal operating load without existing reactor (X1)
Over interrupting 83%, Under interrupting 17%

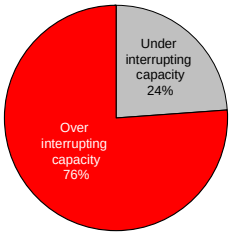

B) Ideal operating load with existing reactor (X1)
Over interrupting 76%, Under interrupting 24%

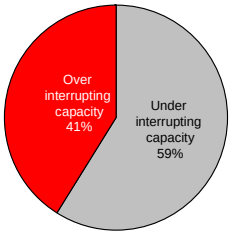

C) Ideal operating load with existing reactor (X1) and the new one (X2)
Over interrupting 41%, Under interrupting 59%

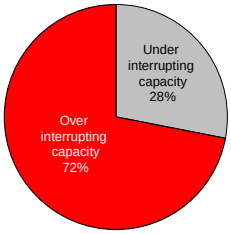

D) Ideal operating load with existing reactor (X1) and the new one (X3)
Over interrupting 72%, Under interrupting 28%

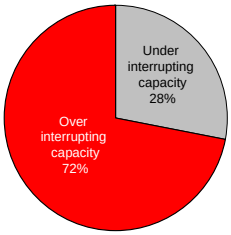

E) Ideal operating load with existing reactor (X1) and the new one (X4)
Over interrupting 72%, Under interrupting 28%

Fig.7. Full load short circuit summary: Reactor(s).

In ideal operating load case, the additional reactor (X2) located between Switchgear bus-1A and bus-1B can effectively reduce the short circuit current and it can increase the percentage of survival buses from 24% to 62% as presented in Fig.7, Case A-C. Therefore, X2 location is the best location to lower the prospective short circuit current in case we use CLR as the fault current reduction device.

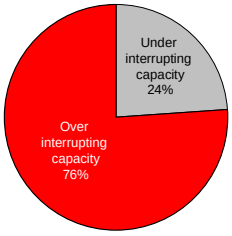

A) Actual operating load without existing reactor (X1)
Over interrupting 76%, Under interrupting 24%

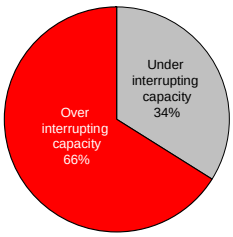

B) Actual operating load with existing reactor (X1)
Over interrupting 66%, Under interrupting 34%

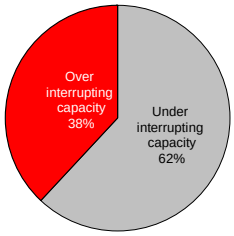

C) Actual operating load with existing reactor and X2
Over interrupting 38%, Under interrupting 62%

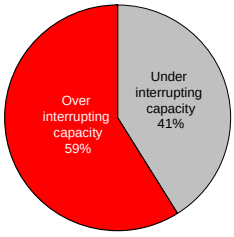

D) Actual operating load with existing reactor and X3
Over interrupting 59%, Under interrupting 41%

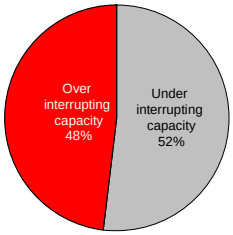

E) Actual operating load with existing reactor and X4
Over interrupting 52%, Under interrupting 48%

Fig.8. Actual load short circuit summary: Reactor(s).

Actual (real) Operating Load with Reactor

In actual operating load case (the case where the actual loads, as given from TPTUC field information are practically in service), the short circuit simulation summary results are summarized in Fig. 8. In case of actual operating load, the additional reactor (X2) located between Switchgear bus-1A and bus-1B can also effectively reduce short circuit current and increase healthy bus bar number from 24% to 62% as full possible connected load operating presented in Fig. 8, Case A-C. Therefore, X2 location is still the best location to lower the prospective short circuit current in case we use CLR as the fault current reduction device. Moreover, in all cases of CLR, load flow simulations using Newton-Raphson method are carried out in order to check the system bus voltage drops and losses. The simulation shows that, with an additional reactor at a time, the voltage drops at all buses are still in allowable limit. Lastly, system losses were also evaluated and shown in Figs. 9 and 10 below.

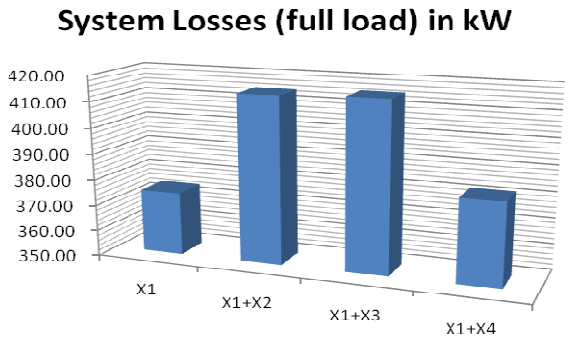

Fig.9. System losses: Full operating load.

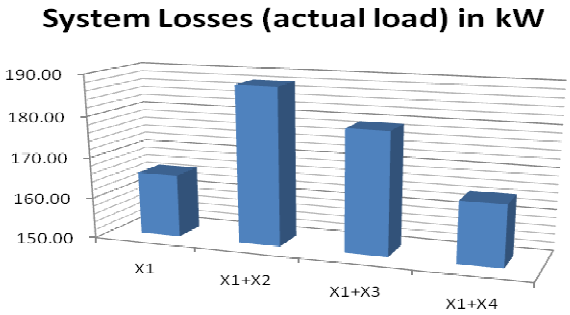

Fig.10. System losses: Actual operating load.

Fault Current Limiter (FCL) Cases

In FCL simulation cases, the additional FCL shall effectively reduce short circuit current contributed from short circuit sources such as generator and utility grid in the same manner as CLR (reactor) cases. As a result, the best locations of FCL to reduce the short circuit current to the lowest value are the combination of those connected between Switchgear bus-1A and bus-1B, after H3 and H4 and after H204 as Fig. 11.

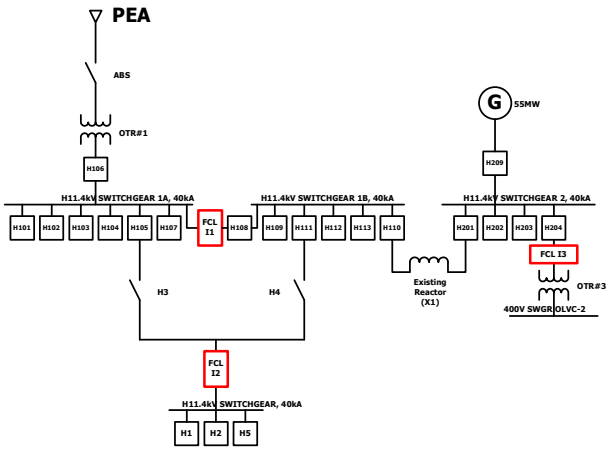

Fig.11. Installation diagram of FCL (I1, I2 and I3).

where:

X1 = Existing reactor (between Bus-1B and Bus-2)

I1 = New FCL#1 (between Bus-1A and Bus-1B)

I2 = New FCL#2 (located in series with H111)

I3 = New FCL#3 (between Bus-2 and OTR#3)

Ideal (Full) Operating Loads with FCL

In case of ideal (full) operating loads, the short circuit simulation results are summarized in Fig.12.

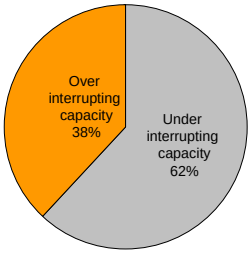

A) Ideal operating load with existing reactor and I1
Over interrupting 38%, Under interrupting 62%

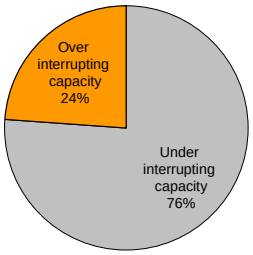

B) Ideal operating load with existing reactor, I1 and I2
Over interrupting 24%, Under interrupting 76%

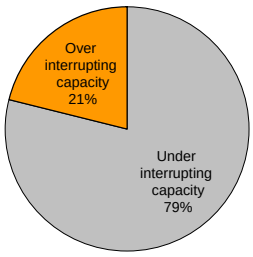

C) Ideal operating load with existing reactor, I1, I2 and I3
Over interrupting 21%, Under interrupting 79%

Fig. 12. Full load short circuit summary: FCL(s).

Actual Operating Load Case with FCL

In actual operating load case, the short circuit simulation results are summarized in Fig. 13.

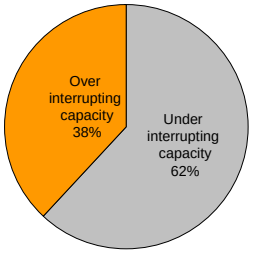

A) Actual operating load with existing reactor and I1
Over interrupting 38%, Under interrupting 62%

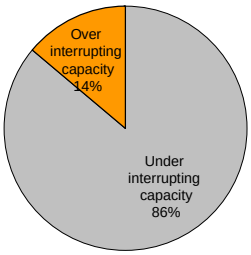

B) Actual operating load with existing reactor, I1 and I2
Over interrupting 14%, Under interrupting 88%

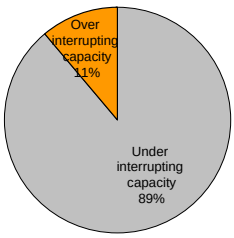

C) Actual operating load with existing reactor, I1, I2 and I3
Over interrupting 10%, Under interrupting 90%

Fig.13. Actual Load Short Circuit Summary: FCL(s)

It is obvious that the most effective scenario is the combined installation of FCL at I1 (one between bus1A and bus1B) and I2 (one in front of lower 11.4 kV bus) locations.

5. COST COMPARISON

Obviously, all simulation results return the best location of FCL and CLR at the one located between Switchgear 1A and 1B. Therefore, estimated investment comparison between those two fault-current reduction techniques is tabulated in table 1 as follows.

Table 1. Fault-current reductions of FCL and CLR

Additional protective devices	FCL (including spare parts)	CLR
Estimated total capital cost (THB)	20,000,000	12,000,000
Cost of additional annual system active power losses (THB)	-	328,320.00
Over interrupting rating before X2 (%)	76.00	76.00
Over interrupting rating after X2 (%)	38.00	38.00

Cost of additional annual system active power (kW) losses caused by insertion of reactor X2 (the one located between Switchgear 1A and 1B) are shown in the middle column above. The system loads are assumed to be constant throughout the whole operation period of 8640 hours per annum with average 2 THB/kWh unit charge. For FCL, the operation and maintenance (O&M) cost in

particular of spare parts might play an important part of capital investment.

6. SUMMARY

Although there are many measures to reduce the fault level in the system but the most applicable techniques for the chosen SPP case are limited to those of Current Limiting Reactor (CLR) and Fault Current Limiter (FCL) applications. CLR is suitable for the system having no limited installation space and in case life cycle cost contributed from kW losses is not seriously taken into account. On the other hand, FCL requiring less space, seems to be one appropriate alternative when the issue of kW losses and voltage drop are of serious concern. In addition, the combination of those two techniques can also be used in order to meet the overall fault level reduction target. In such a study case, even with existing reactor (X1), the percentage of equipment facing through fault current above their interrupting capacities are more than 66%. With the new reactor (X2) or additional FCL (I1) connected between 11.4kV bus 1A and bus 1B, the aforesaid percentage can be improved to 38%. To lower the over-interrupting percentage even more, additional CLRs or FCLs can be put into other parts of the system. Nevertheless, the careful consideration of system losses and voltage drops are needed in the CLR application whereas the investment cost and spare parts are the major concern for the FCL one. The protection coordination aspect and the absence of relevant international standards are also the limit of using FCL application. Lastly, all relevant factors shall be carefully traded off in final decision making.

This study can be used as a guideline for engineers who are responsible for the small scale power plant operation and planning. The authors do hope that this can be the foundation of further study in the related or similar topics.

ACKNOWLEDGMENT

The authors also would like to thanks Mr.Jasada Kudtongngam of National Electronics and Computer Technology Center (NECTEC), Thailand for his valuable suggestion in many aspects of the studies.

REFERENCES

[1] ANSI/IEEE Std. 100-1992
[2] IEEE Std C57.16 – 1996, “IEEE Standard Requirements, Terminology, and Test Code for Dry – Type Air – Core Series – Connected Reactors” 1996
[3] IEC Std 289, “International Standard Reactor”, 1988
[4] http://www.trenchgroup.com
[5] ABB Is – Limiter Handbook, ABB Calor Emag Mittelspannung GmbH, Germany
[6] Presentation Document © ABB Power Technologies / 6-6552 E 11-06-2003
[7] Instruction Manual Is–Limiters in ZS1-Switchgear BA 396/03 E
[8] Is-limiter Technical Development, ABB Power Distribution, Leaflet no. DECMS 2243 00 E Printed in Germany (04.00-2000-PPI).
[9] Schaffer, J. S. Trigged Current Limiters for Closing Bus Ties, Bypassing Reactors and Improving Power Quality.
[10] Wu, A. Y. and Yin, Y. 1998. Fault-Current Limiter Applications in Medium- and High-Voltage Power Distribution Systems. *IEEE Trans. Industry Applications*, vol. 34, no. 1, pp. 236 - 242.
[11] Hartung K.H. and Grafe, V. 2006. Calculation of the Settings for an Is – Limiter Measuring and Tripping Device. ABB AG, Calor Emag Medium Voltage Products.
[12] Final Report. 2004. Development of a Safety Case for the Use of Current Limiting Devices to Manage Short Circuit Current on Electrical Distribution Networks” Parsons Brinckerhoff Ltd.
[13] Fault-Current Limiter (FCL), from the World Wide Web: http://www.wtec.org/loyola/scpa/04_03.htm.

A Fuzzy Multi-Attribute Decision Making Approach for Multi-Objective Thermal Power Dispatch

Saksorn Chalermchaiarbha and Weerakorn Ongsakul

Abstract*— *This paper proposes a fuzzy multi-attribute decision making approach for solving multi-objective thermal power dispatch problem. The fuzzy multi-attribute decision considering the maximum of minimum membership function value of each non-dominated solution could well trade-off the contradicting objective functions consisting of fuel cost, NO_X, SO_2 and CO_2 emission. The weighting aggregation method is employed to generate the non-dominated Newton-Raphson based solutions. Test results on 3 and 6 generating systems indicate that the obtained best optimal solution having more compromise characteristics than the ones derived from fuzzy cardinal priority ranking normalized approach (FCPRN) and technique for order preference by similarity to ideal solution (TOPSIS) when taking account of percentage total deviation from the ideal solution as well as fulfilling preferred zones condition.

***Keywords*— Best Compromise Solution, Fuzzy Multi Attribute Decision Making, Membership Function, Non-Dominated Solutions.**

1. INTRODUCTION

The optimal economic load dispatch in electric power systems has currently gained increasing importance since not only the generation cost keeps on increasing but also pollutant emission level caused by thermal power plants is not allowed to exceed the quantities imposed by environmental laws. In generating electricity, combustion of fossil fuel emits several gaseous pollutant into atmosphere such as nitrogen oxides (NO_x) , sulfur dioxide (SO_2) and carbon dioxide (CO_2). As a result, the allocation of power generation to different thermal power units is to minimize both operating cost and pollutant emission level subject to diverse equality and inequality constraints of the system such as covering power load demand and loss, generating capacities, etc [1]-[5]. Multi-objectives formulation is then implemented to solve for the optimal strategy for electric power generation. The main problem of multi-objective optimization, however, is that such objectives are mostly contradicting one another, where improvements in one objective may lead to an exacerbation in another objective. Trade-off, therefore, exists between such conflicting objectives. Consequently, there are more than one optimal solution for multi-objective problem which is different to the single objective one. Identifying a set of feasible solutions is therefore important for the decision maker to select a compromise solution satisfying the objectives as best possible. Such solutions are referred to as non-dominated solutions [6]-[7].

Traditional techniques which are used for solving multi-objective problem, for example, are goal programming, the, the ε-constraint method, and weighting method, etc [7].

For goal programming, the decision maker has to assign targets or goals that wish to achieve for each objective. These values are included in the problem as additional constraints. The objective function then tries to minimize the absolute deviation from the targets to the objectives

The ε-constraint method is based on optimization of the most preferred objective while considering the other objectives as constraint bounded by some allowable levels (ε). Such levels are altered to generate the non-dominated solutions.

The weighting method uses the concept of combing different objectives through the weighted sum method to convert the multi-objective problem into single objective one. This method generates the non-dominated solution by varying the weight combination.

In addition, the meta-heuristic approaches, such as, evolutionary algorithms and swarm intelligence, is an alternative to aforementioned techniques. A non-dominated sorting genetic algorithm (NSGA) is used to solve for environmental/economic power dispatch (EED). Likewise, a modified multi-objective particle swarm optimization algorithm (MOPSO) and multi-objective evolutionary algorithm (MOEA) is also presented to handle the EED problem [2]-[5]. Importantly, whatever optimization methods are applied to produce the feasible solutions, finally, there is simply one solution chosen as the best that maximizes the satisfaction of all objectives to decision maker [7].

A way that is widely used to extract the best optimal solution in several papers pertaining to electric power generation planning is a fuzzy cardinal priority ranking normalized approach (FCPRN) [2], [3], [5], [8]-[9].

In this paper, a fuzzy multi-attribute decision making (FMADM) approach is proposed to be an alternative decision process for extracting the best compromise solution of multi-objective thermal power dispatch

Saksorn Chalermchaiarbha (corresponding author) is with Power Economics Department, Metropolitan Electricity Authority, 121 Chakpetch Road, Pra Nakorn District, Bangkok, Thailnad. E-mail: saksornarbha@yahoo.com.

Weerakorn Ongsakul is with the Energy field of study, Asian Institute of Technology, P.O. Box 4, Klong Luang, Pathumthani 12120, Thailnad. Email ongsakul@ait.ac.th.

problem. The Newton-Raphson algorithm is utilized, in optimization process, to produce the non-dominated solutions through weighting aggregation method. Test results are demonstrated on 3 and 6 generating systems. The best compromise solution obtained is compared to the ones derived from FCPRN approach as well as an approach that use the technique for order preference by similarity to ideal solution (TOPSIS) [4] in terms of percentage total deviation from the ideal (minimum) solution including checking preferred zones conditions.

2. PROBLEM FORMULATION

In this section, the multi-objective problem of thermal power dispatch with equality and inequality constraints are described. The important objectives considered here are operating fuel cost, NO_X emission, SO_2 emission and CO_2 emission. These objectives are competing one another owing to contradiction characteristics.

2.1 Fuel Cost

The first objective function to be minimized is the total fuel cost for thermal generating units in the system which can be approximately modeled by a quadratic function of generator power output P_i [10], [11]

$$F_1 = \sum_{i=1}^{NG} (a_i P_i^2 + b_i P_i + c_i) \quad (1)$$

where

a_i , b_i , c_i are the fuel cost coefficients.

NG is the total number of generating units.

2.2 Gaseous Pollutant Emission

As thermal power plant uses fossil fuel for power generation, it therefore releases the polluting gases into atmosphere. The most important emission considered in gernerating electric power that effects on the environment are NO_x, SO_2 and CO_2. These emissions can be approximately modeled through a quadratic function in terms of active power generation [10].

The NO_x emission objective can be defined as

$$F_2 = \sum_{i=1}^{NG} (d_{1i} P_i^2 + e_{1i} P_i + f_{1i}) \quad (2)$$

where

d_{1i} , e_{1i} , f_{1i} are the NO_x emission coefficients.

NG is the total number of generating units.

In a similar fashion, SO_2 and CO_2 emission objectives can be defined below:

$$F_3 = \sum_{i=1}^{NG} (d_{2i} P_i^2 + e_{2i} P_i + f_{2i}) \quad (3)$$

where d_{2i} , e_{2i} , f_{2i} are the SO_2 emission coefficients.

$$F_4 = \sum_{i=1}^{NG} (d_{3i} P_i^2 + e_{3i} P_i + f_{3i}) \quad (4)$$

where d_{3i} , e_{3i} , f_{3i} are the CO_2 emission coefficients.

2.3 Equality and Inequality Constraints

The total power generation must cover the total load demand and real power loss in the transmission system. For the fixed network configuration, the equality constraint is represented by the power balance equation stated as:

$$\sum_{i=1}^{NG} P_i = P_D + P_L \quad (5)$$

where P_D and P_L is total load demand and transmission loss, respectively.

The power output limit are imposed as

$$P_i^{\min} \le P_i \le P_i^{\max}, \; i = 1, 2, 3, \ldots, NG \quad (6)$$

2.4 Transmission Loss

One common practice for calculating the effect of transmission losses is to express the total transmission loss as a quadratic function of the generator power outputs. The simplest quadratic form is [11]:

$$P_L = \sum_{i=1}^{NG} \sum_{j=1}^{NG} P_i B_{ij} P_j \quad (7)$$

The coefficients B_{ij} are called loss coefficients or B-coefficients and assumed constant.

Thus, the problem formulation is to minimize all objective functions simultaneously, while satisfying both equality and inequality constraints which can be expressed as follows:

$$\text{Minimize } [F_1, F_2, F_3, F_4]^T \quad (8)$$

subject to

$$\sum_{i=1}^{NG} P_i = P_D + P_L \quad (9)$$

$$P_i^{\min} \le P_i \le P_i^{\max} \quad (10)$$

where F_1, F_2, F_3, and F_4 are the objective functions to be minimized over the set of admissible decision variables P_i.

3. METHODOLOGY

3.1 Optimization Method.

The weighting aggregation method is employed to generate the non-dominated solutions through Newton-Raphson algorithm. This method defines an aggregate objective function as a weighted sum of the objectives. Hence, the multi-objective optimization problem is redefined as [6], [7]:

$$\text{Minimize} \sum_{j=1}^{m} w_j F_j(P_i) \tag{11}$$

subject to

$$\sum_{i=1}^{NG} P_i = P_D + P_L \tag{12}$$

$$P_i^{\min} \le P_i \le P_i^{\max} \tag{13}$$

$$\sum_{j=1}^{m} w_j = 1\,,\ w_j \ge 0\,, \tag{14}$$

where w_j are the weighting coefficients. In this study, the value of weighting coefficients vary in the range of 0 to 1 in steps of 0.1 and the weight of fuel cost, w_1, is not allowed to be zero except in the case of determining the minimum value of other objectives i.e. F_2, F_3, and F_4; m is the total number of objectives.

To solve the scalar optimization problem, the Lagrangian function is defined as

$$L(P_i, \lambda) = \sum_{j=1}^{m} w_j F_j + \lambda\left(P_D + P_L - \sum_{i=1}^{NG} P_i\right) \tag{15}$$

where λ is Lagrangian multiplier and m is the number of objective functions.

The necessary conditions to minimize the unconstrained Lagrangian function are:

$$\frac{\partial L}{\partial P_i} = 0 \quad \text{and} \quad \frac{\partial L}{\partial \lambda} = 0 \tag{16}$$

To implement the Newton-Raphson method, the following equation is solved iteratively until having no further improvement in decision variables.

$$\begin{bmatrix} \nabla_{PP} & \nabla_{P\lambda} \\ \nabla_{\lambda P} & \nabla_{\lambda\lambda} \end{bmatrix} \begin{bmatrix} \Delta P \\ \Delta\lambda \end{bmatrix} = \begin{bmatrix} -\nabla_P \\ -\nabla_\lambda \end{bmatrix} \tag{17}$$

The steps for Newton-Raphson algorithm to produce the admissible solutions can be explained below [10].

Newton-Raphson Algorithm

1. Read data, viz. cost coefficients, emission coefficients and *B*-coefficients, demand, Error (convergence tolerance) and ITMAX (maximum allowed iterations), *M* (number of objectives), NG (number of generators) and *K* (number of non-dominated solutions).
2. Set iteration for non-dominated solutions, $k = 1$.
3. If ($k \ge K$) GOTO step 15
4. Feed weights combination, $w_j : j = 1, 2, \ldots, m$
5. Compute the initial value of P_i ($i = 1, 2, \ldots,$ NG) and λ by assuming that $P_L = 0$. The value of λ and P_i can be calculated using the Eq. (18) and (19).

$$P_i = \frac{\lambda - b_i}{2a_i}\,,\ (i=1, 2, 3, \ldots, \text{NG}) \tag{18}$$

$$\lambda = \frac{P_D + \sum_{i=1}^{NG} \frac{b_i}{2a_i}}{\sum_{i=1}^{NG} \frac{1}{2a_i}} \tag{19}$$

Assume that no generator has been fixed either at lower limit or at upper limit at this step.

6. Set iteration counter, IT = 1.
7. Compute Hessian and Jacobian matrix elements in Eq.(17). Deactivate row and column of Hessian matrix and row of Jacobian matrix representing the generator whose generation is fixed either at lower limit or upper limit in order that those fixed generators cannot participate in allocation.
8. Find ΔP_i (i = 1, 2, …, R) and $\Delta\lambda$ using Gauss elimination method. Here, R is the number of generators that can participate in allocation.
9. Modify control variables,

   $P_i^{new} = P_i + \Delta P_i$ (i = 1, 2, …, R)

   $\lambda^{new} = \lambda + \Delta\lambda$

10. Update old control variable values with new values.

    $P_i = P_i^{new}$ (i = 1, 2, …, R),

    $\lambda = \lambda^{new}$ and GOTO Step 8 and repeat.

11. Check the inequality constraint of generators from the following conditions.

    If $P_i < P_i^{\min}$ then $P_i = P_i^{\min}$

    If $P_i > P_i^{\max}$ then $P_i = P_i^{\max}$

12. Check convergence tolerance condition from $\sqrt{\sum_{i=1}^{R} (\Delta P_i)^2 + (\Delta\lambda)^2} \le \varepsilon$

If convergence condition is satisfied or IT ≥ ITMAX then GOTO Step 13 otherwise update iteration counter, IT = IT+1 and GOTO Step 7.

13. Record the obtained non-dominated solution. Compute F_j ($j=1, 2, \ldots, m$) and transmission loss.
14. Increment count of non-dominated solutions, $k = k+1$ and GOTO step 3.
15. Stop.

3.2 Membership Function

Optimization of multi-objective problem yields a set of non-dominated solutions. However, only one solution would finally be selected as the best that well trades-off the all conflicting objectives.

Typically, it is natural to assume that decision maker may have fuzzy or imprecise goals for each objective function. The membership function based upon fuzzy sets theory, therefore, are introduced to represent the goals of each objective function. The membership function value describes the degree of minimum value attainment of each objective function using values from 0 to 1. The membership value of zero indicates incompatibility with the sets, while one means complete compatibility. Thus, the membership function is a strictly momotonic decreasing and continuous function which is defined as [12]:

$$\mu_j = \begin{cases} 1 & ; \quad F_j \le F_j^{\min} \\ \dfrac{F_j^{\max} - F_j}{F_j^{\max} - F_j^{\min}} & ; \quad F_j^{\min} \le F_j \le F_j^{\max} \\ 0 & ; \quad F_j \ge F_j^{\max} \end{cases} \tag{20}$$

Where μ_j is membership function of objective F_j and $F_j^{\min}, F_j^{\max}$ are minimum and maximum values of the j-th objective, respectively.

3.3 Evaluation of Optimal Solution using the Proposed Fuzzy Multi-attribute Decision Making Approach

The proposed FMADM approach is utilized to elicit the best compromise solution out of a set of non-dominated ones. The concept of FMADM approach can be described as follows. [13]-[16].

Let $X=\{x_1,\ldots, x_n\}$ be a set of optimal solutions. The importance (weight) of the j-th objective is expressed by w_j. The attainment of objective F_j with respect to $F_j^{\min}$ by solution x_i is expressed by the degree of membership $\mu_j(x_i)^{w_j}$.

The procedure for determining the objective weights and the best optimal solution can be described below:

1. Establish by pair-wise comparison the relative importance, α_j, of the fuzzy objectives amongst themselves. Arrange the α_j in a matrix M.

$$M = \begin{bmatrix} \frac{\alpha_1}{\alpha_1} & \frac{\alpha_1}{\alpha_2} & \cdots & \cdots & \frac{\alpha_1}{\alpha_m} \\ \frac{\alpha_2}{\alpha_1} & & & & \\ & & & & \vdots \\ & & & & \vdots \\ \frac{\alpha_m}{\alpha_1} & & & & \frac{\alpha_m}{\alpha_m} \end{bmatrix} \tag{21}$$

2. Determine consistent weights w_j for each objective through approximated Saaty's eigenvector method by normalizing the geometric mean in each row. Thus, the summation of all weights is equal to m, $\sum_{j=1}^{m} w_j = m$.
3. Weight the degrees of objective attainment, $\mu_j(x_i)$ exponentially by the respective w_j. The resulting fuzzy sets are $\mu_j(x_i)^{w_j}$
4. Determine the value of attainment in all objectives of solution x_i via intersection of all $\mu_j(x_i)^{w_j}$:

$$\tilde{D}(x_i) = \mu_1(x_i)^{w_1} \cap \mu_2(x_i)^{w_2} \cap \ldots \cap \mu_m(x_i)^{w_m} \tag{22}$$

5. The best optimal solution, $\tilde{D}(x^*)$, is defined as that achieving the largest degree of membership in $\tilde{D}(x_i)$.

$$\tilde{D}(x^*) = \max\{\tilde{D}(x_i) \mid i = 1,2,\ldots,n\} \tag{23}$$

3.4 Evaluation of Optimal Solution using Fuzzy Cardinal Priority Ranking Normalized Approach

For this approach, the accomplishment of each non-dominated solution is considered with respect to all the n non-dominated solutions by normalizing its accomplishment in all objectives over the sum of the accomplishments of n non-dominated solutions as follows [2], [3], [5], [8]-[9]:

$$\mu_{\tilde{D}}(x_i) = \frac{\sum_{j=1}^{m} \mu_j(x_i)}{\sum_{i=1}^{n}\sum_{j=1}^{m} \mu_j(x_i)} \tag{24}$$

where $\mu_{\tilde{D}}(x_i)$ represents the normalized fuzzy membership function of the the i-th solution. The solution that attains the maximum membership constitutes the best one, $\mu_{\tilde{D}}(x^*)$, owing to having highest cardinal priority ranking. Hence, the best optimal solution is obtained from

$$\mu_{\tilde{D}}(x^*) = \max\{\mu_{\tilde{D}}(x_i) \mid i = 1,2,\ldots,n\} \tag{25}$$

3.5 Evaluation of Optimal Solution through Technique for Order Preference by Similarity to Ideal Solution (TOPSIS)

The concept of TOPSIS is that the most preferred solution should have the shortest distance from the positive ideal solution and, in the meantime, also have the longest distance from the negative ideal solution [4],[17].

The entropy measure of importance is used to score the contrast intensity of the j-th objective. Specifically, the larger entropy is, the less information is transmitted by the j-th objective leading to being removed from further consideration.

Let $R=\{R_{ij} \mid i=1, \ldots, n; j=1, \ldots, m\}$ be performance rating matrix of the i-th solution with respect to the j-th objective where each element represents the degrees of closeness of F_{ij} to $F_j^{\min}$.

$$R = \begin{bmatrix} R_{11} & R_{12} & ... & R_{1m} \\ R_{21} & R_{22} & ... & R_{2m} \\ ... & ... & ... & ... \\ R_{n1} & R_{n2} & ... & R_{nm} \end{bmatrix} \quad (26)$$

Then, normalizing the performance rating matrix in Eq.(26) for each objective as

$$p_{ij} = \frac{R_{ij}}{\sum_{k=1}^{n} R_{kj}} \quad (27)$$

The contrast intensity of the *j*-th objective can now be measured to consider the amount of decision information contained in and transmitted by the objective by means of Shannon's entropy measure (e_j) which is defined as.

$$e_j = -\frac{1}{\ln n} \sum_{i=1}^{n} p_{ij} \ln p_{ij} \quad (28)$$

Thus, a total entropy is

$$E = \sum_{j=1}^{m} e_j \quad (29)$$

The objective weight ($\tilde{\lambda}_j$), therefore, is given by

$$\tilde{\lambda}_j = \frac{1}{m-E}(1-e_j) \quad (30)$$

The normalized performance rating element in Eq.(27) is now weighted as

$$v_{ij} = \tilde{\lambda}_j p_{ij} \ , \ j = 1, 2,\ldots, m; i=1, 2,\ldots, n \quad (31)$$

The next step is to find the set of positive ideal solution (A^+) and negative ideal solution (A^-) which are defined by

$$A^+ = (\max(v_{i1}), \max(v_{i2}),..., \max(v_{im})) = (v_1^+, v_2^+,..., v_m^+) \quad (32)$$

$$A^- = (\min(v_{i1}), \min(v_{i2}),..., \min(v_{im})) = (v_1^-, v_2^-,..., v_m^-) \quad (33)$$

Hence, the distance of each solution from the positive ideal solution is given as

$$d_i^+ = \sqrt{\sum_{j=1}^{m} (v_{ij}^+ - v_{ij})^2} \quad (34)$$

Likewise, the distance of each solution from the negative ideal solution is given as

$$d_i^- = \sqrt{\sum_{j=1}^{m} (v_{ij} - v_{ij}^-)^2} \quad (35)$$

The relative closeness to the positive ideal solution of the *i*-th solution is defined as

$$c_i = \frac{d_i^-}{d_i^+ + d_i^-} \quad (36)$$

The most preferred solution is the solution having the highest c_i value.

3.6 Comparing FMADM Approach to FCPRN Approach and TOPSIS Approach

The objective of comparing the proposed FMADM approach to FCPRN approach and TOPSIS approach is to demonstrate that the best optimal solution obtained from the proposed FMADM approach having more compromise characteristics than both FCPRN and TOPSIS approach in terms of both percentage total deviation from the ideal solution and fulfilling the preferred zones condition.

As the ideal solution that one wishes to attain in multi-objective problem is the solution consisting of minimum value in all objectives, therefore, it can be represented as $F^{ideal} = \left\{F_1^{\min}, F_2^{\min},..., F_m^{\min}\right\}$ when let F^{ideal} be a set of the ideal solution. Such a solution, however, is impossible one due to all objectives having conflicting characteristics one another. Nonetheless, there is an attempt to elicit the best optimal solution which has the values in the vicinity of the minimum in all objectives as best possible

Accordingly, two measures below are utilized to compare the solution qualities obtained from FMADM, FCPRN and TOPSIS approach.

3.6.1 Percentage Total Deviation from the Ideal Solution (ε_i) . This measure uses the concept of Euclidean distance between two points in *n*-dimensions. Hence, the percentage total deviation between the chosen optimal solution and the ideal solution can be defined as.

$$\varepsilon_i = 100 * \sqrt{\sum_{j=1}^{m} \left(\frac{F_j^* - F_j^{\min}}{F_j^{\min}} \right)^2} \quad (37)$$

where

F_j^* is the optimal value of objective F_j of the chosen solution.

$F_j^{\min}$ is the minimum value of objective F_j

m is the number of objectives.

3.6.2 Preferred Zones Condition (PZ_j) Here is the condition to check whether the objective values of the obtained solution is in the preferred zones by vetting from

$$PZ_j = \left(\frac{F_j^{\max} + F_j^{\min}}{2} \right) - F_j^* \geq 0 \quad (38)$$

Specifically, this condition help check whether the

chosen solution has a well-balanced characteristics in all objectives. Only the criterion of percentage total deviation from the ideal solution (ε_i) is not enough to indicate that the solution with lower value of ε_i is the better one since certain objectives may have the dominant tendency towards the minimum value whereas the others probably rather away from the their respective minimum. As a result, it would be more favorable should all objectives of the chosen solution is in the preferred zones. In other words, they all have a good tendency towards the minimum value. The term in the bracket of Eq.(38) is referred to as threshold value.

4. NUMERICAL RESULTS

In this section, two numerical examples are provided to demonstrate the main features of the proposed approach. The simulation program of the proposed approach is written in MATLAB and run on 1.6 GHz Pentium M processor with 512 MB of RAM.

In this study, all objective functions are assumed to have an equal importance. That means all w_j of Eq.(22) having the value of one in order that the obtained results are compared basing upon the same underlying hypotheses as above-mentioned FCPRN and TOPSIS approach. Also, it should be noted that such weight combinations do not involve the weight used in Eq.(11) since those weight combinations are simply employed to produce the different non-dominated solutions. They, therefore, do not involve in decision making for extracting the best optimal solution. The input information for the first test system is given below.

Test System 1: Three Generators with Four Objectives

Fuel Cost Characteristics of Thermal Plants($/h)

$$F_{11} = 5.25x10^{-3}P_1^2 + 8.6625P_1 + 328.125$$

$$F_{12} = 6.085x10^{-3}P_2^2 + 10.0403P_2 + 136.9125$$

$$F_{13} = 5.9155x10^{-3}P_3^2 + 9.7606P_3 + 59.155$$

NO_X Emission Characteristics of Thermal Plants (kg/h)

$$F_{21} = 0.006323P_{g1}^2 - 0.38128P_{g1} + 80.9019$$

$$F_{22} = 0.006483P_{g2}^2 - 0.79027P_{g2} + 28.8249$$

$$F_{23} = 0.003174P_{g3}^2 - 1.36061P_{g3} + 324.1775$$

SO_2 Emission Characteristics of Thermal Plants (kg/h)

$$F_{31} = 0.001206P_{g1}^2 + 5.05928P_{g1} + 51.3778$$

$$F_{32} = 0.002320P_{g2}^2 + 3.84624P_{g2} + 182.2605$$

$$F_{33} = 0.001284P_{g3}^2 + 4.45647P_{g3} + 508.5207$$

CO_2 Emission Characteristics of Thermal Plants (kg/h)

$$F_{41} = 0.265110P_{g1}^2 - 61.01945P_{g1} + 5080.148$$

$$F_{42} = 0.140053P_{g2}^2 - 29.95221P_{g2} + 3824.770$$

$$F_{43} = 0.105929P_{g3}^2 - 9.552794P_{g3} + 1342.851$$

The B-Coefficients (MW^{-1})

$$B_{ij} = \begin{bmatrix} 1.36255x10^{-4} & 1.753x10^{-5} & 1.8394x10^{-4} \\ 1.754x10^{-5} & 1.5448x10^{-4} & 2.82765x10^{-4} \\ 1.8394x10^{-4} & 2.82765x10^{-4} & 1.6147x10^{-3} \end{bmatrix}$$

Power output constraint

$$50 \le P_1 \le 250\,\text{MW}$$

$$5 \le P_2 \le 150\,\text{MW}$$

$$15 \le P_3 \le 100\,\text{MW}$$

The load demand is 190 MW

Table 1. Comparison of the Best Compromise Solution derived from FMADM , FCPRN and TOPSIS Approach (3 Generators, 4 Objectives)

Approach		F1	F2	F3	F4
FCPRN	Value	2,450.84	*392.09*	1,637.92	5,286.81
	PZ	+	-	+	+
	Weight	0.3	0.3	0.4	0.0
TOPSIS	Value	*2,657.82*	302.26	*1,706.41*	*6,637.65*
	PZ	-	+	-	-
	Weight	0.0	1.0	0.0	0.0
FMADM	Value	2,487.43	369.18	1,635.50	5,556.68
	PZ	+	+	+	+
	Weight	0.2	0.4	0.4	0.0
MDS	Value	2,509.35	343.46	*1,674.95*	5,642.26
	PZ	+	+	-	+
	Weight	0.3	0.7	0.0	0.0
Minimum Value		2,393.91	302.26	1,604.01	5,183.75
Maximum Value		2,657.82	475.01	1,706.73	6,637.76
Threshold Value		2,525.87	388.64	1,655.37	5,910.76

The 224 non-dominated solutions are produced considering all the objectives concurrently through 224 different weight combinations using Newton-Raphson algorithm. The running time for eliciting the best compromise solution from the proposed FMADM approach takes 872.30 s.

Table 1 illustrates the comparison of the best

compromise solutions obtained from the FMADM, FCPRN and TOPSIS approach in terms of objective value including checking the preferred zones condition. The percentage total deviation from the minimum of the solution obtained from FMADM, FCPRN and TOPSIS approach are shown in Table 2.

As seen from Table 1, the FMADM approach is the only one approach which is satisfied with preferred zones condition since all PZ_j have positive sign. That means the obtained solution having a good balance towards the minimum in all objectives.

Minimum deviation solution (MDS) shown in Table 1 is the solution yielding the lowest percentage total deviation from the ideal solution which can be seen in Table 2. It is noted that despite MDS having the lowest percentage total deviation, it still have certain objectives having the value higher than the threshold value. In other words, some objectives of MDS have the values further away from the ideal solution than the best optimal solution derived from FMADM approach.

Table 2. Percentage Total Deviation from the Ideal Solution (3 Generators, 4 Objectives)

Approach	Deviation from the Ideal Value (%)				Total Deviation (%)
	F1	F2	F3	F4	
FCPRN	2.38	29.72	2.11	1.99	29.96
TOPSIS	11.02	0.00	6.38	28.05	30.80
FMADM	3.91	22.14	1.96	7.19	23.69
MDS	4.82	13.63	4.42	8.85	17.52

As seen from Table 2, the FMADM approach yields the solution having percentage total deviation from the ideal solution lower than both FCPRN and TOPSIS approach. Also, it should be noted that TOPSIS approach does not yield the lowest percentage total deviation despite the fact that it uses the concept of selecting the solution which has the shortest distance from the positive ideal solution, meanwhile, also has the longest distance from the negative ideal solution. This is because the weight of second objective ($\tilde{\lambda}_2$), for decision making according to Eq.(30), has the value much higher than the others especially when compared to $\tilde{\lambda}_1$ and $\tilde{\lambda}_3$ as shown below

$$\tilde{\lambda}_1 = 0.035891 \qquad \tilde{\lambda}_2 = 0.636456$$

$$\tilde{\lambda}_3 = 0.011373 \qquad \tilde{\lambda}_4 = 0.316280$$

This is resulted from objective F2 having high contrast intensity when compared to the objective F1 and F3

TOPSIS's mechanism for selecting the most preferred solution, therefore, boils down to attempting to elicit the solution which has the value of objective F2 approaching its minimum as nearest as possible. From calculating the value of relative closeness to the positive ideal solution (c_i) using Eq.(36), the solution that produces the highest c_i is the solution yielding the minimum value of objective F2 thereby making the percentage total deviation of objective F2 zero.

Importantly, it should be noticed that the best optimal solution obtained from TOPSIS approach is the one which also provides the maximum value of objective F1, in the meantime, the value of both objective F3 and F4 is approaching their respective maximum. Hence, it is considered as an extreme solution thereby making it rather difficult to be chosen in real-world application.

Test System 2: Six Generators with Three Objectives

The information for the second test system is given below.

Fuel Cost Characteristics of Thermal Plants($/h)

$$F_{11} = 0.002035P_{g1}^2 + 8.43205P_{g1} + 85.6348$$

$$F_{12} = 0.003866P_{g2}^2 + 6.41031P_{g2} + 303.7780$$

$$F_{13} = 0.002182P_{g3}^2 + 7.42890P_{g3} + 847.1484$$

$$F_{14} = 0.001345P_{g4}^2 + 8.30154P_{g4} + 274.2241$$

$$F_{15} = 0.002182P_{g5}^2 + 7.42890P_{g5} + 847.1484$$

$$F_{16} = 0.005963P_{g6}^2 + 6.91559P_{g6} + 202.0258$$

NO_X Emission Characteristics of Thermal Plants (kg/h)

$$F_{21} = 0.006323P_{g1}^2 - 0.38128P_{g1} + 80.9019$$

$$F_{22} = 0.006483P_{g2}^2 - 0.79027P_{g2} + 28.8249$$

$$F_{23} = 0.003174P_{g3}^2 - 1.36061P_{g3} + 324.1775$$

$$F_{24} = 0.006732P_{g4}^2 - 2.39928P_{g4} + 610.2535$$

$$F_{25} = 0.003174P_{g5}^2 - 1.36061P_{g5} + 324.1775$$

$$F_{26} = 0.006181P_{g6}^2 - 0.39077P_{g6} + 50.3808$$

SO_2 Emission Characteristics of Thermal Plants (kg/h)

$$F_{31} = 0.001206P_{g1}^2 + 5.05928P_{g1} + 51.3778$$

$$F_{32} = 0.002320P_{g2}^2 + 3.84624P_{g2} + 182.2605$$

$$F_{33} = 0.001284P_{g3}^2 + 4.45647P_{g3} + 508.5207$$

$$F_{34} = 0.000813P_{g4}^2 + 4.97641P_{g4} + 165.3433$$

$$F_{35} = 0.001284P_{g5}^2 + 4.45647P_{g5} + 508.5207$$

$$F_{36} = 0.003578P_{g6}^2 + 4.14938P_{g6} + 121.2133$$

The B-Coefficients (MW^{-1})

$$B_{ij} = \begin{bmatrix} 20 & 1 & 1.5 & 0.5 & 0 & -3 \\ 1 & 30 & -2 & 0.1 & 1.2 & 1 \\ 1.5 & -2 & 10 & -1 & 1 & 0.8 \\ 0.5 & 0.1 & -1 & 15 & 0.6 & 5 \\ 0 & 1.2 & 1 & 0.6 & 25 & 2 \\ -3 & 1 & 0.8 & 5 & 2 & 21 \end{bmatrix} \text{x}10^{-5}$$

Power output constraint

$90 \le P_1 \le 350$ MW

$100 \le P_2 \le 500$ MW

$200 \le P_3 \le 800$ MW

$100 \le P_4 \le 500$ MW

$150 \le P_5 \le 600$ MW

$100 \le P_6 \le 500$ MW

The load demand is 1800 MW.

The different 58 weight combinations are used to generate the 58 non-dominated solutions. The running time for this test system takes 676.52 s to derive the best compromise solution from the proposed approach.

Table 3. Comparison of the Best Compromise Solution obtained from FMADM, FCPRN and TOPSIS Approach (6 Generators, 3 Objectives)

Approach		F1	F2	F3
FCPRN	Value	18,745.90	2,165.21	11,236.45
	PZ	+	+	+
	Weight	0.4	0.3	0.3
TOPSIS	Value	*18,950.86*	2,070.13	*11,356.50*
	PZ	-	+	-
	Weight	0.0	1.0	0.0
FMADM	Value	18,778.75	2,122.26	11,255.47
	PZ	+	+	+
	Weight	0.4	0.5	0.1
MDS	Value	*18,862.17*	2,079.83	*11,304.31*
	PZ	-	+	-
	Weight	0.2	0.8	0.0
Minimum Value		18,721.38	2,070.13	11,222.94
Maximum Value		18,950.86	2,282.97	11,356.50
Threshold Value		18,836.12	2,176.55	11,289.72

The comparison of objective value and checking the preferred zones condition of the best optimal solution obtained from the FMADM, FCPRN and TOPSIS approach are given in Table 3. Percentage total deviation from the ideal solution is shown in Table 4. It can be seen in Table 3 that both the FMADM and FCPRN approach yields all objective values satisfied with preferred zones condition due to all PZ_j having positive sign. On the contrary, TOPSIS and MDS approach has certain objectives unsatisfied with the preferred zones condition which is likewise the above result in test system 1.

Table 4. Percentage Total Deviation from the Ideal Solution (6 Generators, 3 Objectives)

Approach	Deviation from the Ideal Value (%)			Total Deviation (%)
	F1	F2	F3	
FCPRN	0.13	4.59	0.12	4.60
TOPSIS	1.23	0.00	1.19	1.71
FMADM	0.31	2.52	0.29	2.55
MDS	0.75	0.47	0.73	1.14

Given the percentage total deviation, FCPRN approach still has the value higher than the proposed approach which is similar to the results of test system 1. The percentage deviation value of objective F2 derived from TOPSIS approach is zero since the objectives weight $\tilde{\lambda}_2$ is much more dominant than the others, namely $\tilde{\lambda}_2 =$ 0.985941 whereas $\tilde{\lambda}_1$ and $\tilde{\lambda}_3$ is 0.007258 and 0.006801 respectively. Thus, both $\tilde{\lambda}_1$ and $\tilde{\lambda}_3$ hardly effects decision making. Consequently, the mechanism for selecting the most preferred solution of TOPSIS approach is an attempt to choose the solution approaching F2 as closet as possible.

Incidentally, the percentage total deviation of TOPSIS approach becomes lower than the FMADM approach in this test system as the obtained solution yields the minimum value to the objective which has high contrast intensity, F2, meanwhile the rest of objectives having low contrast intensity have been decreased.

In addition, it should also be observed that the best optimal solution obtained from the TOPSIS approach gives the minimum value of objective F2, meanwhile, it also provides the maximum value for objective F1 and F3. It is obvious that the consequence is likewise the result in test system 1. Therefore, the solution obtained from TOPSIS approach is regarded as an extreme solution and is less compromise than the one derived from the FMADM approach. In practical way, despite the fact that the objectives for reducing environmental effects is increasingly concerned, the operating fuel cost objective (F1), however, is still the important one that always have to be considered and can not be neglected.

Thus, it is unfavorable to choose the best optimal solution yielding the maximum operating fuel cost or so since it is a key factor that determines viability of a utility. Consequently, it would be more favorable should the best optimal solution of multi-objective problem have well-balanced characteristics in all objectives towards their respective minimum.

5. CONCLUSION

The proposed fuzzy multi-attribute decision making approach was applied to help system operators extract the best compromise solution out of a set of non-dominated solutions of multi-objective thermal power dispatch problem. The obtained best compromise solution is compared to the ones derived from fuzzy cardinal priority ranking normalized approach (FCPRN) and the technique for order preference by similarity to ideal solution (TOPSIS) by means of two measures viz. percentage total deviation from the ideal solution and preferred zones condition

Given the percentage total deviation from the ideal solution, it is evident that the solution obtained from the FMADM approach is superior to the one derived form FCPRN approach. For TOPSIS approach, when the number of objectives has been increased, the value of percentage total deviation becomes larger, in the meantime, also higher than the value obtained from the proposed approach. Moreover, the solution obtained from TOPSIS approach is considered an extreme solution since it has an inclination to produce the minimum in an objective, meanwhile, they also yields the maximum or so for others.

For preferred zones condition, it helps check the quality of balance in all objectives towards the minimum. The simulation results demonstrate that the proposed FMADM approach is superior to TOPSIS approach. For the FCPRN approach, even it has fulfilled the condition in the case of the reducing the number of objective functions from four to three, however, its percentage total deviation still has the value higher than the proposed approach.

Thus, taking these two measures into account concurrently, the FMADM approach demonstrates that it can elicit the best optimal solution which has characteristics more compromise and favorable than its counterparts. The further research will be focused on the effects of the best compromise solution obtained from FMADM, FCPRN and TOPSIS approach when each objective has different important degree.

REFERENCES

[1] El-Waki M.M. (1984). *Power Plant Technology*. Singapore: McGraw-Hill, Inc.

[2] Wang Lingfeng & Singh Chanan (2007). Environmental/economic power dispatch using a fuzzified multi-objective particle swarm optimization algorithm. *Electric Power Systems Research*, 77 (2007), 1654–1664

[3] Bo Zhao & Yi-jia Cao (2005). Multiple objective particle swarm optimization technique for economic load dispatch. *Electric Power Systems Research*, 77, 1654–1664

[4] Xuebin Li. (2009). Study of multi-objective optimization and multi-attribute decision making for economic and environmental power dispatch. *Electric Power Systems Research*, 79 (2009), 789–795.

[5] Abido M.A. (2003). A novel multiobjective evolutionary algorithm for environmental/economic power dispatch. *Journal of Zhejiang University Science*, 6A(5), 420-427

[6] Engelbrecht Andries P. (2005) *Fundamentals of Computational Swarm Intelligence*. Great Britain: John Wiley & Sons, Ltd.

[7] Coello Coello Carlos A. (2002). *Evolutionary Algorithms for Solving Multi-Objective Problems*. New York: Kluwer Academic/Plenum Publishers.

[8] Dhillon J.S., Parti S.C., Kothari D.P. (2001). Fuzzy decision making in multiobjective long-term scheduling of hydrothermal system. *Electrical Power and Energy Systems*, 24, 19-29.

[9] Dhillon J.S., Parti S.C., Kothari D.P. (2002). Fuzzy decision making in stochastic multiobjective short-term hydrothermal scheduling. *Proceedings Generation, Transmission & Distribution*, (pp. 191-200), vol. 149, no. 2.

[10] Kothari D.P. & Dhillon (2004). *Power System Optimization*. New Delhi: Prentice-Hall of India Private Limited.

[11] Hadi Saadat (2004). *Power System Analysis.* Singapore: The McGraw-Hill Companies.

[12] Zimmermann, H.-J. (1991). *Fuzzy Set Theory and Its Application*. Boston: Kluwer Academic Publishers.

[13] Zimmermann, H.-J. (1987). *Fuzzy Set, Decision Making, and Expert Systems*. Boston: Kluwer Academic Publishers.

[14] Saaty, Thomas L. (1980). *The Analytic Hierarchy Process. Planning, Priority Setting, Resource Allocation*. New York: McGrw-Hill, Inc.

[15] Saaty, Thomas L. (1990). *The Analytic Hierarchy Process Planning, Priority Setting, Resource Allocation*. United States of America: RWS Publications.

[16] Saaty, Thomas L. (1996). *Decision Making with Dependence and Feedback. The Analytic Network Process*. United States of America: RWS Publicaions.

[17] M. Zeleny (1982), *Multiple Criteria Decision Making*, McGraw-Hill, New York.

Optimal Capacitor Placement in Unbalanced Loading Distribution System with Nonlinear Loads by Adaptive Particle Swarm Technique

S. Auchariyamet and S. Sirisumrannukul

***Abstract*—** *A capacitor placement problem in an unbalanced loading distribution system with the presence of nonlinear loads is formulated in this paper. The objective function of the problem is to minimize the total annual cost comprising the costs of energy loss, peak demand loss, and capacitor investment. This objective function is subjected to power flow equations, bus voltage limits, voltage distortion constraint, and also maximum capacitor kVAr to be installed at each bus. An adaptive particle swarm optimization (PSO) is proposed to search for an optimal or near-optimal solution. This adaptive technique appropriately activates the last obtained solution to seek for better solutions when a fixed number of iterations are reached or when no improvement solution is observed over the course of iterations. A radial distribution system of Provincial Electricity Authority (PEA), Thailand, which consists of 28 buses and 19 load points with a two-step load pattern, is studied to demonstrate the effectiveness of the proposed methodology. Test results indicate that the obtained optimal solutions give a saving in the total cost while satisfying all the specified constraints. In addition, the effects of unbalanced loading and nonlinearity of load on the optimal solutions are investigated. It is found that increases of these two factors introduce more total loss in the network and more total capacitor kVAr required for reactive power compensation, and therefore the saving in the total cost is decreased due to more investment cost for capacitors.*

***Keywords*— Capacitor placement, Nonlinear loads, Particle swarm optimization, Unbalanced distribution system.**

1. INTRODUCTION

Electrical energy from power plants is transmitted to end-use customers by transmission and distribution systems. Around 13% of power generated is consumed as power loss at the distribution levels [1]. The power loss is determined as function of square of branch current which consists of real and reactive component. A portion of power loss in distribution systems, produced by reactive current, could be diminished by capacitor placement which is one of the most effective and useful methods.

With shunt capacitors, reactive power compensation is provided to reduce power and energy loss, to regulate bus voltages, to improve power quality, and to release feeders and system capacity. The extent of these advantages depends on how capacitors are placed in the distribution system. For this reason, it is necessary to solve capacitor placement problem to simultaneously determine the optimal locations, sizes, and types of capacitors.

Special attention should be paid to capacitor placement when nonlinear loads appear in the distribution system owing to widely used power electronics-base devices. This is because nonlinear loads behave as harmonic current sources. Sizes and locations of shunt capacitor are significant factors that response to harmonics. The combination of harmonic sources, system reactance, and capacitors introduce both series and parallel resonant frequencies to the networks. Due to the resonant conditions, the total harmonic distortion can be magnified greater than the permissible level. The capacitor placement problem, therefore, should take harmonic constraint into account to assure that the obtained optimal solution does not result in an excessive harmonic distortion.

The practical aspects of distribution system should also be considered when the capacitor placement problem is formulated. The actual distribution feeders are unbalanced because of the existence of single-phase and two-phase line segments as well as the three-phase unbalanced loads and the mutual coupling among phase conductors [2]. With unbalanced conditions, the generation and propagation of harmonics are more complicated [3]. Furthermore, the inclusion of system unbalances increases the dimension of the capacitor placement problem because all three phases have to be considered instead of the single phase balanced representation.

The capacitor placement problem is a zero-one decision with discrete step of standard capacitor bank size, each step of which has a different installation cost. Such zero-one decision and discrete steps make the problem as a nonlinear and non-differentiable mixed integer optimization problem. In addition, the solutions to be analyzed generally increase with the size of distribution system. The capacitor placement problem is, therefore, a hard and large-scale combinatorial problem, where most of conventional optimization tools find it difficult to search for the optimal solution.

One efficient method to solve the capacitor placement problem is particle swarm optimization (PSO). PSO is a heuristic search technique inspired by social interaction

S. Auchariyamet (corresponding author) and S. Sirisumrannukul are with Department of Electrical Engineering, Faculty of Engineering, King Mongkut's University of Technology North Bangkok, 1518, Pibulsongkram Rd., Bangsue, Bangkok, 10800, Thailand. Phone: +66-81-930-0211; E-mail: s4910190042@kmutnb.ac.th and spss@kmutnb.ac.th.

in herd of animals (e.g. bird flocks or fish schools). It was first introduced in 1995 [4]. Many advances in PSO development extend its abilities to handle difficult optimization problems in science and engineering fields. Key attractive advantages of PSO are its simplicity in concept and implementation, less computation time, and inexpensive memory for computer resource.

The capacitor placement problem is a combinatorial optimization problem that features a multimodal landscape of locally optimal solutions scattering throughout the search space. In some cases where the globally optimal solutions are slightly different from locally optimal solutions, the use of a conventional PSO algorithm would get trapped at local optimums. For this reason, the conventional PSO algorithm requires some variations to remedy this drawback. This paper presents an adaptive PSO technique to seek for an optimal or near-optimal solution at some other regions in the search space. The key of the approach is a modification on the last obtained solution with the proper number of activations during the computational process. The effectiveness of the proposed methodology is illustrated by test results of an 85-bus distribution system.

The objective function of capacitor placement problem in unbalanced loading distribution system connected to nonlinear loads is to minimize the total annual cost comprising the costs of energy loss, peak demand loss, and capacitor investment. This objective function is subjected to power flow equations, bus voltage limits, voltage distortion constraint, and number of discrete capacitors to be installed at each bus. A 28-bus distribution system with a two-step load pattern of Provincial Electricity Authority (PEA), Thailand, is used to investigate the effects of unbalanced loading and nonlinearity of load on the optimal solutions.

2. PROBLEM FORMULATION

The objective function of the capacitor placement problem is to minimize the total annual cost due to energy loss cost, peak power loss cost, and the investment cost of fixed and switched type capacitors. It can be stated as:

$$\min F = (\sum_{i=1}^{nl} k_{e,i} T_i P_i) + k_p P_{lp} + (\sum_{j \in SCf} k_{cf} Q_j^{cf}) + (\sum_{j \in SCs} k_{cs} Q_j^{cs}) \quad (1)$$

where F = total cost ($, Baht)

nl = number of load levels

$k_{e,i}$ = cost of energy loss for load level i ($/kWh, Baht/kWh)

T_i = time duration for load level i (hr)

P_i = power loss for load level i (kW)

k_p = cost of peak power loss ($/kW, Baht/kW)

P_{lp} = peak power loss (kW)

SC_f, SC_s = set of buses for fixed and switched type capacitor placement

k_{cf}, k_{cs} = investment cost for fixed and switched type capacitor ($/kVAr, Baht/kVAr)

Q_j^{cf}, Q_j^{cs} = fixed and switched type capacitor installed at bus j (kVAr)

Power loss, P_i, in Equation (1) is the summation of losses from all branches in the system being considered. Since branch loss is determined from loss in each phase of that branch. P_i, therefore, can be written as [5]:

$$P_i = \sum_{k=1}^{L} [\mathbf{I}_{k,i}]^T [\mathbf{R}_k] [\mathbf{I}_{k,i}] \quad (2)$$

where P_i = power loss for load level i (kW)

L = number of branches in the system

$[\mathbf{I}_{k,i}]$ = three-phase rms current matrix in branch k for load level i (A)

$[\mathbf{R}_k]$ = three-phase resistance matrix of branch k (ohm)

$[\mathbf{I}_{k,i}]$ and $[\mathbf{R}_k]$ in Equation (2) are expressed as:

$$[\mathbf{I}_{k,i}] = \begin{bmatrix} \sqrt{\sum_{h=1}^{nh} \left| I_{k,i}^{A,h} \right|^2} \\ \sqrt{\sum_{h=1}^{nh} \left| I_{k,i}^{B,h} \right|^2} \\ \sqrt{\sum_{h=1}^{nh} \left| I_{k,i}^{C,h} \right|^2} \end{bmatrix} \quad (3)$$

$$[\mathbf{R}_k] = \begin{bmatrix} r_k^{AA} & r_k^{AB} & r_k^{AC} \\ r_k^{BA} & r_k^{BB} & r_k^{BC} \\ r_k^{CA} & r_k^{CB} & r_k^{CC} \end{bmatrix} \quad (4)$$

where nh = maximum harmonic order

$\left| I_{k,i}^{p,h} \right|$ = current magnitude of phase p in branch k for load level i at harmonic order h

p = $\{A, B, C\}$

$r_k^{AA}, r_k^{BB}, r_k^{CC}$ = self resistance of conductor in phase A, B, C of branch k (ohm)

$r_k^{AB}, r_k^{AC}, r_k^{BA}$ $r_k^{BC}, r_k^{CA}, r_k^{CB}$ = mutual coupling resistance between phase conductor of branch k (ohm)

The objective function is subjected to the following operational constraints.

- Three-phase power balance equations at fundamental frequency.
- Bus voltage and voltage distortion contraints:

$$V_{\min} \le \sqrt{\left|V_{j,i}^{p,1}\right|^2 + \sum_{h\neq 1}^{nh}\left|V_{j,i}^{p,h}\right|^2} \le V_{\max} \quad (5)$$

$$THD_{j,i}^{p}(\%) = 100\times\frac{\sqrt{\sum_{h\neq 1}^{nh}\left|V_{j,i}^{p,h}\right|^2}}{\left|V_{j,i}^{p,1}\right|} \le THD_{\max} \quad (6)$$

where $\left|V_{j,i}^{p,1}\right|$ = voltage magnitude in phase p of bus j for load level i at fundamental frequency

$\left|V_{j,i}^{p,h}\right|$ = voltage magnitude in phase p of bus j for load level i at harmonic order h

nh = maximum harmonic order

$V_{\min}$ = minimum limit of bus voltage

$V_{\max}$ = maximum limit of bus voltage

$THD_{j,i}^{p}$ = total harmonic distortion of voltage in phase p at bus j for load level i

$THD_{\max}$ = maximum permissible limit for total harmonic distortion of voltage

- Limitation of capacitor kVAr to be placed at each bus:

$$0 \le Q_{j,i}^{c} \le Q_{\max}^{c} \quad (7)$$

where $Q_{j,i}^{c}$ = capacitor to be placed at bus j for load level i (kVAr)

$Q_{\max}^{c}$ = maximum capacitor to be placed at any bus (kVAr)

3. THE CONVENTIONAL PSO ALGORITHMS

The PSO technique conducts the searching process using a population of particles. Each particle represents a potential solution in n -dimensional search space of the problem being considered. Particles change their positions, from current iteration to next iteration, based on their velocities to locate a good optimum. In general, the implementation of a conventional PSO algorithm consists of three main steps, namely, 1) generate initial particle's positions and velocities, 2) evaluate fitness value of each particle, and 3) update velocity and position of all particles [6].

First, the positions and velocities of the initial swarm of particles are randomly generated to allow all particles randomly distributed across the search space. The fitness value of each particle is evaluated in the second step to determine the best position of each particle and also to reveal the particle that has the best global fitness value in the current swarm. Next, the velocities of all particles are updated by using the information from the current velocity, the best solution of each particle, and the best solution found by the best particle in swarm. The velocity update from iteration t to $(t+1)$ can be expressed as [7]:

$$\begin{aligned} v_{id}(t+1) &= wv_{id}(t) + c_1 r_{1d}(t)[y_{id}(t) - x_{id}(t)] \\ &\quad + c_2 r_{2d}(t)[\hat{y}_d(t) - x_{id}(t)] \end{aligned} \quad (8)$$

where x = position of particle

v = velocity of particle

w = inertia weight

c_1, c_2 = positive acceleration constants

r_{1d}, r_{2d} = uniformly distributed random values in the range [0,1]

y = personal best position

$\hat{y}$ = global best position

i = i^{th} particle

d = d^{th} dimension

id = particle i in dimension d

Position update is the last step. The new position of each particle is calculated by [7]:

$$x_{id}(t+1) = x_{id}(t) + v_{id}(t+1) \quad (9)$$

The step of velocity and position update is repeated and will terminate when a stopping criterion is met, e.g. maximum number of iteration is reached or the change in solution is smaller than the pre-specified tolerance.

4. THE PROPOSED ADAPTIVE PSO FOR CAPACITOR PLACEMENT PROBLEM

When a conventional PSO algorithm is applied to solve the capacitor placement problem, each particle will represent the size of capacitor to be placed at each bus for all load levels. Power flow is employed to calculate bus voltages and power losses, while the total cost is defined as a fitness value.

Since the capacitor placement problem has multimodal of locally optimal solutions [8], if solutions during the iterative process of conventional PSO are detected no improvement, it may result from convergence to an optimal solution or from being trapped at any local optimums. For the later case, a conventional PSO search algorithm should be tried to seek for better solutions at some other regions in the search space. This could be done by activating the position of particles (i.e., randomly generate with a uniform probability distribution) at the prespecified iteration instead of updating them by Equation (9). After activation, the process of position update in the conventional PSO algorithm resumes as normal. In this work, the PSO algorithm combined with the activation of particles is called adaptive PSO.

The key point of the adaptive PSO technique is to identify the appropriate numbers of activation. Two methods are suggested as follows:

1) Activate the solution when a fixed number of iterations are reached.

2) Activate the solution when no improvement solution is observed over the course of iterations.

The numerical results from 300 independent experimental runs with 10-, 15-, 23-, 34-, 69- and 85-bus systems indicate that when the proposed adaptive PSO is implemented with the proper numbers of activation, it can introduce an improvement in optimal solution which results in the reduction of total cost about 5-10% compared with that given by the conventional PSO. However, there is a probability about 0.3 that this technique will offer worse solutions compared with those without the activation. For this reason, the solution before activation should be stored and compared with the solution after the activation. The one with a better total cost will be selected as the final solution.

To demonstrate the performance of the proposed adaptive PSO, the test results of three cases from one experiment with an 85-bus system are presented in Table 1.

Table 1. Summary of test results from an 85-bus system

	Case A	Case B	Case C
Loss at light load (kW)	124.37	104.39	92.13
Loss at medium load (kW)	154.21	146.12	146.54
Loss at peak load (kW)	261.43	254.21	252.23
Total capacitor (kVAr)	7,350	6,150	5,700
Peak power loss cost ($)	31,372	30,505	30,268
Energy loss cost ($)	70,668	65,619	63,979
Capacitor cost ($)	2,595	2,198	2,018
Total cost ($)	104,635	98,322	96,265
Reduction in total cost (%)	-	6.03	7.99

The solution in case A is obtained from a conventional PSO algorithm while the solutions in cases B and C are calculated from the adaptive PSO. For case B, the activation point, identified by method 1, is set at iteration 150, whereas the activation points in case C are defined by method 2; that is, if the total cost remains unchanged for 30 iterations, the solution will be activated. The convergence characteristics for the three cases are given in Figures 1 to 3.

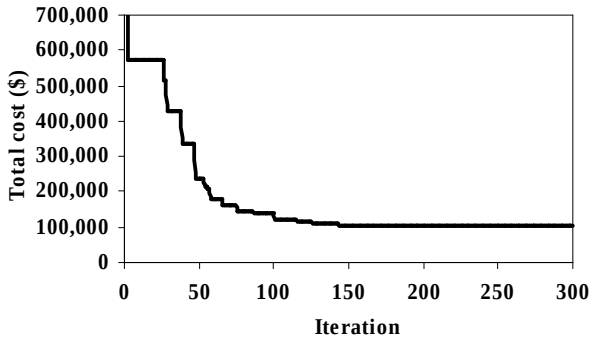

Fig. 1. Convergence characteristic of total cost in an 85-bus system obtained from Case A.

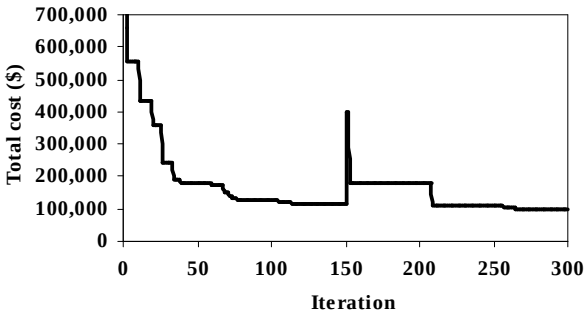

Fig. 2. Convergence characteristic of total cost in an 85-bus system obtained from Case B.

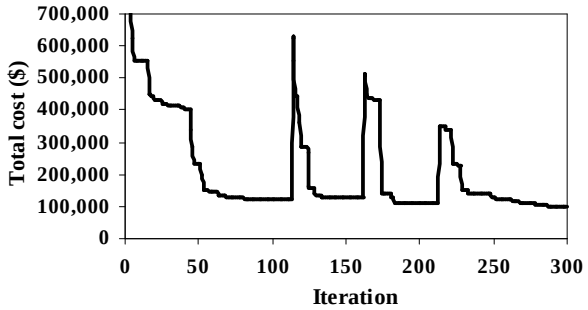

Fig. 3. Convergence characteristic of total cost in an 85-bus system obtained from Case C.

It can be seen from Table 1 that the proposed adaptive PSO have lower total capacitor, peak power loss cost, energy cost, capacitor cost, and total cost. In Figure 1, the solution of case A converges at iteration 160 with a total cost of $104,635. Case B, whose solution is activated just only one time at iteration 150 as shown in Figure 2, gives a total cost of $98,322. In case C, the solution is activated three times at iterations 113, 162, and 212 as shown in Figure 3, gives a total cost of $96,265. The total cost of cases B and C are about 6% and 8% lower than that of case A respectively.

The tests results of an 85-bus distribution system demonstrate that with activation, better solutions are found, indicating the effectiveness of the proposed adaptive PSO. However, because the appropriate number of activations for both methods cannot be determined in advance, experimental runs are still required but it is worth doing so as there is a high possibility to obtain improved solutions. Note that this proposed technique, as in many heuristic techniques, does not guarantee the globally optimal solution, but at least this adaptive strategy could be useful.

5. SOLUTION TECHNIQUE BY ADAPTIVE PSO

The adaptive PSO based approach takes the following steps:

Step 1: Input the line and bus data of a distribution system, all operational constraints, the values of all the variables associated with Equation (1), and PSO parameters.

Step 2: Generate an initial population of particles with random positions and velocities. The dimension

of each particle is $m \times nl$, where m is the number of buses in the system and nl is the number of load levels.

Step 3: Set iteration index $t = 0$

Step 4: For each particle, perform an AC three-phase distribution power flow and harmonic power flow to obtain a power losses, bus voltages, and THD values for all the load levels.

Step 5: Calculate the total cost of each particle using Equation (1) and check all the constraints. If any of the constraints is violated, a penalty term is added to the total cost. The calculated total cost is served as a fitness value of particle.

Step 6: Compare the fitness value of each particle with the personal best, *Pbest*. If the fitness value is lower than *Pbest*, set this value as the current *Pbest*, and record the particle corresponding to this *Pbest* value.

Step 7: Select the minimum value of *Pbest* from all particles to be the current global best, *Gbest*, and record the particle corresponding to this *Gbest* value.

Step 8: Check whether $t = t_a$, where t_a is the activation point. If yes, all particles should be activated, or else the velocity and position of particles are updated by Equations (8) and (9).

Step 9: If the maximum number of iteration is reached, the particle associated with the current *Gbest* is the optimal solution, and then go to Step 10. Otherwise, set $t = t + 1$ and return to Step 4.

Step 10: From the optimal solution obtained in Step 9, the types and sizes of capacitors to be placed at each bus are identified. If the sizes of capacitor for all load levels are different, then the capacitor at this bus can be considered as switched type. On the other hand, if the sizes of capacitor are identical for all load levels, the capacitor at this bus is fixed type. The capacitor size for each bus is defined as the maximum value of capacitor found in any load level at that bus.

Step 11: Calculate energy loss cost, peak power loss cost, capacitor placement cost, the total cost, voltages and THD levels for all buses using the obtained optimal solution.

Step 12: Print out the results.

6. THREE-PHASE POWER FLOW AND HARMONIC POWER FLOW

For an unbalanced distribution system, a power flow algorithm with complete three-phase model is required to determine power losses and bus voltages at fundamental frequency. The technique in [9], based on the backward-forward sweep technique and tailored for radial distribution systems, is employed. This three-phase power flow algorithm develops a "bus-injection to branch-current matrix (BIBC)" based on the topological structure of distribution system to indicate the relationship between load currents and branch currents. All bus voltages are then computed by iterative process using BIBC matrix. The three-phase bus voltage in the k^{th} iteration of power flow calculation is stated by:

$$[\mathbf{V}]^{(k)} = [\mathbf{V_0}] - [\mathbf{BIBC}]^T [\mathbf{Z}][\mathbf{BIBC}][\mathbf{I}]^{(k)} \quad (10)$$

where $[\mathbf{V}]^{(k)}$ = vector of three-phase bus voltages

$[\mathbf{V_0}]$ = vector of three-phase voltage at the slack bus

$[\mathbf{BIBC}]$ = three-phase bus-injection to branch-current matrix

$[\mathbf{Z}]$ = three-phase primitive impedance matrix

$[\mathbf{I}]^{(k)}$ = three-phase vector of load currents

$[\mathbf{V}]^{(k)}$ and demand load at every bus are used to calculate $[\mathbf{I}]^{(k+1)}$, so that $[\mathbf{V}]^{(k+1)}$ in the next iteration can be evaluated. This process is repeated until the difference of bus voltages between a current iteration and the previous one is smaller than the prespecified tolerance. Note that all vectors and matrices in Equation (10) are in three-phase format; therefore, elements in $[\mathbf{V}]^{(k)}$, $[\mathbf{V_0}]$, and $[\mathbf{I}]^{(k)}$ are 3×1 subvectors and elements in $[\mathbf{Z}]$ and $[\mathbf{BIBC}]$ are 3×3 submatrices.

The harmonic power flow is performed under different harmonic orders to find harmonic voltages and harmonic losses. In this paper, harmonic power flow is based on the technique proposed in [10], where harmonic voltages are computed by:

$$[\mathbf{V}_i^h] = [\mathbf{Y}_i^h]^{-1}[\mathbf{I}_i^h] \quad (11)$$

where $[\mathbf{V}_i^h]$ = vector of three-phase bus voltages at harmonic order h for load level i

$[\mathbf{Y}_i^h]$ = three-phase bus admittance matrix at harmonic order h for load level i

$[\mathbf{I}_i^h]$ = vector of three-phase harmonic current at harmonic order h for load level i

All the variables in Equation (11) are expanded to three-phase format, so that elements in $[\mathbf{V}_i^h]$ and $[\mathbf{I}_i^h]$ are 3×1 subvectors whereas elements in $[\mathbf{Y}_i^h]$ are 3×3 submatrices.

$[\mathbf{Y}_i^h]$ is formulated from the feeder admittances of the network, all load admittances, and all shunt capacitor admittances. The values of all the admittances are varied with harmonic order as defined in [10]. Nonlinear loads are treated as harmonic sources which inject harmonic currents into the system. Elements in $[\mathbf{I}_i^h]$ are, therefore, calculated by:

$$I_{j,i}^{p,h} = \rho_j^p \frac{P_{L(j,i)}^p - jQ_{L(j,i)}^p}{h(V_{j,i}^{p,1})^*} \quad (12)$$

where $I_{j,i}^{p,h}$ = injection current in phase p of bus j for load level i at harmonic order h

ρ_j^p = nonlinear portion of load in phase p of bus j

$P_{L(j,i)}^{p}$ = real power demand in phase p of bus j for load level i

$Q_{L(j,i)}^{p}$ = reactive power demand in phase p of bus j for load level i

$(V_{j,i}^{p,1})*$ = conjugate of voltage in phase p of bus j for load level i at fundamental frequency

p = $\{A, B, C\}$

h = order of harmonic being considered

7. CASE STUDY

The distribution system of PEA, designated as Kalasin Feeder 5, is used as the test system in this work. The system has 28 buses and 19 load points. Its configuration, load data including feeder data are provided in Figure 4 [11].

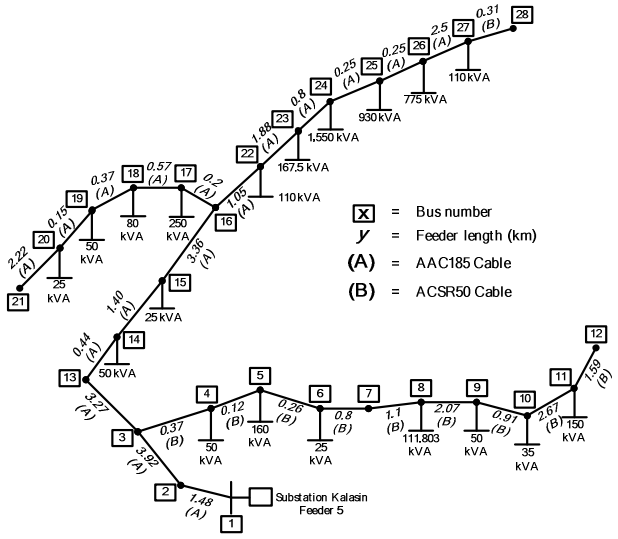

Fig. 4. Kalasin feeder 5 distribution system.

The base values for voltage and power are 22 kV and 100 MVA. The power factor of all load points is assumed as 0.85. The harmonic orders of interest are 5, 7, 11, 13, 17, 19, 23, and 25. It is assumed that capacitors are placed or replaced to each bus by discrete size of 300 kVAr three-phase fixed capacitor or switched capacitor bank. The reactive power from capacitors at each bus is, therefore, equally divided to install at each phase by the same amount.

A two-step load pattern, peak and off-peak period, is given in Table 2. The off-peak duration is 11 hours a day and the peak duration is 13 hours a day. The operational constraints and cost data are listed in Table 3. Note that cost of peak power loss (k_p) is zero because from the view point of PEA, who purchases electricity from Electricity Generating Authority of Thailand (EGAT), PEA is not obliged to pay the cost of peak demand.

For PSO parameters, the number of particles in swarm and maximum number of iteration are 100 and 300. The values of PSO acceleration constants are given as 2.0, the PSO inertia weigh is linearly decreased from 0.9 to 0.4 in each iteration and the activation point for the adaptive PSO technique is set at iteration 150.

In order to examine the effects of unbalanced loading and nonlinearity of load on the optimal solution of capacitor placement problem, 15 cases are investigated with different values of these two factors as shown in Table 4. Case 1 represents the base case in which all three phase loads are balanced and entirely linear. For other case, for example in case 5, 5% unbalanced loading means that the load of phase A is 5% higher that of phase B but lower than that in phase C by the same amount, while 15% nonlinearity of load indicates 15% of the loads are assumed to be nonlinear.

Table 2. Load duration data

Load level	Load (p.u.)	Duration (hr)
Off-peak	1.0	4,015
Peak	1.2	4,745

Table 3. Operational constraints and cost data

Minimum voltage limit	0.95 p.u.
Maximum voltage limit	1.05 p.u.
Maximum THD limit	5%
Maximum capacitor for each bus	1,500 kVAr
Cost of energy loss (off-peak period)	1.1154 Baht/kWh
Cost of energy loss (peak period)	2.9278 Baht/kWh
Cost of peak power loss	-
Cost of fixed type capacitor	32,000 Baht/bank
Cost of switched type capacitor	43,200 Baht/bank

Table 4. Fifteen cases

Case	%UB	%NL	Case	%UB	%NL
1	0	0	9	10	30
2	0	15	10	15	0
3	0	30	11	15	15
4	5	0	12	15	30
5	5	15	13	20	0
6	5	30	14	20	15
7	10	0	15	20	30
8	10	15			

%UB = %Unbalanced loading %NL = %Nonlinearity of load

8. RESULTS AND DISCUSSION

8.1 Results before capacitor placement

At first, three-phase power flow and harmonic power

flow algorithms are performed to obtain the bus voltages, THD levels, and total losses of all cases before capacitor placement. Numerical results from case 15 (extreme case) during peak period, as shown in Figures 5 and 6, indicate the effect of unbalanced loading and nonlinearity of load on voltage profile and THD values of phases A, B, and C. As expected, the voltage and THD of each phase vary with its loading.

Before capacitor placement, the minimum voltage including maximum THD level found in any phase of all buses at any load levels, and total loss are graphically summarized in Figures 7 to 9. It is found that there are some bus voltages which are lower than the minimum voltage (0.95 p.u.) as shown in Figure 7 for all cases. It is very interesting to note that with the same unbalanced loading, a greater nonlinearity of load results in a higher minimum voltage. The maximum voltages for all cases are always at slack bus, so they are not shown in the figure.

Voltage distortions are presented in the system in the cases with nonlinear loads as seen in Figure 8. From this figure, the highest values of THD found in the system are violated the maximum permissible THD level (5%) only in the cases with 30% nonlinearity of load (i.e. case 3, 6, 9, 12, and 15). The total losses of all 15 cases are shown in the bar graph of Figure 9. This figure indicates that more total losses are introduced due to an increase in unbalanced loading, while a change of load nonlinearity in the same value of unbalanced loading results in slight difference in the total loss.

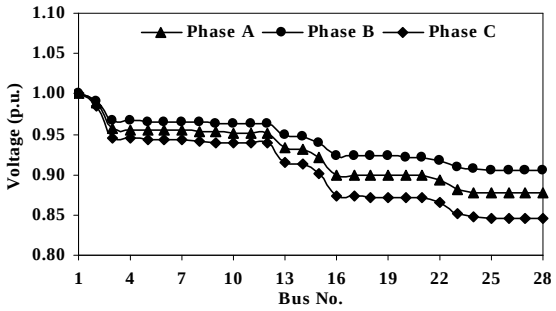

Fig. 5. Bus voltage profile at peak period for Case 15 before capacitor placement.

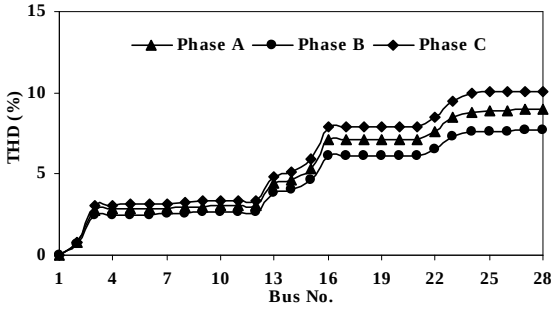

Fig. 6. THD values along the feeders at peak period for Case 15 before capacitor placement.

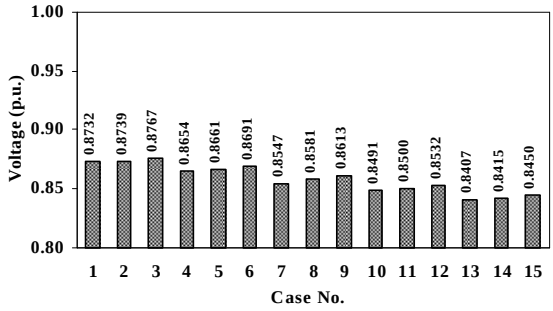

Fig. 7. Minimum voltages found in all cases before capacitor placement.

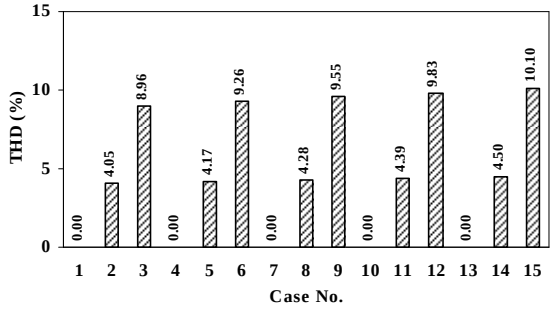

Fig. 8. Maximum THD values found in all cases before capacitor placement.

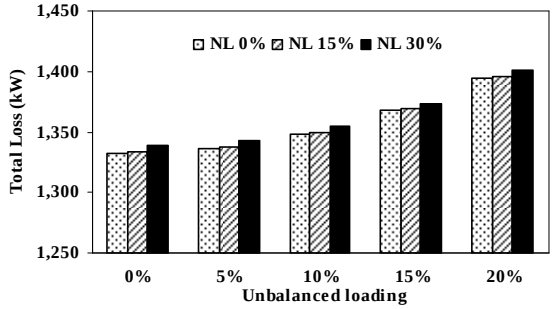

Fig. 9. Total loss of all cases before capacitor placement.

8.2 Performance of the adaptive PSO

Based on the fifteen cases shown in Table 4, their total costs can be calculated by the conventional PSO and the proposed adaptive PSO, as illustrated in Figure 10. It is obviously seen that the solutions obtained from the proposed adaptive PSO can offer lower total costs compared with those derived by the conventional PSO for every scenario appearing in the fifteen cases. These results confirm the advantages of the adaptive PSO technique in searching for better solutions.

8.3 Effects of unbalanced loading and nonlinearity of load on the optimal solutions

The effects of unbalanced loading and nonlinearity of load are investigated using the optimal solutions determined by the proposed adaptive PSO approach. The summary of constraint satisfaction, fixed and switched type capacitor kVAr to be placed, and the comparison of total loss and total cost between before and after capacitor placement are presented in Tables 5 to 7. Figures 11 to 13 graphically show the total

capacitor kVAr required for reactive power compensation, as well as reduction in the total loss and total cost respectively.

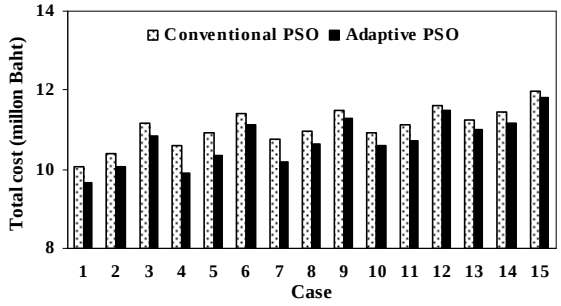

Fig. 10. Comparison of total cost between conventional PSO and adaptive PSO

It can be seen from Table 5 that the obtained optimal solutions of 15 cases satisfy all the constraint given in Section 2, namely, bus voltages, THD levels, and maximum capacitor kVAr for each bus. Table 6 indicates that the total capacitor kVAr associated with the obtained optimal solution vary with the change of unbalanced loading and nonlinearity of load. It is also found in Figure 11 that the increasing of these two factors gives the more total capacitor kVAr required for compensation.

The optimal capacitor placements introduce the reduction in total loss and total cost compared with that before capacitor placement as listed in Table 7. The percentage in reduction of total loss is slightly different regard to the variation of unbalanced loading and nonlinearity of load as shown in Figure 12. It is around 33-37% for all cases. On the other hand, the percentage in reduction of total cost is decreased with increased unbalanced loading and nonlinearity of load as seen in Figure 13. This is expected as an increase of these two factors needs more investment on capacitor. The maximum reduction in total cost of about 28% is taken place in case 1 with entirely linear and balanced load connected to the network, while the minimum reduction of total cost of around 17%, is given in case 15.

The above observations are evidences for the effects of unbalanced loading and load nonlinearity on the optimal solution of capacitor placement problem. For this reason, both unbalanced loading and the presence of nonlinear loads should be considered when the optimal location and size of capacitors are determined. Otherwise, a solution without concerning these two factors is a non-optimal solution.

Table 5. Summary of constraints satisfaction for optimal solution in all cases

Case	Min. voltage (p.u.)	Max. voltage (p.u.)	Max. THD (%)	Max. capacitor placed at any bus (kVAr)
1	0.9546	1.000	0.00	1,200
2	0.9541	1.0012	3.43	1,500
3	0.9750	1.0060	4.81	1,500
4	0.9504	1.0000	0.00	1,500
5	0.9546	1.0009	4.11	1,200
6	0.9695	1.0125	4.99	1,500
7	0.9505	1.0009	0.00	1,500
8	0.9519	1.0055	3.96	1,200
9	0.9648	1.0178	4.99	1,500
10	0.9503	1.0061	0.00	1,500
11	0.9521	1.0123	3.18	1,500
12	0.9633	1.0238	4.88	1,500
13	0.9501	1.0099	0.00	1,500
14	0.9502	1.0121	3.24	1,500
15	0.9676	1.0231	4.75	1,500

Table 6. Fixed and switched type capacitors required for optimal solution in all cases

Case	Fixed type capacitor (kVAr)	Switched type capacitor (kVAr)	Total kVAr (kVAr)
1	9,600	2,100	11,700
2	8,700	4,800	13,500
3	5,100	12,000	17,100
4	5,700	6,300	12,000
5	7,800	6,300	14,100
6	10,200	7,500	17,700
7	8,100	5,700	13,800
8	6,300	9,000	15,300
9	7,800	10,500	18,300
10	7,800	7,800	15,600
11	10,200	6,000	16,200
12	7,500	11,700	19,200
13	4,200	12,300	16,500
14	6,900	10,500	17,400
15	8,700	11,100	19,800

Table 7. Total loss and total cost before and after capacitor placement

Case	Total loss (kW)		Total cost (Baht)	
	Before	After	Before	After
1	1,322.76	829.02	13,530,285	9,675,243
2	1,334.10	841.01	13,543,364	10,072,660
3	1,338.83	857.28	13,589,995	10,821,851
4	1,336.61	837.99	13,570,495	9,896,125
5	1,337.94	857.76	13,583,569	10,337,989
6	1,342.67	896.14	13,630,200	11,107,645
7	1,348.15	845.06	13,691,338	10,179,085
8	1,349.49	870.24	13,704,392	10,631,717
9	1,354.22	905.06	13,751,025	11,271,614
10	1,367.47	855.68	13,893,610	10,579,519
11	1,368.81	882.86	13,906,634	10,709,031
12	1,373.54	925.72	13,953,268	11,506,100
13	1,394.68	881.21	14,178,653	10,996,677
14	1,396.01	891.79	14,191,634	11,154,244
15	1,400.75	940.96	14,238,271	11,801,461

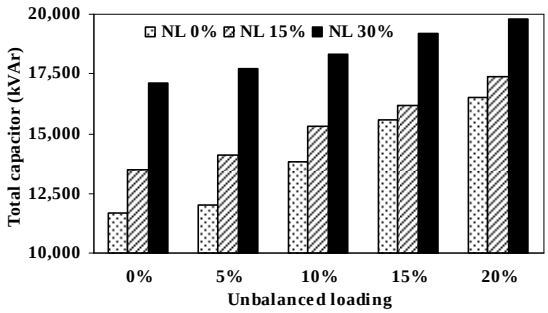

Fig. 11. Total capacitor kVAr required for optimal solution for all cases.

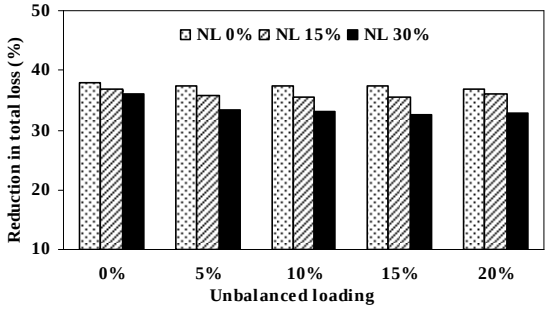

Fig. 12. Reduction in total loss for all cases after optimal capacitor placement.

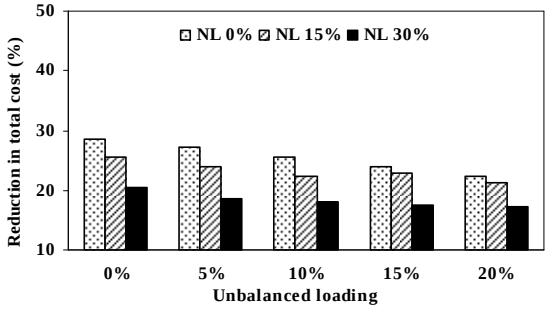

Fig. 13. Reduction in total cost for all cases after optimal capacitor placement.

9. CONCLUSION

This paper has presented an adaptive PSO-based optimization technique to determine optimal capacitor placement in an unbalanced loading distribution system connected to nonlinear loads. A distribution system of PEA, which consists of 28 buses and 19 load points with a two-step load pattern, is used to illustrate the performance of this proposed technique. Numerical results from different values of unbalanced loading and nonlinearity of load demonstrate that the obtained optimal solutions introduce a saving in total cost while satisfying all the specified constraints. The effects of unbalanced loading and load nonlinearity on the optimal solution are also examined. It is found that total loss in the network and total capacitor kVAr required for reactive power compensation are increased when unbalanced loading and load nonlinearity are increased whereas the saving in total cost is decreased owing to the more investment cost for capacitors.

ACKNOWLEDGMENT

The first author would like to express his sincere thanks to the Ministry of Science and Technology (MOST), Thailand and Thailand Institute of Scientific and Technological Research (TISTR), Thailand for their financial supports.

REFERENCES

[1] Ng, H.N., Salama, M.M.A., and Chikhani, A.Y. 2000. Classification of capacitor allocation techniques. *IEEE Transactions on Power Delivery* 15(1): 387-392.

[2] Chen, C.S., Hsu, C.T., and Yan, Y.H. 1995. Optimal distribution feeder capacitor placement considering mutual coupling effects of conductors. *IEEE Transactions on Power Delivery* 10(2): 987-994.

[3] Xu, W., Marti, J.R., and Dommel, H.W. 1991. A multiphase harmonic load flow solution technique. *IEEE Transactions on Power Systems* 6(1): 174-182.

[4] Eberhart, R., and Kennedy, J. 1995. A new optimizer using particle swarm theory. In *Proceedings of the Sixth International Symposium on Micro Machine and Human Science.* Nagoya, Japan. 4-6 October. IEEE Press.

[5] Chiang, H.D., Wang, J.C., Tong, J., and Darling, G. 1995. Optimal capacitor placement, replacement and control in large-scale unbalanced distribution system: system modeling and a new formulation. *IEEE Transactions on Power Systems* 10(1): 356-362.

[6] Lee, K.W., and El-sharkawi, M.A. 2008. *Modern heuristic optimization techniques: theory and applications to power system*. New Jersey: John Wiely & Sons, Inc.

[7] Engelbrecht, A. P. 2005. *Fundamentals of computational swarm intelligence*. West Sussex: John Wiley & Sons.

[8] Gallego, R.A., Monticelli, A.J., and Romero, R. 2001. Optimal capacitor placement in radial distribution networks. *IEEE Transactions on Power Systems* 16(4): 630-637.

[9] Teng, J.H. 2000. A network-topological-based three-phase load flow for distribution systems. *Pro. Natl. Sci. Counc. ROC(A)* 24(4): 259-264.

[10] Baghzouz, Y. 1991. Effects of nonlinear loads on optimal capacitor placement in radial feeders. *IEEE Transactions on Power Delivery* 6(1): 245-251.

[11] Nethan, C. 2006. Optimal shunt capacitor sizing and location on the radial distribution system with microsoft excel solver. M.Eng Thesis. Khon Kaen University, Khonkaen, Thailand.

GMSARN International Journal
NOTES FOR AUTHORS

Editorial Policy

In the Greater Mekong Subregion, home to about 250 million people, environmental degradation - including the decline of natural resources and ecosystems will definitely impact on the marginalized groups in society - the poor, the border communities especially women and children and indigenous peoples. The complexity of the challenges are revealed in the current trends in land and forest degradation and desertification, the numerous demands made on the Mekong river - to provide water for industrial and agricultural development, to sustain subsistence fishing, for transport, to maintain delicate ecological and hydrological balance, etc., the widespread loss of biological diversity due to economic activities, climate change and its impacts on the agricultural and river basin systems, and other forms of crises owning to conflicts over access to shared resources. The *GMSARN International Journal* is dedicated to advance knowledge in energy, environment, natural resource management and economical development by the vigorous examination and analysis of theories and good practices, and to encourage innovations needed to establish a successful approach to solve an identified problem.

The *GMSARN International Journal* is a biannual journal published by GMSARN in June and December of each year. Papers related to energy, environment, natural resource management, and economical development are published. The papers are reviewed by world renowned referees.

Preparation Guidelines

1. The manuscript should be written in English and the desired of contents is: Title, Author's name, affiliation, and address; Abstract, complete in itself and not exceeding 200 words; Text, divided into sections, each with a separate heading; Acknowledgments; References; and Appendices. The standard International System of Units (SI) should be used.

2. Illustrations (i.e., graphs, charts, drawings, sketches, and diagrams) should be submitted on separate sheets ready for direct reproduction. All illustrations should be numbered consecutively and given proper legends. A list of illustrations should be included in the manuscript. The font of the captions, legends, and other text in the illustrations should be Times New Roman. Legends should use capital letters for the first letter of the first word only and use lower case for the rest of the words. All symbols must be italicized, e.g., α, θ, Q_{wt}. Photographs should be black and white glossy prints; but good color photographs are acceptable.

3. Each reference should be numbered sequentially and these numbers should appear in square brackets in the text, e.g. [1], [2, 3], [4]–[6]. All publications cited in the text should be presented in a list of full references in the Reference section as they appear in the text (not in alphabetical order). Typical examples of references are as follows:

   - **Book references** should contain: name of author(s); year of publication; title; edition; location and publisher. Typical example: [2] Baker, P.R. 1978. Biogas for Cooking Stoves. London: Chapman and Hall.
   - **Journal references** should contains: name of author(s); year of publication; article title; journal name; volume; issue number; and page numbers. For example: Mayer, B.A.; Mitchell, J.W.; and El-Wakil, M.M. 1982. Convective heat transfer in veetrough liner concentrators. Solar Energy 28 (1): 33-40.
   - **Proceedings reference** example: [3] Mayer, A. and Biscaglia, S. 1989. Modelling and analysis of lead acid battery operation. Proceedings of the Ninth EC PV Solar Conference. Reiburg, Germany, 25-29 September. London: Kluwer Academic Publishers.
   - **Technical paper** reference example: [4] Mead, J.V. 1992. Looking at old photographs: Investigating the teacher tales that novice teachers bring with them. Report No. NCRTL-RR-92-4. East Lansing, MI: National Center for Research on Teacher Learning. (ERIC Document Reproduction Service No. ED346082).
   - **Online journal** reference example: [5] Tung, F. Y.-T., and Bowen, S. W. 1998. Targeted inhibition of hepatitis B virus gene expression: A gene therapy approach. Frontiers in Bioscience [On-line serial], 3. Retrieved February 14, 2005 from http://www.bioscience.org/1998/v3/a/tung/a11-15.htm.

4. Manuscript can be uploaded to the website or sent by email. In case of hard copy, three copies of the manuscript should be initially submitted for review. The results of the review along with the referees' comments will be sent to the corresponding author in due course. At the time of final submission, one copy of the manuscript and illustrations (original) should be submitted with the diskette. Please look at the author guide for detail.

GMSARN Members

Asian Institute of Technology

Hanoi University of Technology

Ho Chi Minh City University of Technology

Institute of Technology of Cambodia

Khon Kaen University

Kunming University of Science and Technology

National University of Laos

Royal University of Phnom Penh

Thammasat University

Yangon Technological University

Yunnan University

Guangxi University

Associate Members

Nakhon Phanom University

Mekong River Commission

Ubon Rajathanee University

Published by the **Greater Mekong Subregion Academic and Research Network (GMSARN)**
c/o Asian Institute of Technology (AIT)
P.O. Box 4, Klong Luang
Pathumthani 12120, Thailand
Tel: (66-2) 524-5437; Fax: (66-2) 524-6589
E-mail: gmsarn@ait.ac.th
Website: http://www.gmsarn.org